DOT/FAA/TC-20/2

Federal Aviation Administration
William J. Hughes Technical Center
Aviation Research Division
Atlantic City International Airport
New Jersey 08405

A Summary of Results from Two Full-Scale Fokker F28 Fuselage Section Drop Tests

May 2020

Final Report

U.S. Department of Transportation
Federal Aviation Administration

NOTICE

Technical Report Documentation Page

1. Report No.	2. Government Accession No.	3. Recipient's Catalog No.
DOT/FAA/TC-20-2		

4. Title and Subtitle	5. Report Date
A Summary of Results from Two Full-Scale Fokker F28 Fuselage Section Drop Tests	May 2020
	6. Performing Organization Code

7. Author(s)	8. Performing Organization Report No.
Justin D. Littell	

9. Performing Organization Name and Address	10. Work Unit No. (TRAIS)
NASA Langley Research Center Hampton, VA 23681	11. Contract or Grant No.

12. Sponsoring Agency Name and Address	13. Type of Report and Period Covered
U.S. Department of Transportation Federal Aviation Administration Office of Aviation Research Washington, DC 20591	Final Report
	14. Sponsoring Agency Code AIR-600

15. Supplementary Notes

The Federal Aviation Administration William J. Hughes Technical Center Aviation Research Division COR was Allan Abramowitz.

16. Abstract

The Federal Aviation Administration (FAA) and NASA Langley Research Center (LaRC) collaborated on a research effort to obtain data through a series of drop tests for developing airframe-level crash requirements for transport category airplanes.

This research was conducted on two Fokker F28 MK4000 fuselage sections (FS). The first test was a pure vertical drop test of a relatively uniform forward section, which included an underfloor area for luggage. The second test was a canted drop test onto a sloped surface of a portion of the fuselage representing the wingbox stiffened structure. In both tests, accelerometers were installed on the floor, seat track, luggage, and overhead bin to measure responses in the two airframe sections. In addition, ten Anthropomorphic Test Devices (crash test dummies) were included in each test to measure the potential of onboard occupant injury. Self-contained data recorders, which logged accelerations and rotational rates, were also used on the seat tracks and the lower structure for evaluation as potential crash recording devices in future tests. Finally, the starboard side of each section was painted with a stochastic black and white speckle pattern for use in full field photogrammetric imaging techniques.

The results show notable differences in the forward and wingbox section FS responses. The forward section floor accelerations had an initial peak of approximately 21 g and a relatively uniform response of approximately 7 g throughout the impact event. This section exhibited large amounts of subfloor crushing, floor stiffener failures, and seat deformation on impact. These results are contrasted by the wingbox section accelerations, which showed large differences when comparing accelerations from the rear and the front of the FS. The rear had an initial peak of 39 g and the front section only 32 g, and uniform responses of 12.2 and 9.8 g, respectively.

17. Key Words	18. Distribution Statement
Drop test, airframe, anthropomorphic test devices, ATD, crash dummies, Fokker F28	This document is available to the U.S. public through the National Technical Information Service (NTIS), Springfield, Virginia 22161. This document is also available from the Federal Aviation Administration William J. Hughes Technical Center at actlibrary.tc.faa.gov.

19. Security Classif. (of this report)	20. Security Classif. (of this page)	21. No. of Pages	22. Price
Unclassified	Unclassified		

TABLE OF CONTENTS

LIST OF FIGURES

LIST OF TABLES

LIST OF ACRONYMS

ATD	Anthropomorphic Test Device
CBR	California Bearing Ratio
CDR	Crash data recorder
CFR	Code of Federal Regulations
CG	Center of gravity
DAS	Data acquisition system
FS	Frame Section
LandIR	Landing and Impact Research Facility
LaRC	Langley Research Center
SC	Special Condition

EXECUTIVE SUMMARY

During 2017, two vertical drop tests were conducted on two partial sections removed from a Fokker F28 MK4000 aircraft. This was part of a joint NASA/Federal Aviation Administration (FAA) effort to investigate the crashworthiness characteristics of Transport Category Aircraft, as defined by 14 Code of Federal Regulations, Part 25. The first test was a pure vertical drop of a relatively uniform forward section, which included an underfloor area for luggage. The second test was a canted drop onto a sloped part of the fuselage representing the wingbox stiffened structure. In both tests, accelerometers were installed on the floor, seat track, luggage, and overhead bin to measure responses in the two airframe sections. In addition, ten Anthropomorphic Test Devices (ATDs, a.k.a. crash test dummies) were used in each test to measure the potential of onboard occupant injury. Self-contained data recorders, which logged accelerations and rotational rates, were also used on the seat tracks and the lower structure. These were evaluated for use as potential crash recording devices in future tests. Finally, the starboard side of each section was painted with a stochastic black and white speckle pattern for use in full field photogrammetric imaging techniques.

The results show notable differences in the forward and wingbox section responses. The forward section floor accelerations showed an initial peak of approximately 21 g and a relatively uniform response of approximately 7 g throughout the impact event. This section exhibited large amounts of subfloor crushing, floor stiffener failures, and seat deformation on impact. These results are contrasted by the wingbox section accelerations, which showed large differences when comparing accelerations from the rear and the front of the FS. The rear had an initial peak of 39 g and the front section only 32 g, and uniform responses of 12.2 and 9.8 g, respectively. Additionally, the wingbox section test induced a forward motion caused from the rotation at impact. With the exception of the lower cavity, there was minimal deformation in the wingbox section, and ATD responses were consistently higher than those for the forward section.

A complete set of results are presented for the airframe, seat, ATD, overhead bin, and subfloor regions for each section. The ATD results are compared to current injury criteria and determinations made on the likelihood of injury. Additional results for cargo-hold stored luggage are included to try and provide a component-level characterization to better understand under-floor loading. Finally, there is a discussion of the relevance of the results for a proposed airframe level crashworthiness guideline.

Current FAA certification requirements do not consider the size of Part 25 aircraft. The size of the F28 sections (and corresponding aircraft) are much smaller than an A350-900 or other wide-body aircraft. The size of these sections made them potentially unable to demonstrate adequate crashworthiness at the 30 ft/s impact velocity. Had the sections been tested at 20 ft/s vertical velocity, representing a reduction of the kinetic impact energy by 44%, all four criteria might have been met. Thus, it is important to consider different limits in the criteria based on aircraft size, weight, or other defining factors.

1. INTRODUCTION

The Federal Aviation Administration (FAA) and NASA Langley Research Center (LaRC) collaborated on researching and obtaining data through a series of drop tests to development airframe-level crash requirements for transport category airplanes (FAA, 2015). This research was conducted on two Fokker F28 MK4000 fuselage sections in 2017. The Fokker F28 MK4000 is a high-performance twin-turbo fan narrow-body aircraft. Seating is in a triple configuration on the starboard side and a double configuration on the port side. This aircraft can carry up to 85 passengers on medium range routes. The original F28 aircraft was type certified by the FAA in 1969 and had major operations in the US up through the 1990s. The majority of the F28 fleet has been retired from service. Only a handful of still airworthy aircraft are operated by African commercial carriers. NASA LaRC acquired a full F28 aircraft, along with three additional partial fuselage section test articles, in the early 2000s time frame.

Drop tests of partial fuselage sections (commonly called "barrel drops" or "barrel section drops") have been done for a variety of aircraft over the past 30 years. A set of drop tests were conducted in the 1980s by NASA LaRC for the preliminary acquisition of occupant, structural, and seat loadings from Boeing 707 fuselage sections (Williams & Hayduk, (NASA-TM-85706) 1983, Fasanella & Alfaro-Bou (NASA-TM-89025), 1986, and Williams & Hayduk, (NASA-TM-85679) 1983). This was to prepare for a full-scale crash test, known as the Controlled Impact Demonstration, conducted in 1984 (Fasanella et al., 1986). More recently, the FAA conducted a series of barrel section drops for both Boeing 737 and Boeing 707 fuselages. A subset of these tests was used to evaluate airframe interaction with auxiliary fuel tanks (FAA, 2000). These tests also collected airframe, seat, and occupant loads to valuate injury metrics (FAA, 1995). The FAA used this preliminary information for a series of vertical drop tests of full aircraft, including an ATR42-300 (FAA, 2006), Metro III (FAA, 1993), Beechcraft 1900C (FAA, DOT/FAA/AR-05/56, 1998), and Shorts 3-30 (FAA, 1999). All these drop tests were conducted to investigate the structural response of the aircraft and occupant injury under severe but survivable conditions.

2. TEST SETUP

There were two intact and untested F28 barrel sections located at LaRC, their locations in the aircraft are highlighted in Figure 2.1. The first section is a forward section, which consists of five windows and six frames between Frame Stations (FS) 5305 and 7805. (For the Fokker 28 aircraft, these FS numbers are designated in units of centimeters). All the interior paneling, overhead bins, floor, and windows were removed in this section. There is a functional cargo door on the starboard side of the section, but otherwise the section has a uniform cross section. The second section is a wingbox section, which consists of 5 windows, 6 frames, and two emergency exit doors between FS 9805 and 12405. As with the forward section, the interior paneling, overhead bins, floor and windows were removed. The emergency exits were functional before being used for testing. The wings were disconnected from the wingbox attachment points on either side.

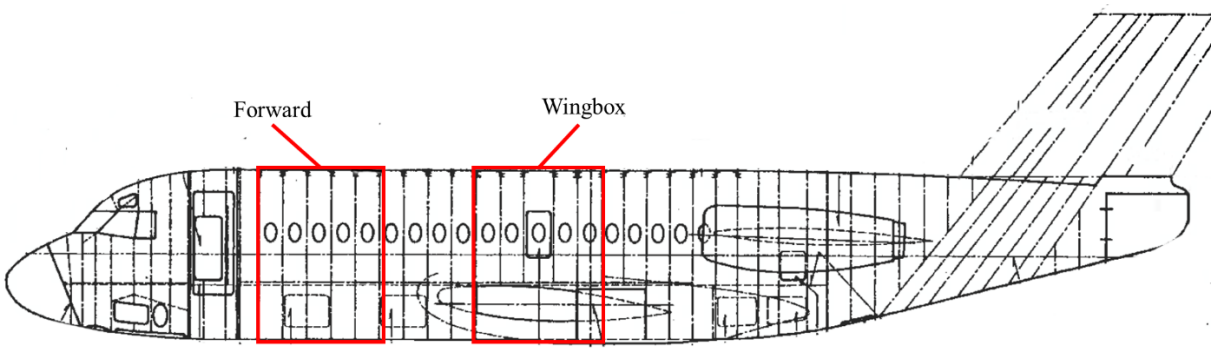

Figure 2.1. Schematic of F28 section locations

Each section was approximately 9 ft long and 9 ft wide when measured at the floor level. The sections were of a semi-monocoque design with skin-stringer-stiffener frame construction. Frame sections were spaced approximately 20 inches apart throughout each section, and the forward section floor was stiffened with lower stanchions. The wingbox section floor structure was supported by the wingbox itself. All electronic wiring was removed, and all fluids drained. In the wingbox section, the existing mechanical linkages were cut at the ends of the section, but the mechanical components already in the structure remained for the test. The underfloor wing truss structure was left unmodified. The unmodified sections are shown in Figure 2.2.

Figure 2.2. Unmodified F28 test article sections—forward (left), and wingbox (right)

All tests were conducted at NASA LaRC's Landing and Impact Research Facility (LandIR), shown in Figure 2.3. LandIR is a 240-ft high, 400-ft long steel A-frame gantry structure built in 1965. LandIR is used to conduct full-scale crash testing under combined horizontal and vertical loading

(Annett, et al., 2014, Littell, 2015) or under vertical loading only (Kellas & Jackson, 2008) through a series of overhead cabling and release mechanisms.

Figure 2.3. Landing and Impact Research Facility (LandIR)

To populate a fully instrumented test article from the unmodified sections, floor panels, seats, Anthropomorphic Test Devices (ATDs), overhead mass, and underfloor luggage were all installed into the sections. The original floor panels, which were in storage, were reused in testing. The floor panels were a sandwich composite structure, fabricated from either a fiberglass face sheet with Nomex® core or aluminum face sheet with balsa wood core. Each floor panel was fit for a specific location on the floor, so the two types of floor designs were used at their correct positions during installation. Care was taken to identify where each type of material was installed at which position. It is not clear why two different types of floor panel materials were used interchangeably in various locations. Each floor panel was fastened to the seat track flanges through a series of quarter turn fasteners along their edges.

Two rows of seats were installed in a triple-double configuration, with the triple seats installed on the starboard side of the section and the double seats installed on the port side. These seats were (FAA, 1998 CFR § 25.562) certified and removed from an in-service Boeing 737 aircraft. However, all seats had a triple configuration and needed modification to be used in testing. Figure

2.4 shows a schematic taken from the Fokker F28 Weight and Balance Manual (Fokker, 1999) of the F28 seat configuration.

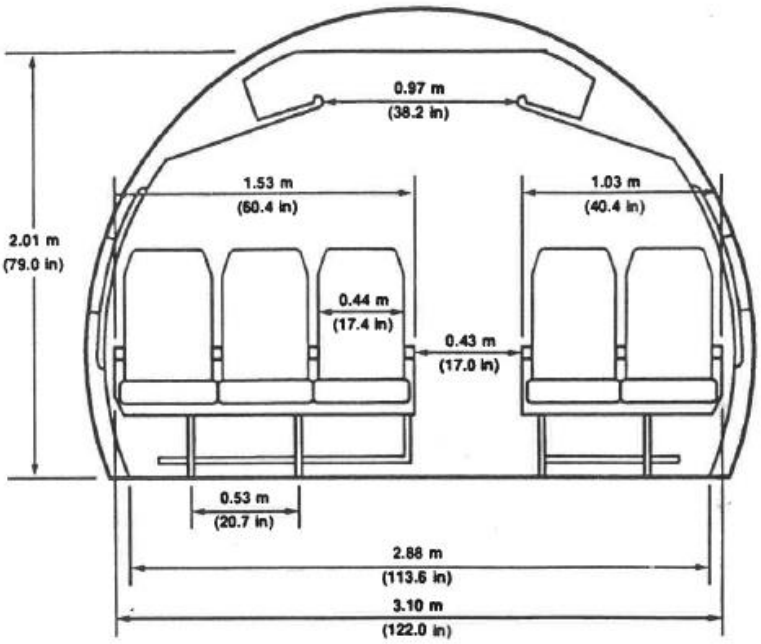

Figure 2.4. Original F28 seating configuration from the F28 weight and balance manual

Care was taken to adhere to the original F28 configuration as much as possible. The seat legs were reconfigured to interface with the seat track dimensions for the F28. For the triple seats located on the starboard side of the fuselage, this involved moving both of the seat legs outward to interface with the starboard side seat track spacing. For the double seats, the process involved removing the original window seat and then re-spacing the seat legs inward to interface with the F28 port side seat track spacing. The original window seat was not used in testing, and the old middle seat became the window seat. For the remainder of this report, the old middle/new window seat is referred to as the port side window seat. Figure 2.5 shows the modifications made on both the starboard side triple seat and the port side double seat. Note that the aisle seat in the triple configuration was overhung up to 25 in. after the modifications were complete.

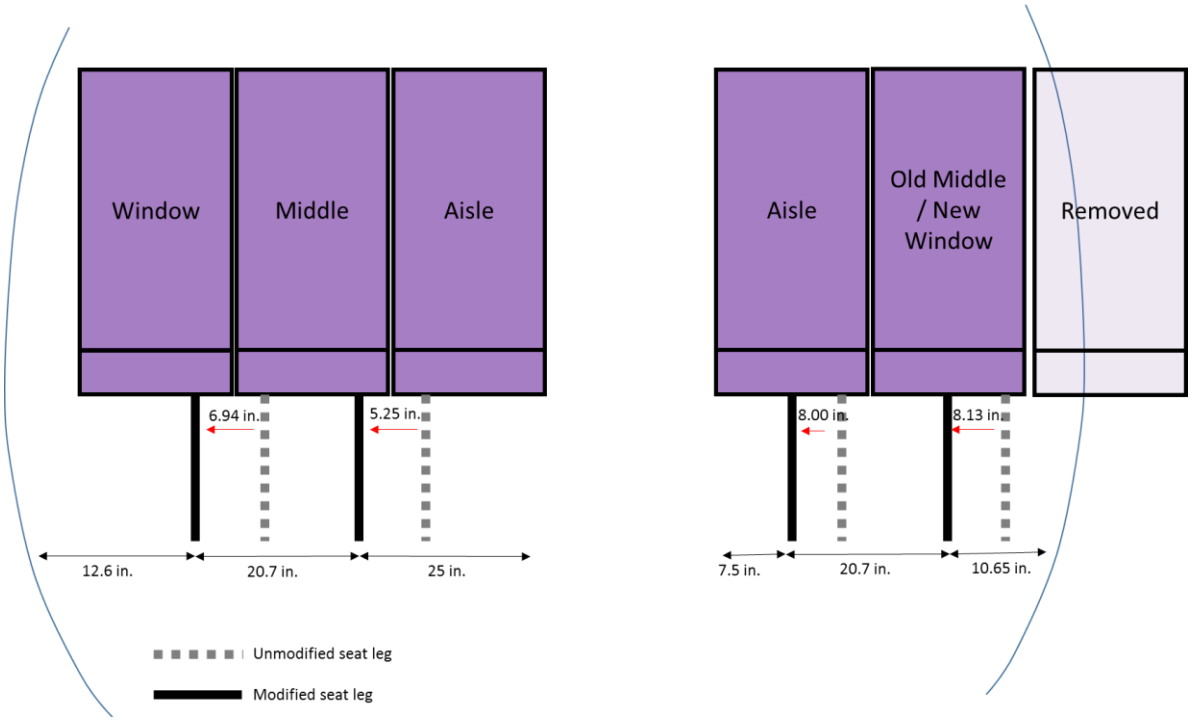

Figure 2.5. Seat modification illustration

Figure 2.6 shows the unmodified and modified triple seat configuration. The window seat is on the left side and the aisle seat is on the right side in both views. The modification and layout of the double seat is shown in Figure 2.7. The existing lap belts in the seats were unmodified and used to restrain all the ATDs.

(a) (b)

Figure 2.6. Triple seat configuration for starboard side—unmodified (a) and modified (b)

(a) (b)

Figure 2.7. Double seat configuration for port side—unmodified triple (a) cut and modified into a double (b)

Underfloor luggage was included in the forward section test to simulate a fully loaded fuselage condition. Packed luggage was acquired from the FAA containing clothing, shoes, toiletries, and other typical items. Bags were loosely placed and stacked up to the required loading limit in the subfloor luggage compartment between the stanchions. This configuration approximated a packing sequence of three bags wide, four bags deep, and three bags stacked high. The intent was to have some realistic nonuniformity in the luggage configuration due to the construction, size, and contents of the individual bags. This would accurately replicate a real aircraft containing underfloor luggage. The compartment was held by a safety net on each end. The total weight of luggage in the subfloor compartment was 922 lb. Figure 2.8 shows a close-up of the forward section luggage compartment. After the test, the luggage was discarded.

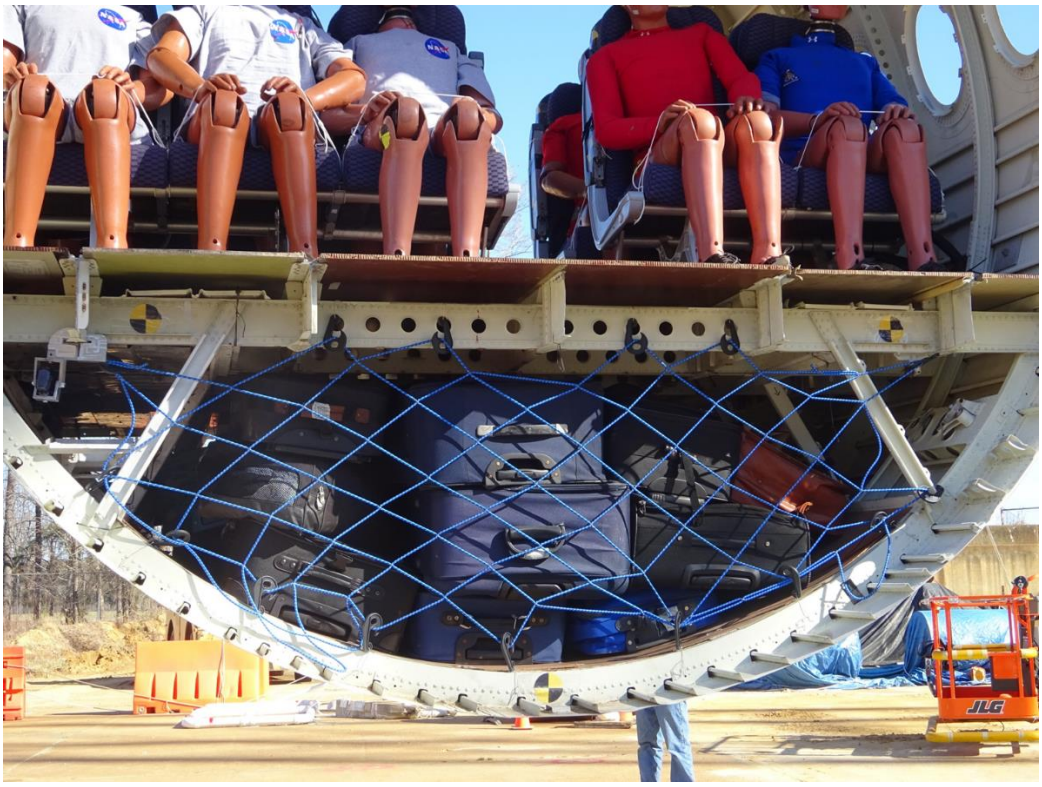

Figure 2.8. Underfloor luggage configuration for the forward section test

Overhead compartments, called “hat racks” were originally installed on the F28, but were not available for the tests. Note that hat racks have similar functionality to overhead bins but lack a door. Overhead bins have since replaced hat racks on current aircraft fleets because stowed items in hat racks could come loose during flight. In Figure 2.4, simulated hat racks are at the top of the fuselage section, over the seats. They are simulated with ballast mass and aluminum c-channels. A section of aluminum c-channel was fastened to both sides of the interior four frames of each test article through links connected to the three original overhead hat rack attachment locations. The links were sized so that the overall center of gravity (CG) position of the structure was 71.6 in. above the floor and 25.25 in. off the fuselage centerline. These dimensions located the CG in the middle of the hat rack opening shown in Figure 2.4. Lead ballast, in the form of 25 lb. weights was fastened to the three interior center spans of the c-channel. The onboard cameras were attached to the underside of the c-channel. In total, the weight for each side was 116 lb., giving a running load of 33.2 lb./ft. Figure 2.9 shows the overhead mass configuration.

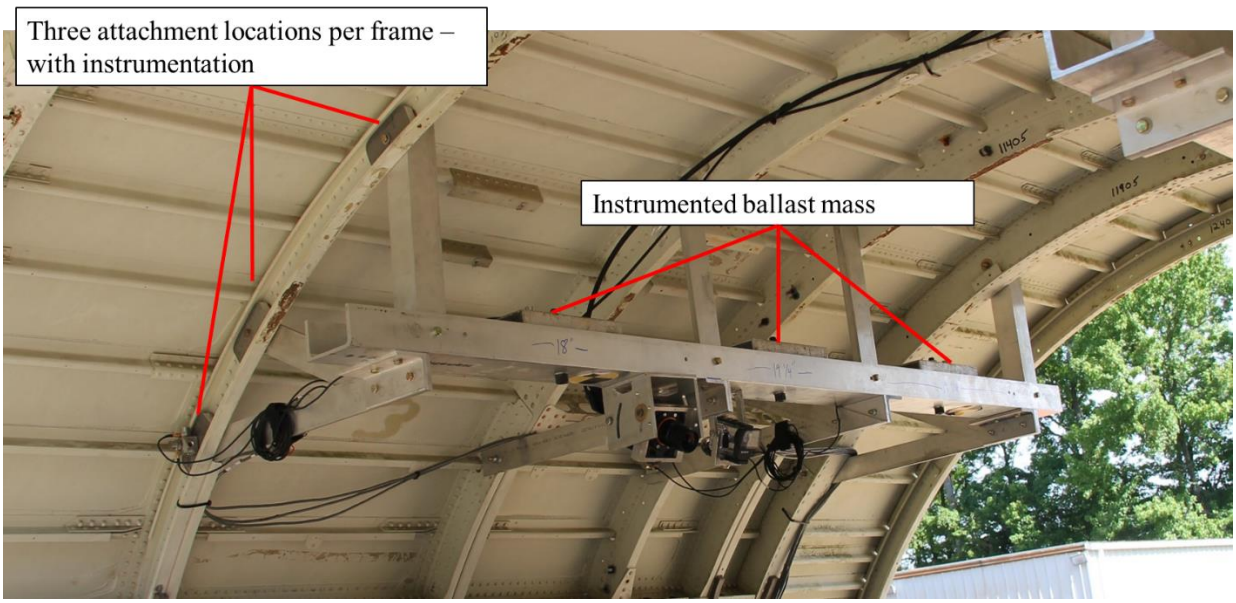

Figure 2.9. Overhead mass configuration

In the forward section test, the rear row of seats was centered over FS 6805. The forward row of seats was positioned over FS 5805. In the wingbox section, the rear row of seats was centered over FS 11405, and the front row of seats was positioned over FS 10305. For both tests, the seat pitch was 32 in between rows. All seats were in their most upright position and all armrests placed up to avoid interfering with the ATD and ATD arm motion. Rear seat back monitors and corresponding electronics were removed for the tests. Aluminum plates were installed in their place to determine possible ATD head contact.

Ten ATDs seated in the 10 seats were supplied by NASA LaRC and the FAA Civil Aerospace Medical Institute. There was a combination of Hybrid II (H2), Hybrid III (H3), and FAA H3 (Gowdy, et al., 1999) ATDs in different sizes ranging between a 110 lb. (5^{th} percentile), a 170 lb. (50^{th} percentile), and a 237 lb. (95^{th} percentile). Each Hybrid III ATD was instrumented with head, chest, and pelvic accelerometers. They also had upper and lower neck and lumbar load cells. Each Hybrid II was only instrumented with head, chest, and pelvic accelerometers and a lumbar load cell. Figure 2.10 on the left shows the ATD make, size, and seat positioning for both tests. The setup for both tests was identical. Figure 2.10 on the right shows an overhead view of the ATDs in their test configuration. This report uses the following nomenclature to identify the ATD along with its seat position as ATD #. For example, the ATD seated in seat 3 is identified as ATD 3.

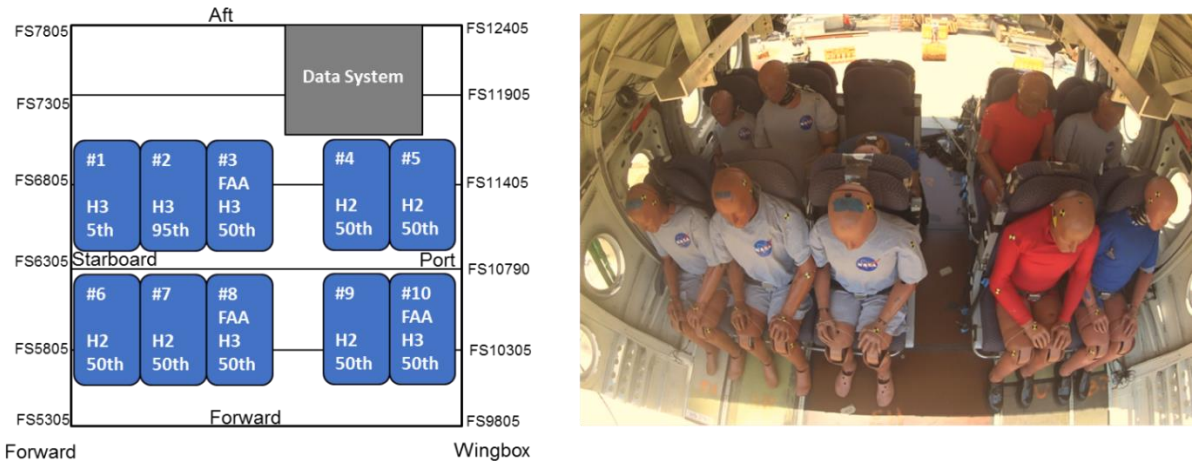

(a) (b)

Figure 2.10. Seat schematic (a) and ATDs in test configuration (b)

Airframe data via accelerometers placed in various locations throughout the fuselage sections. Accelerometers along the floor at the floor/frame junctions along the port and starboard sides were used to measure floor accelerations. Small holes were drilled into the base of the seat legs for the placement of seat leg accelerometers used to measure seat base accelerations. Accelerometers were also mounted directly to the overhead lead ballast mass and at the c-channel attachment locations at the forward and aft frame attachments. These accelerometer locations were common to both fuselage sections. Sample positions of these locations are shown in Figure 2.11.

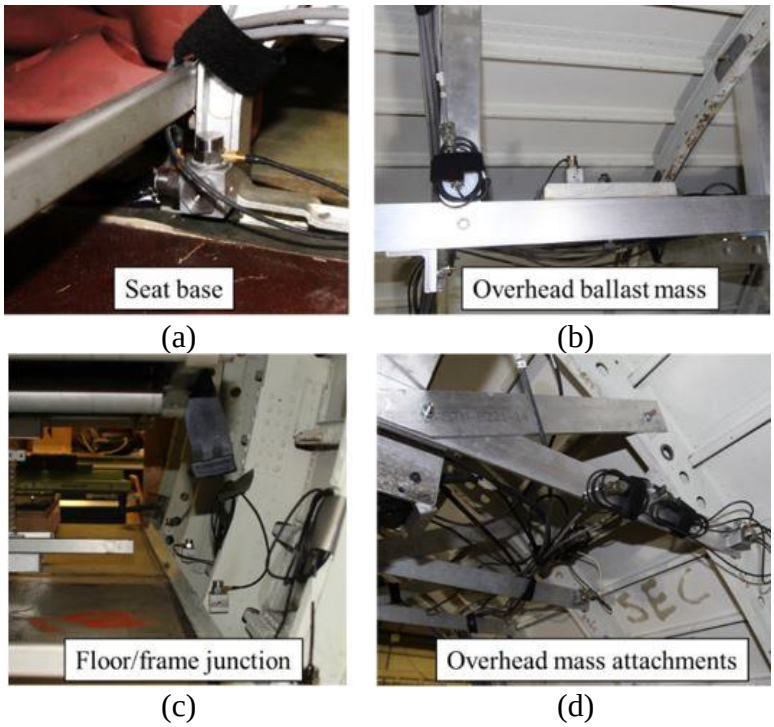

Figure 2.11. Accelerometer locations—seat base (a), overhead ballast mass (b), floor / frame junction (c), and overhead mass attachments (d)

For the forward section test, additional accelerometers were placed near the lower stanchion/frame attachment points on the port and starboard sides at FS 5805 and 6805 to measure underfloor accelerations. Because the forward section test was designed for a purely vertical impact, accelerometers primarily measured vertical acceleration. Several accelerometers measured horizontal (forward/aft) accelerations for potential test anomalies. The forward section channel count was 145 total, which included the entirety of the airframe and ATD sensors.

Two additional crash data recorders (CDRs) were placed on the rear starboard side floor. Each of the CDRs was a standalone data logging unit. Their physical dimensions measured approximately 3 in. x 3 in. x 1 in. The CDRs had acceleration sensors in three axes, non-volatile memory, a circuit board with computer USB connection, and a battery. Each was armed independently of all other sensors and triggered at impact via a sensed acceleration threshold. There were two types of CDRs–a blue unit with a 500-g range recording at 10 kHz and a brown unit with a 6000-g range recording at 75 kHz. The CDRs were included to evaluate their robustness as an alternative means of measuring acceleration through a portable measurement system. In the forward section test, an additional blue CDR in one of the luggage bags was used to measure the acceleration of the luggage during the test event. Figure 2.12 shows two CDRs used in the forward section test.

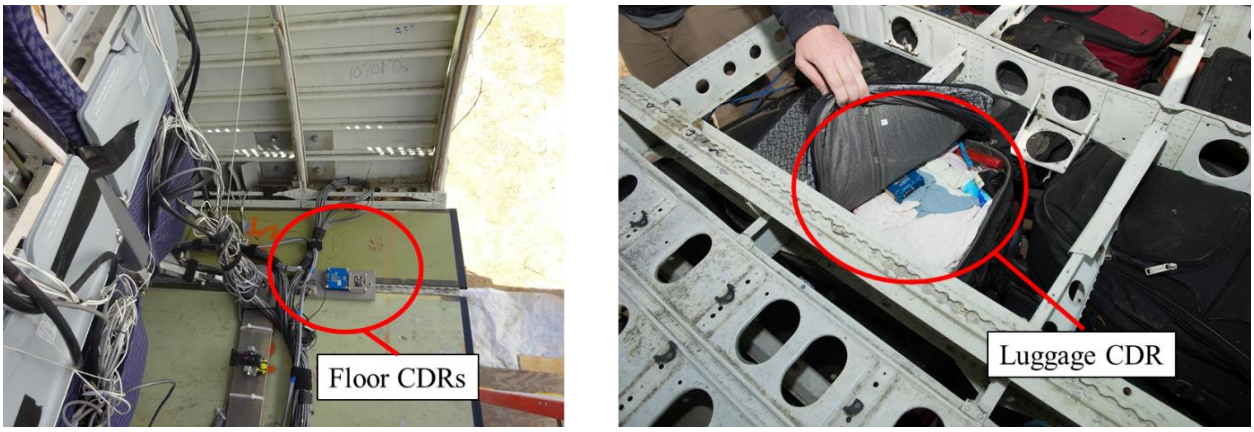

(a) (b)

Figure 2.12. Forward section CDRs—floor level (a) and luggage (b)

In the wingbox section test, it was expected that the test conditions would produce both vertical and horizontal accelerations. Therefore, accelerometers were positioned to measure horizontal accelerations on the seat leg bases and at the frame/floor junctions. Additional rotational rate sensors in the front and rear of the wingbox truss structure were used to measure the rotation rate of the test article during the impact. Like the forward section, a plate containing both blue and brown CDR, along with the data acquisition system (DAS) sensors measuring vertical and horizontal accelerations, were attached to the starboard window seat track. This provided a second data point to evaluate these measurement systems. Because there was no luggage compartment on the wingbox section, a blue CDR was placed at the base of the lower cavity. Figure 2.13 shows the CDRs in the wingbox section.

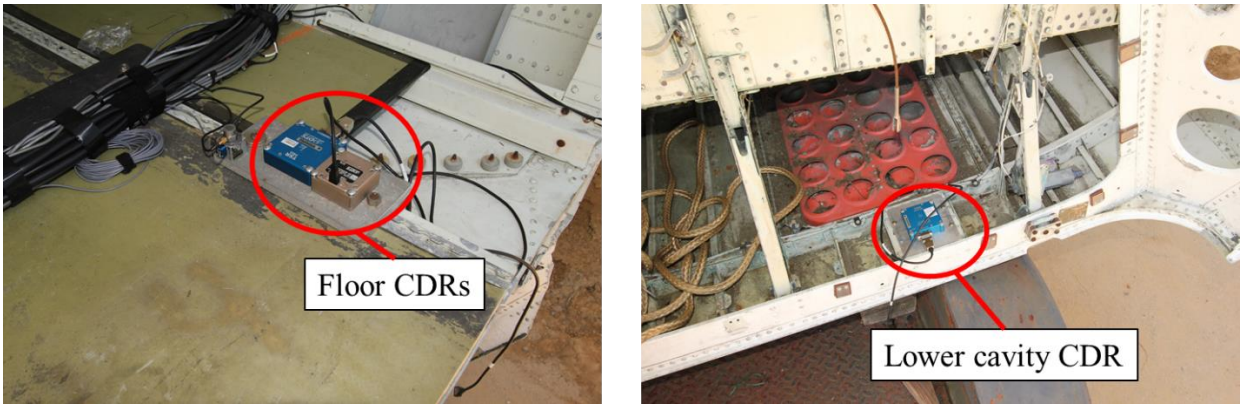

(a) (b)

Figure 2.13. Wingbox section CDRs—floor level (a) and lower cavity (b)

The majority of the airframe and occupant data were collected via the DAS, an onboard ruggedized data acquisition system. The DAS was on a pallet located at the rear port side of the test articles, mounted to the port side seat track rails. It consisted of three 64-channel data collection racks, battery, power distribution box, and time code generator mounted on a rigid aluminum plate. Data were collected at a sampling rate of 10 kHz and triggered via a start trigger initiated in the LandIR control room. Additionally, ATD 7 had its own internal DAS being evaluated for use in this and

future test series. For this ATD, a separate arming and triggering mechanism was used for data collection. It was also controlled from the LandIR control room. All the standalone CDRs for both tests were armed pre-test and triggered on reaching a predetermined acceleration level threshold at impact. All airframe and occupant data were filtered according to guidelines specified by SAE J-211 (SAE, 1995), unless noted.

External high-speed cameras were placed around the perimeter of the test area. Most of these cameras recorded the test events with a resolution of 2 megapixels (MP) at a speed of 1 kHz. There were two photogrammetric cameras used for full field Digital Image Correlation (DIC) (Littell, 2016). These cameras had a resolution of 4 MP and recorded at a speed of 500 Hz. The starboard side of each test article was painted with a black and white stochastic pattern for the acquisition of DIC results. The DIC results will be covered in a separate report. Two high-speed onboard cameras were mounted to the overhead hat rack bin ballast. These cameras viewed all the ATDs on the double or triple sides. Additional onboard high definition (HD) cameras were mounted at various locations of interest for each test article. For the forward section, camera locations included underfloor cargo area. For the wingbox section, camera locations included inside the subfloor wingbox truss structure and in the lower cavity below the wingbox truss structure near the bottom skin. Additional HD and ultra-high definition (4k) cameras were placed on the ground and perimeter of the test area. A series of photogrammetric yellow and black “bowtie” targets were applied to specific areas along the forward and port sides of the test articles to aid in determining the impact conditions during the tests.

The forward section test article weighed 4,465 lb. This weight included 814 lb. for the empty section, 922 lb. of underfloor luggage, 232 lb. of overhead hat rack bin ballast, and 2,496 lb. for the floors, ATDs, seats, and DAS. The CG was located at FS 6524, which was 1.3 in. forward of the geometrical center and 0.75 in. starboard of the geometrical center of the section. The vertical CG position was not measured. Figure 2.14 shows the fully instrumented section before the test.

Figure 2.14. Forward section test article

The wingbox section test article weighed 5,182 lb. This weight included 2,454 lb. for the empty section, 232 lb. of overhead hat rack bin ballast, and 2,496 lb. for the weight of the floors, ATDs, seats, and DAS. The CG was located 2.1 in. forward and 1.4 in. starboard of the geometrical center of the section. The vertical CG position was not measured. Figure 2.15 shows the fully instrumented section before the test.

Figure 2.15. Wingbox section test article

For each test, the test article was lifted into position using a combination of LandIR overhead cables. The test articles were lifted though four soft straps located near the four corners of each test article. In the forward section test, they were attached to locally reinforced attachments above the windows at approximately FS 5305 for the forward straps and at approximately FS 7305 for the aft straps. For the wingbox section test, the straps were attached to the original wing attachment fastener locations for the forward and aft lifting points used in the forward section test. The required nose down pitch in the wingbox section test was achieved using different vertical locations on the wing attachment fastener pattern. Test articles were released via a release hook operated by personnel in the LandIR control room.

The nominal impact velocities for both tests were expected to be 30 ft/s onto a bed of soil. The forward section was expected to impact at a nominal pitch angle of zero degrees, corresponding to a purely vertical flat impact. The wingbox section was intended to impact pitched at a 4-degree nose down angle as measured on the floor and onto a 10-degree forward sloping soil bed. The differences in the contact angle allowed for the rear portion of the wingbox section to rotate about the rear impact point, inducing a locally perceived forward velocity into the ATDs during the rotation. This resulted in a two-dimensional loading condition. Figure 2.16 shows the test articles at their respective drop positions just before release.

(a) (b)

Figure 2.16. Forward section (a) and wingbox section (b) at release position

3. FORWARD SECTION STRUCTURAL RESPONSE RESULTS

The forward section test occurred on March 23, 2017. The forward section impacted the soil surface at a velocity of 28.9 ft/s using data obtained through both the forward and port side photogrammetry bowtie targets. The photogrammetric data also showed the forward section with a 1.3-degree nose down pitch and 0.7-degree starboard downward roll at impact. A forward high-speed camera captured the fuselage horizontal deformation or "ovalization" of the test article at impact by measuring the change in distance between targets located on the port and starboard sides of FS 5305 during the impact. A time history of the ovalization of the fuselage and data locations are shown in Figure 3.1.

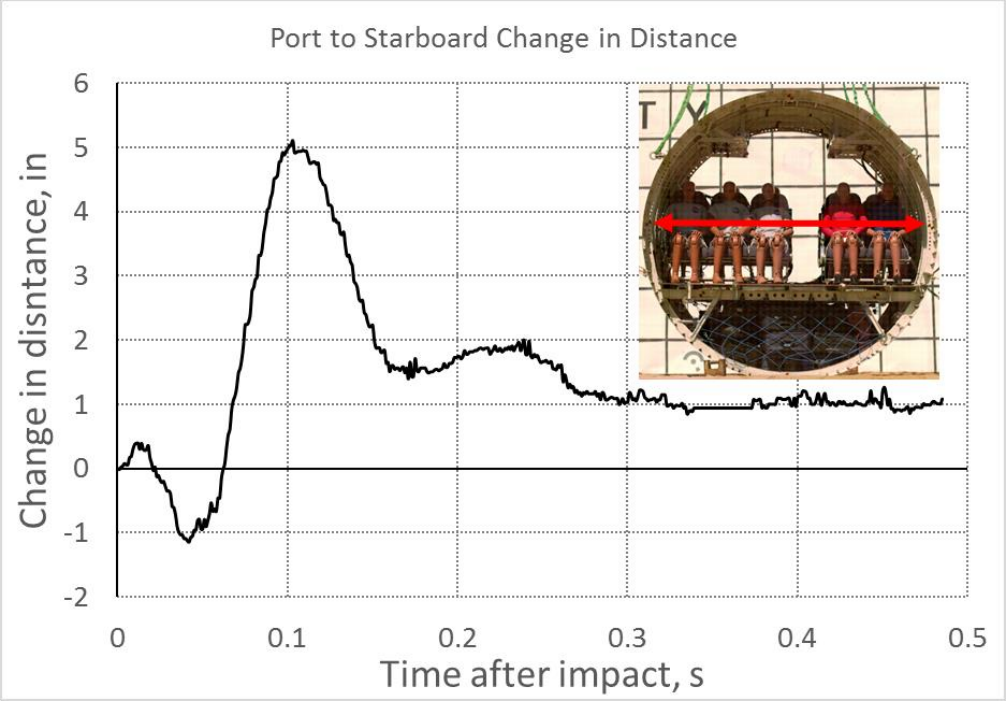

Figure 3.1. Forward section ovalization

The negative values shown before 0.06 s were caused by inward motion of the port and starboard targets, which indicated an initial vertical ovalization of the fuselage at impact. This vertical ovalization was caused by floor bending, which pulled the sidewalls of the fuselage inward. After the initial vertical ovalization, the sides of the fuselage deformed outward to a maximum value of 5.1 in at 0.103 s after impact. The late time history in Figure 3.1 showed that the fuselage sustained a permanent deformation of approximately 1 in. post-test. The test sequence as captured from the forward viewing high-speed camera is shown in Figure 3.2 with highlighted notable events. Note the initial floor bending in the upper right image.

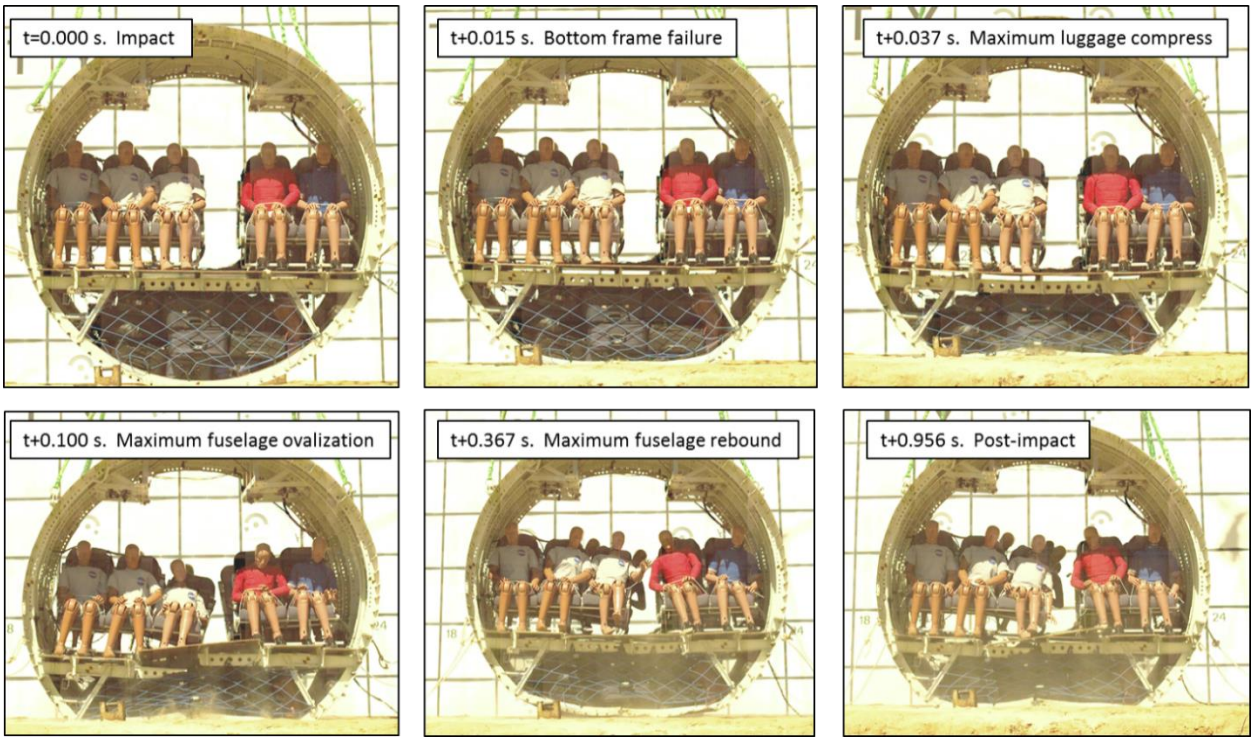

Figure 3.2. Sequence of events for forward section test

The upper left image shows the test article at impact where first ground contact was made. This time was also the datum time used for calculating the ovalization. The upper middle image shows the first visible failure in the test article, which occurred at FS 5305 at the bottom skin/soil impact location. The upper right image shows where the subfloor luggage had maximum compression. This time was noted because it affected both the airframe and ATD responses. The lower left image shows the fuselage at 0.100 s after impact, which was where maximum lateral ovalization occurred. This event was important due to its effect on the ATD response, described later in this section. The lower middle image shows the fuselage when it underwent a small rebound. Finally, the lower right image shows the last acquired frame of the high-speed camera almost one second after the impact event. This frame was beyond the time the major events occurred during the impact, although the onboard motion after the test did not stop until a full 2.5 seconds after impact. Between these two times, the fuselage gently rocked back and forth because of the dynamics in the still attached, but slack, lifting straps.

Crush displacement of the fuselage subfloor structure was next examined using the photogrammetric data acquired from the two targets placed on FS 5305 subfloor. These targets were placed directly on FS5305 outboard of the stanchions and equidistant between the stanchions and outboard seat rail. The vertical displacements of these two targets were tracked throughout the impact event and plotted in Figure 3.3.

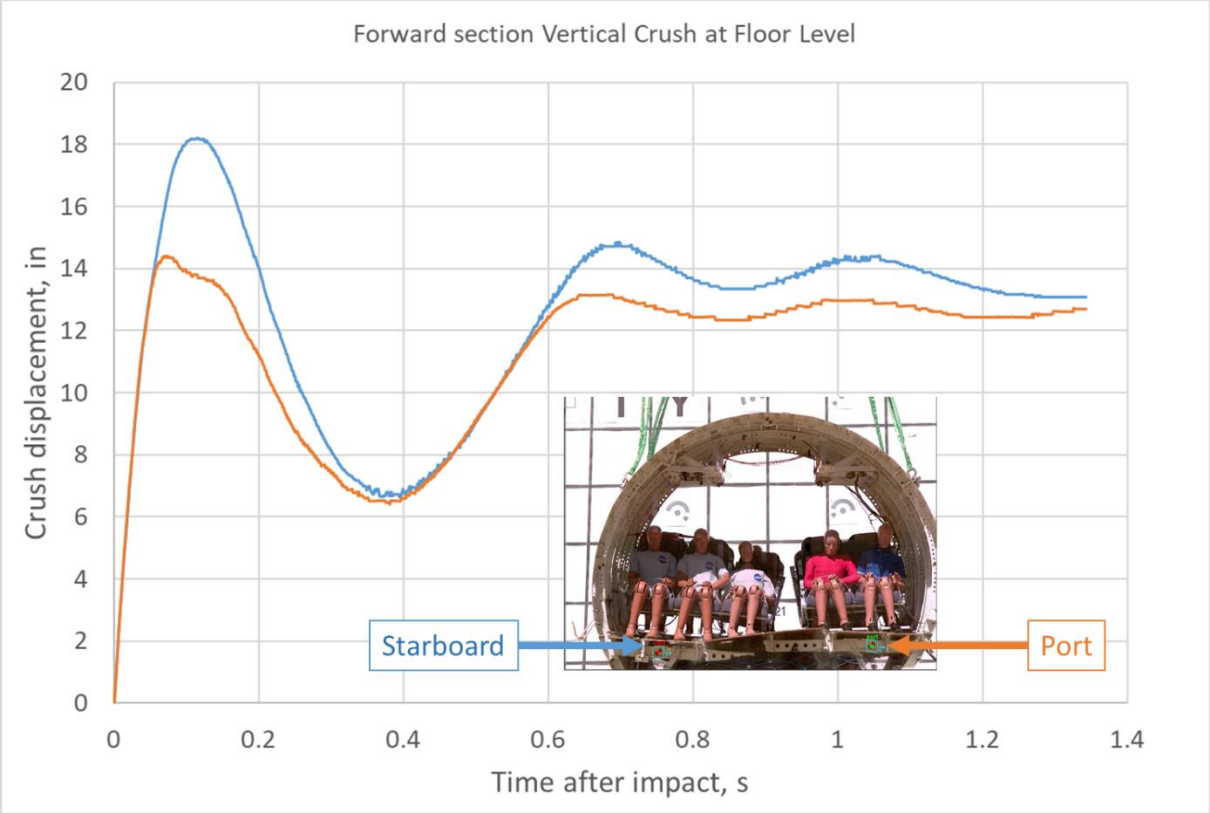

Figure 3.3. Forward section subfloor crush deformation

The two positions tracked in Figure 3.3 show an initial maximum crush displacement immediately after impact before rebounding at approximately 0.4 s. after impact. The initial crush displacement reached 18.2 inches for the starboard side and 14.4 inches on the port side. The difference is attributed to the failure of FS 5305 at approximately 0.1 s. after impact, causing the two sides to penetrate the underfloor luggage unevenly and independently. After the rebound at 0.4 s., the data begins to converge as the two sides settle into a post-impact deformed state. The convergence begins at approximately 0.7 s. Although the two sides did not reach identical crush values, they were in an equilibrium state. The data at the end of the tracking shows a starboard side total displacement of 13.1 inches and a port side displacement of 12.7 inches. The average subfloor crush was 12.9 inches.

Post-test inspections of the airframe showed failures in all of the floor support lateral stiffeners. However, they were not uniform and did not have a discernable pattern. A diagram highlighting complete failures of floor support stiffeners, indicated by a red dash, is shown in Figure 3.4. The numbered items only show where a stiffener completely separated in half. Much of the other floor support structure also buckled, bent, and partially tore but, for clarity, are not included in Figure 3.4.

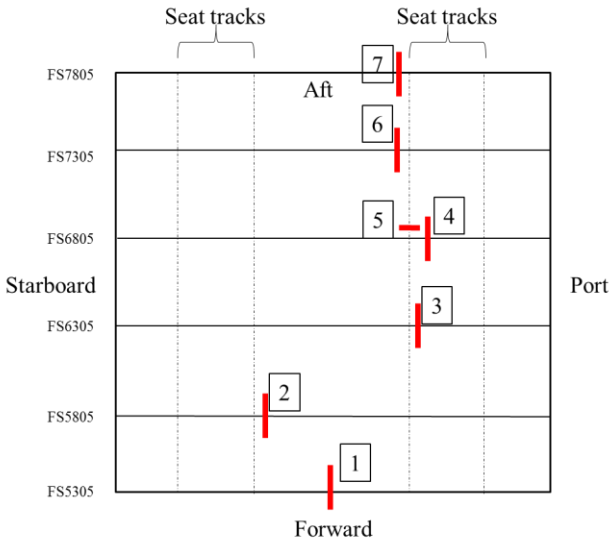

Figure 3.4. Failure locations in the floor support structure and seat tracks

The failure pattern in the floor support structure at first appeared to be random and did not correlate to either a seating position or place of overall stiffness discontinuity leading to high stress concentration (i.e. the cargo door). On closer inspection it was determined that many of the specific failure locations were caused by the luggage interaction with the specific floor stiffener locations throughout the impact. The onboard and ground cameras captured some of the exterior failures but could not cover all of the interior failures due to blockage of the failure from the luggage, floor, or both. Post-test inspections provided guidance in failure initiation and propagation for the interior members. The first interior failure inspected post-test was at location #2. A picture of the failure in location #2 from Figure 3.4 is shown in Figure 3.5. This failure was only visible once the floor and seats were removed.

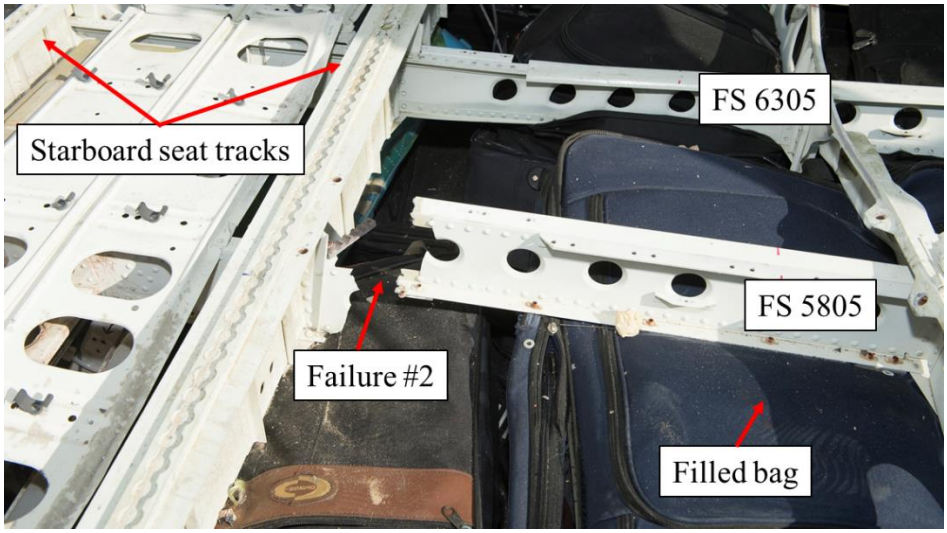

Figure 3.5. Failure of FS 5805 at location #2

A detailed inspection at failure location #2 revealed a probable cause. Inboard of the starboard seat tracks, there was a fully filled dark blue bag located at the top of the underfloor luggage stack centered underneath FS 5805. To the left of this bag was a black-with-brown-striped bag, stacked at a lower height. The difference in height was either from the black and brown striped bag being partially filled or simply from being stacked on top of slightly shorter bags. At impact and during the maximum luggage rebound, the upward bearing of only the blue bag against FS 5805, the highest in the stack, caused the failure to occur near the seat track junction. This was an area of differing localized stiffness. After the failure, the bag itself provided a surface for which FS 5805 to rest. Additionally, it is important to note that the blue bag was centered along FS 5805 and did not extend under either FS 5305, which is not shown, or FS 6305, which is shown in Figure 3.5. If this bag extended into the area underneath FS 6305, FS 6305 might have failed in a similar way. Failures #3, #4, and #5 also occurred adjacent to each other and are shown next in Figure 3.6.

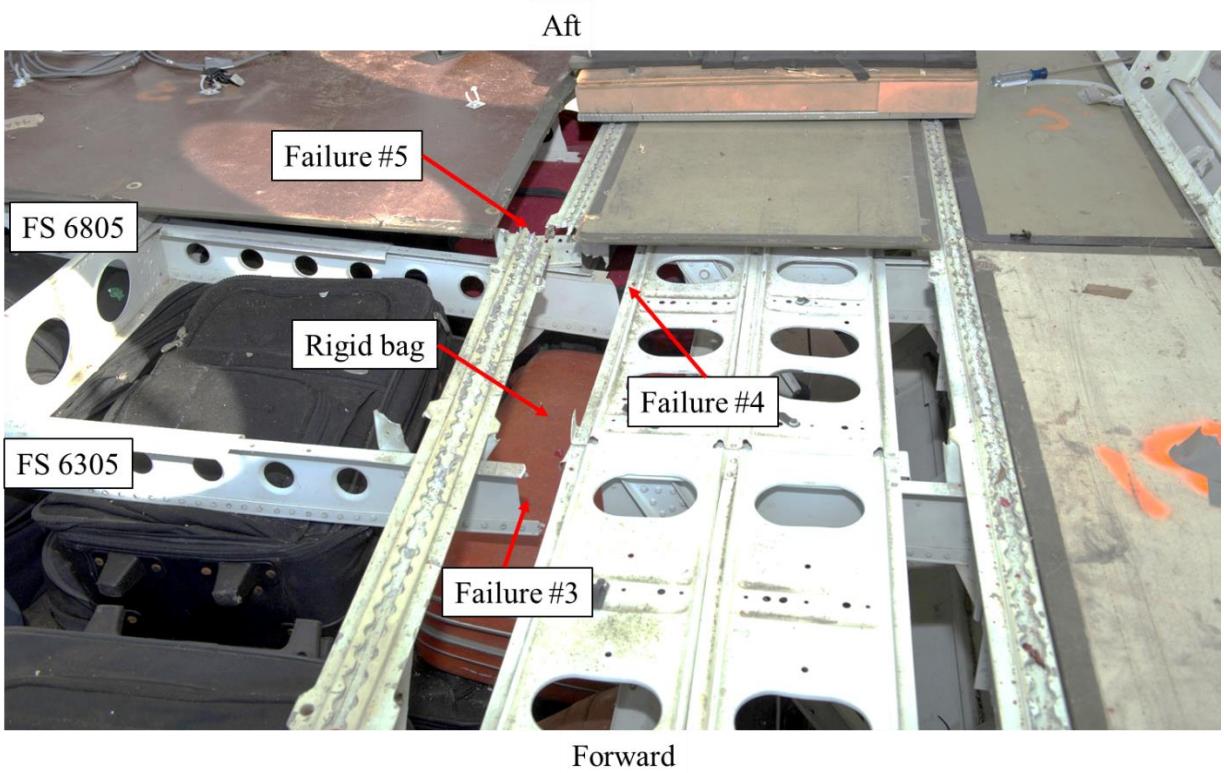

Figure 3.6. Failure locations #3, #4, and #5

The root cause of the failure in FS 6305 (failure #3), FS 6805 (failure #4), and the inboard port seat track (failure #5) was attributed to the rigid brown bag underneath this area of the floor. The bag was unintentionally centered between FS 6305 and FS 6805 slightly outboard of the port inner seat track position. The impact and, more importantly, the rebound of this bag against these areas caused failures in these locations. The failures at FS 6305 and FS 6805 occurred at almost identical locations, immediately outboard of the inner seat track and positioned directly over the bag. The reason for the failure of the seat track (failure #5) was not as straightforward. However, it is suspected that a combination of the failure of the two adjacent frame sections (failures #3 and #4), the added loading from the rear row double seat inboard leg attachment directly over FS 6805, and

the added localized rigidity in the adjacent rear structure due to the DAS pallet attachment just aft of the seat track failure location.

Similarly, failures in locations #6 and #7 occurred due to the luggage impacting the lateral support stiffeners inboard of the seat tracks near the rear of the fuselage section. The failures occurred inboard of the seat tracks due to the presence of the DAS pallet, which effectively caused the area to be rigid between the seat tracks at its attachments.

After the underfloor failures were thoroughly documented and photographed, the underfloor luggage was carefully removed to aid in the examination of the lower cavity and bottom skin areas of the test article. There were several failures in the lower section that were commonly seen in previous testing and in-service accident data. The first was the failure of the frame sections along the centerline at the very base of the fuselage. These failures were tensile failures at the inner end of the frame section caused by the ovalization of the test article in the bottom skin region. The second prominent failure was the crushing of the frame sections immediately inboard of the lower-stanchion-to-subfloor attachment locations. This crush was caused both by subfloor deformation from the under-floor luggage loading along with the outward motion of the frames during ovalization. These two failures are shown in Figure 3.7.

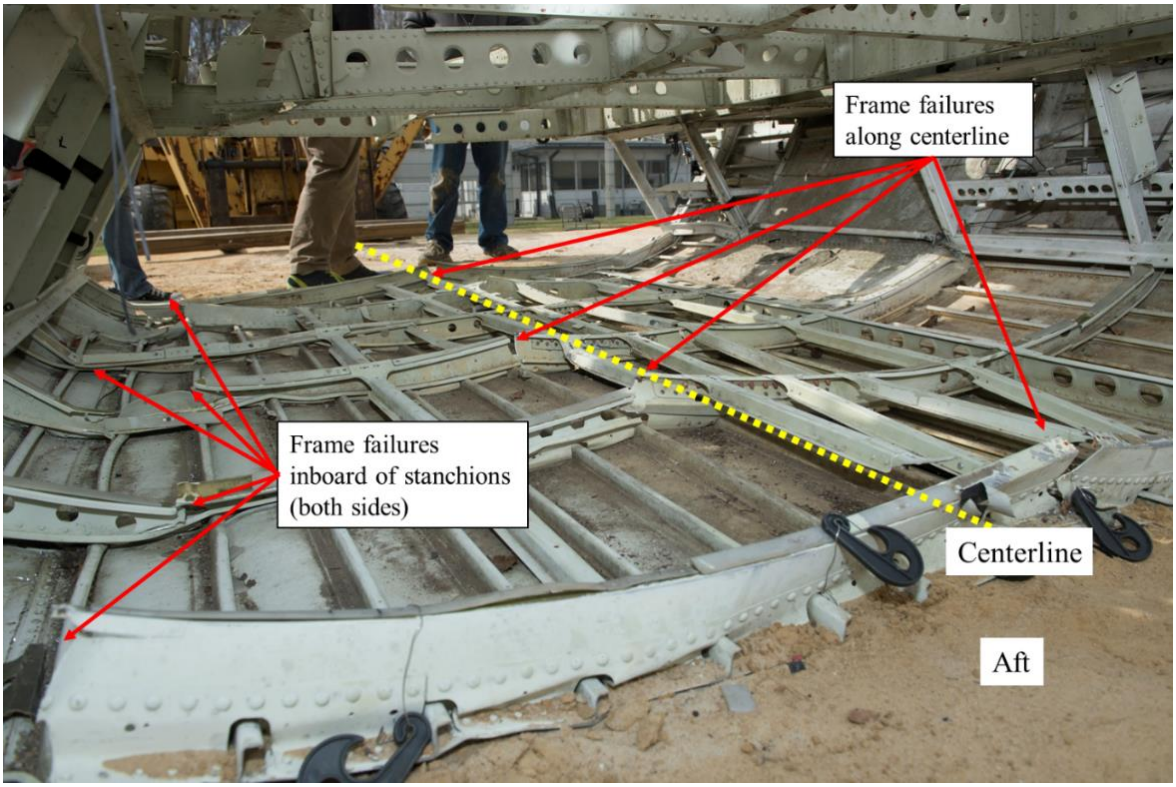

Figure 3.7. Lower cavity failure locations

The upper portion of the fuselage section above the floor level was undamaged. The overhead ballast attachment points did not show signs of deformation or fastener tear out, and the ceiling was intact. The major deformations and failures in the test occurred for the major items of mass such as where the luggage and seats interacted with the lower support.

The acceleration data at the starboard floor/frame junction locations were examined to determine airframe response, see Figure 3.8. The data showed the fuselage section exhibited a nearly uniform response, which was the first indication that the test was a (nearly) pure vertical drop. In addition, the fuselage, at least for the starboard side at the floor/frame junctions, reacted uniformly during the impact event. The different colored data series show the response at different FS locations on the section, which are defined by starred locations in the legend in Figure 3.8.

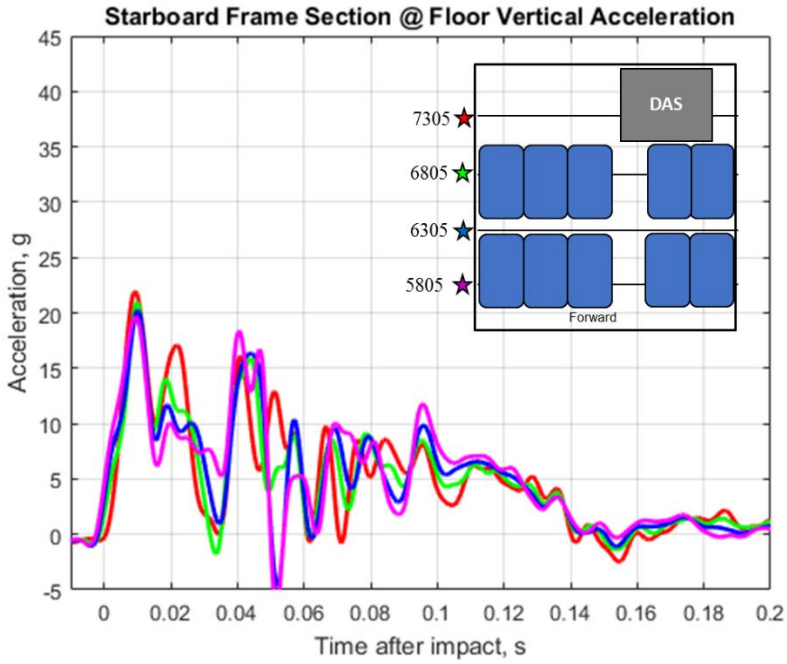

Figure 3.8. Starboard floor/frame accelerations from forward section test

The accelerations reached initial peak values ranging between 19.7 g to 21.9 g, depending on location. This occurred approximately 0.010 s after initial ground contact. A large valley occurred at 0.033 s after impact, which was close to when the change in the fuselage ovalization measurement shown in Figure 3.1. This was also the same approximate time there was maximum luggage compression, shown in Figure 3.2. The acceleration had oscillatory motion through the major portion of the impact event. The overall shape of the acceleration data can be approximated as an acute trapezoid with a rise time of 0.015 s, a plateau until 0.120 s, and a fall time of 0.031 s. Average accelerations were computed using the plateau region starting at 0.015 s and ending at 0.120 s. The average values of 7.2 g, 6.8 g, 6.8 g, and 6.9 g were obtained for FS 5805, FS 6305, FS 6805, and FS 7305, respectively.

Acceleration results for the port side of the airframe are shown in Figure 3.9. Although there was a large amount of noise in the accelerometer located at FS 6805, the general shape in the data matched the starboard side results. The cause of the noise is currently unknown and was only seen at this location. Thus, the large oscillations produced between 0.035 s and 0.070 s were based on a type of localized motion and did not represent the test article. Additionally, the sensor at FS 6305 failed and did not record data, which might have been due to the localized phenomena recorded in the sensor at FS 6805. If local oscillations are neglected, the acceleration time histories for all three locations resemble a trapezoid in shape with a duration of approximately 0.086 s for FS 7305 and

FS 6805, and a duration of 0.103 s for FS 5805. The end points of the plateau were measured between the times in which the acceleration response crossed the zero-g mark after impact. The initial peak accelerations were 19.4 g, 25.3 g, and 26.4 g when examining the response from FS 7335, FS 6805 and FS 5805 respectively. The peak increased going from aft to forward in the test article, primarily due to the slight pitch down impact condition from the photogrammetric results. When averaging the acceleration values between the end points in the plateau, values of 9.8 g, 9.7 g, and 9.6 g were obtained for FS 5805, FS 6805, and FS 7305, respectively. These numbers are slightly higher than the starboard side accelerations and might be caused by the small amount of starboard roll at impact.

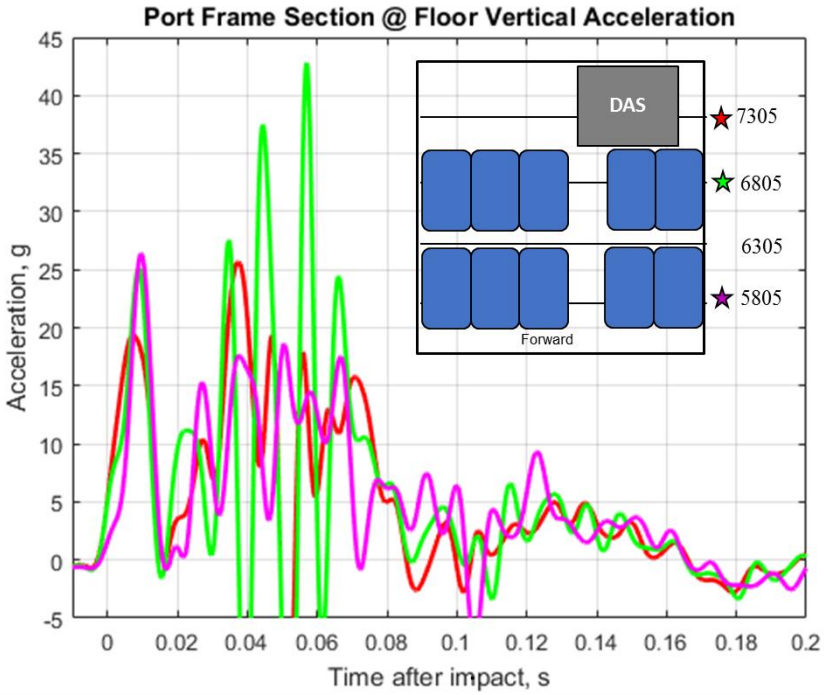

Figure 3.9. Port floor/frame accelerations from forward section test

Seat accelerations were measured on the floor of the base of each seat leg for both the double and triple seats. The seat base accelerations were crucial to determine the exact loading characteristics being input into the seated ATDs during the impact. The rear seat base accelerations are first plotted in Figure 3.10. Note that the color in the figure corresponds to the seat leg. For example, the red curve is the response on the triple seat, measured at the outboard seat leg position. The blue curve represents the response on the double seat, measured at the inboard set leg position.

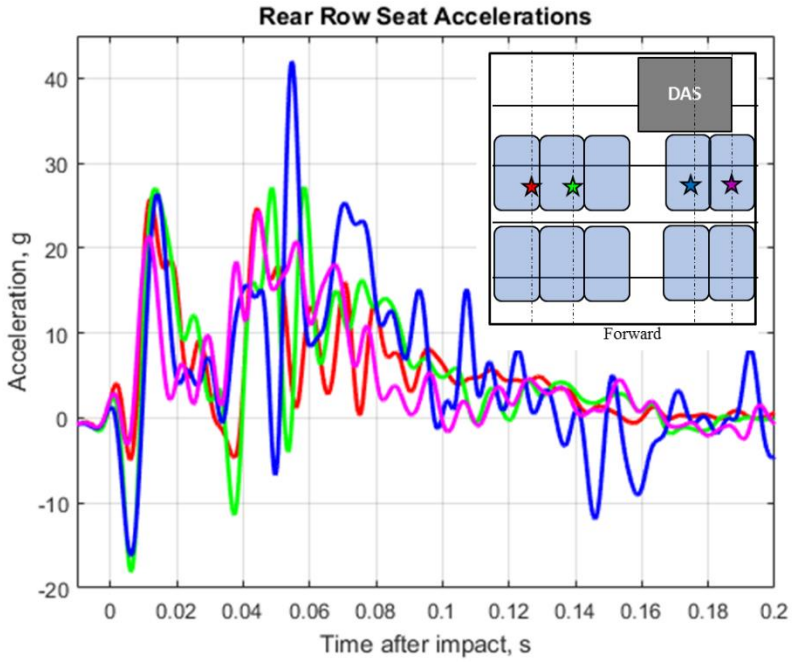

Figure 3.10. Rear row seat accelerations from forward section test

An initial negative peak acceleration at 0.006 s occurred in all seat leg positions immediately after test article impact. The negative peaks, which reached a maximum of 18.0 g at the triple inboard seat leg position, were caused by the floor bending at impact. All seat leg accelerations then measured a positive peak between 21.4 g and 27.0 g and between 0.012 s and 0.014 s after initial test article impact. When examining the acceleration pulses in their entirety, all seat leg positions exhibited similar characteristics in shape, which was approximated as triangular with vertex around the 0.060 s mark. The total pulse durations were similar for all seat leg positions, lasting between 0.134 s at the double inboard seat leg position to 0.166 s at the triple inboard seat leg position. The forward row seat accelerations are plotted in Figure 3.11.

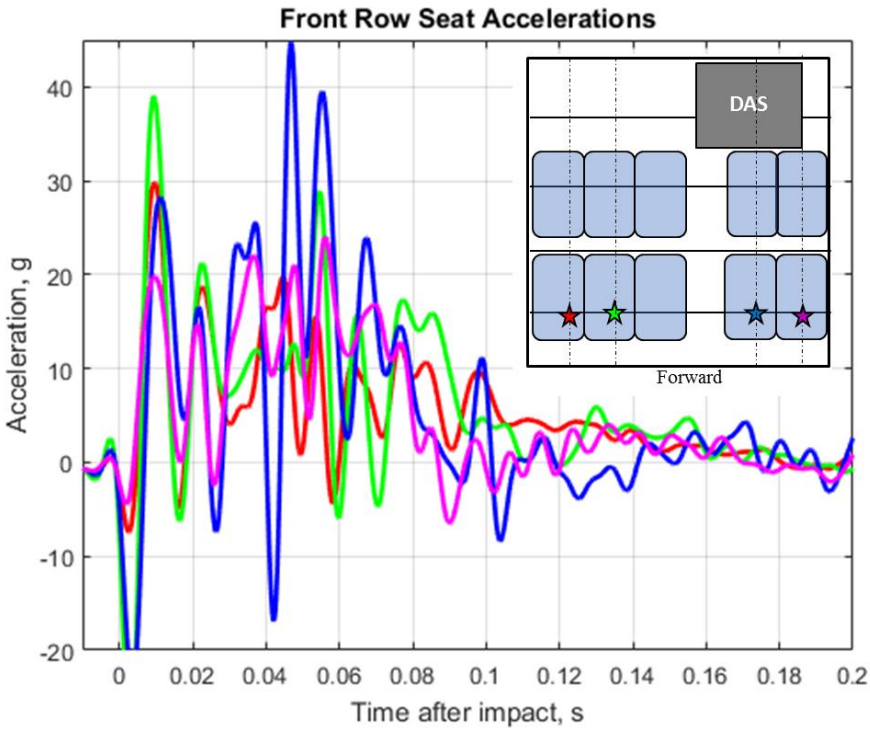

Figure 3.11. Front row seat accelerations from forward section test

The front row seat leg responses exhibited the same general trends as the rear seat leg response results. The same initial negative peak in acceleration occurred at an earlier time in the response approximately 0.003 s after initial impact. The peaks were highest on the inboard locations and consistent with the largest floor deformations on the middle of the fuselage. The downward pitch angle was determined to cause the time differences. The downward pitch angle caused the forward portion of the test article, corresponding to the forward row of seats, to impact first. The responses then showed positive peak accelerations between 19.8 g at the double outboard location to 39.0 g at the triple inboard location. Large oscillations occurred in the double inboard seat leg location between 0.040 s and 0.072 s after impact. The generalized shape for all responses were either triangular or trapezoidal, depending on how the data were interpreted. If assuming a trapezoid, the average acceleration values ranged from 9.7 g at the triple outboard seat leg location to 15.5 g at the double inboard seat leg location. This was determined from examining the data starting after the initial dip at 0.007 s through 0.080 s. For either shape, the durations ranged between 0.087 s at the double outboard set leg location to almost 0.180 s at the triple outboard seat leg location.

Hat rack bin ballast attachment accelerations were next examined for the determination of the response in the overhead structures. Two out of the four attachment locations were instrumented on both the port and starboard sides. These locations, along with the corresponding acceleration data appear in Figure 3.12.

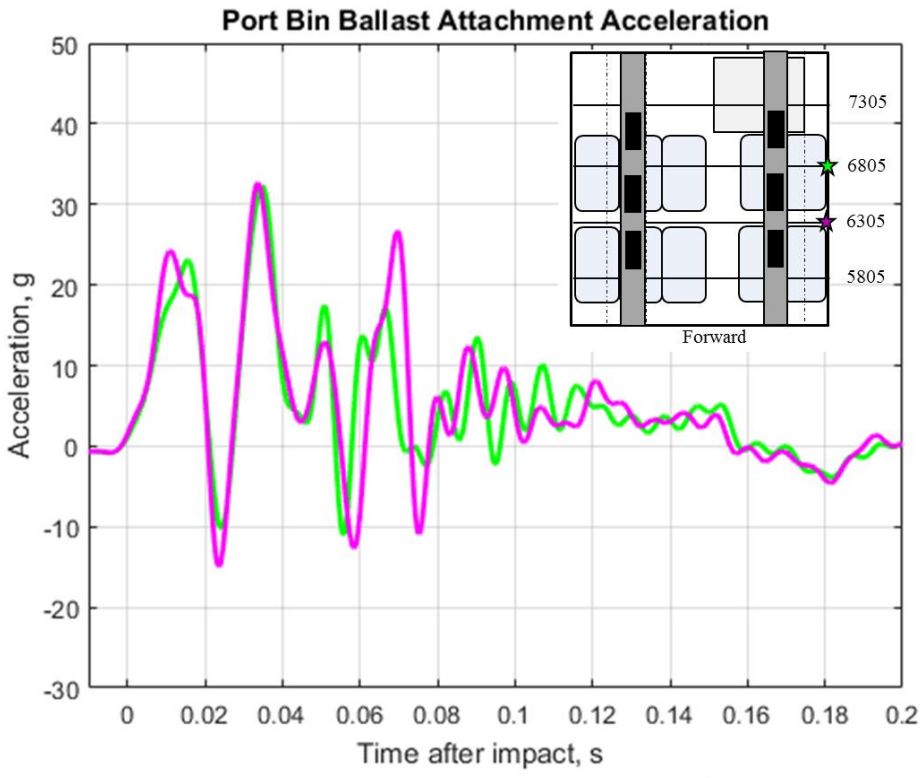

Figure 3.12. Port side bin attachment accelerations from forward section test

Large oscillations occurred in the hat rack bin ballast attachment locations, both at FS 6305 and FS 6805. There was no discernable shape for the first 0.080 s due to the oscillatory nature of the signals., The signals were similar for both locations. The oscillations tapered off to a sustained average acceleration of 4.1 g and 4.3 g for FS 6305 and FS 6805 respectively, between 0.080 s and 0.160 s after impact. This was at the end of the loading in the attachment locations. The response was due to the large amount of mass cantilevered off these attachment points and the structural response of the test article, which did not deform at the upper attachment locations. The accelerations on two of the three bin masses are plotted in Figure 3.13.

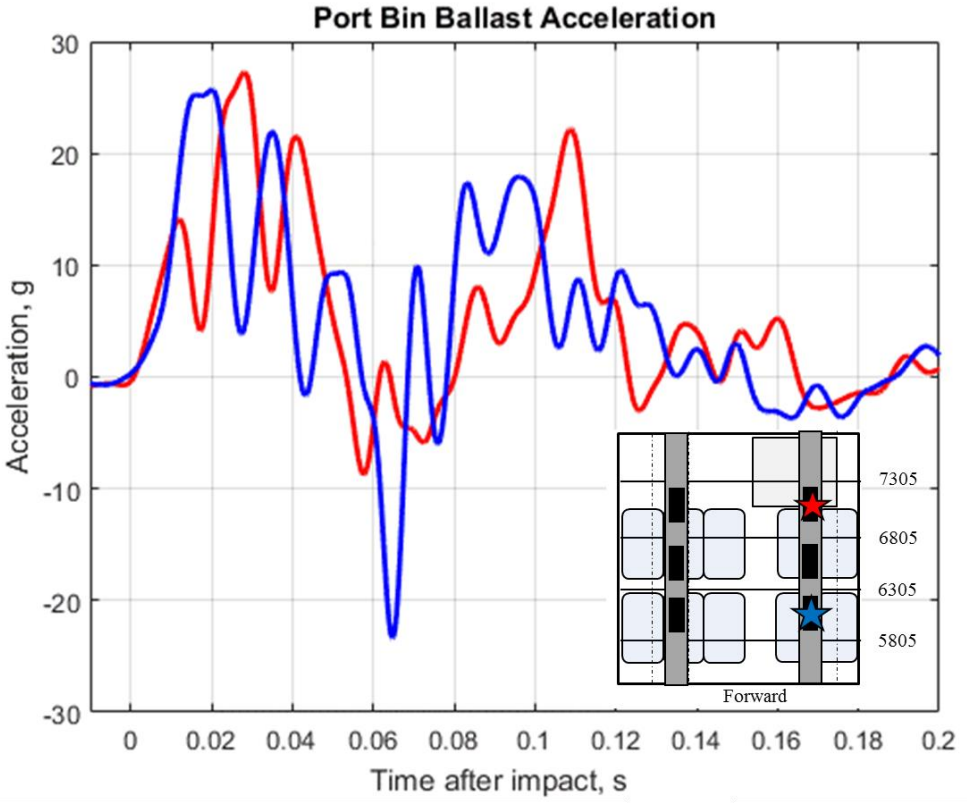

Figure 3.13. Port side bin ballast accelerations from forward section test

The rear ballast mass between FS 6805 and 7305 is plotted in red. The forward ballast mass between FS 5805 and 6305 is plotted in blue in Figure 3.13. Similar responses were measured for both masses that included an initial peak acceleration reaching 25.7 g in the forward ballast and 27.1 g in the rear. The forward ballast produced a large negative acceleration afterward, reaching 23.1 g. The rear ballast reached a minimum of only 8.6 g. Both curves had a noticeable sinusoidal shape with an overall frequency of approximately 11 Hz. The sinusoidal response was caused by the mass movement off the cantilever attachment points. The measured peak accelerations multiplied by the total overhead mass had a maximum dynamic load of 3,143.6 lb., which acted on the bin attachment points at their respective frame section locations. Both the starboard side bin ballast and bin attachment accelerations were of similar magnitude, shape, and duration in nature.

The results from the CDRs were examined and compared to measurements obtained by the onboard DAS system. The CDRs, along with an adjacent DAS accelerometer, were rigidly mounted to the starboard outer seat rail at FS 7305. The location of the CDRs, along with the data obtained, appears in Figure 3.14.

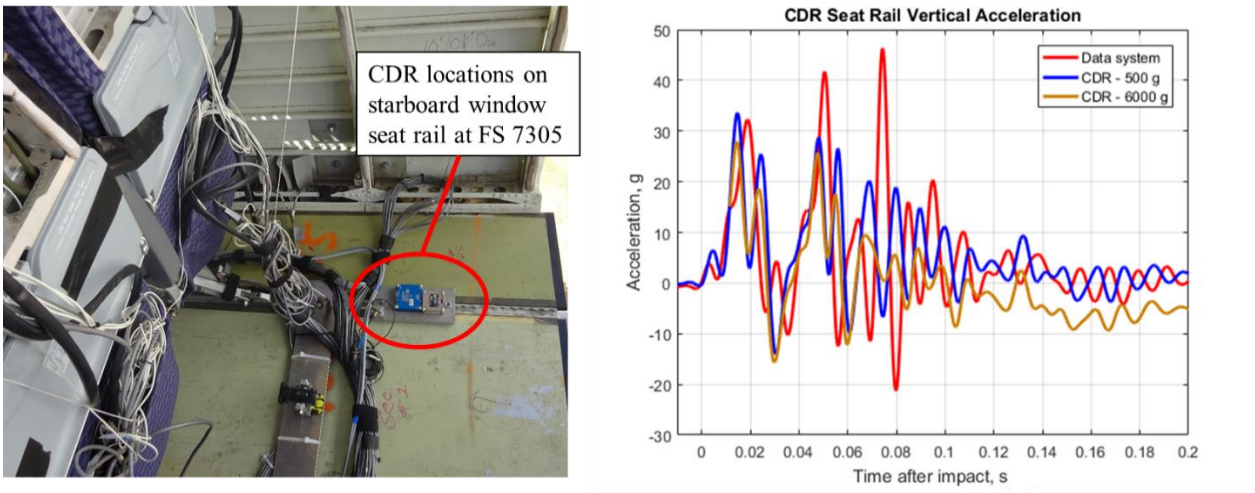

Figure 3.14. CDR seat rail acceleration for forward section test

The red curve in Figure 3.14 is the accelerometer attached to the DAS. The blue curve is the blue 500-g CDR, and the brown curve is the brown 6000-g CDR. All curves were in good agreement. The DAS data exhibited a first peak value of 32.2 g approximately 0.019 s after initial impact. The blue CDR exhibited a peak of 33.5 g, and the brown CDR exhibited a peak of 27.8 g. Because the CDRs were not time-synchronized with the DAS or camera systems, analysis on the timing could not be completed. Also, the curves were arbitrarily time shifted using manual offsets, so timing information was not heavily scrutinized. Where possible, the DAS timing information was used to identify important event markers. After the initial peak value, all three curves showed a localized minimum in the acceleration at 0.030 s and showed a second peak at approximately 0.051 s. All three curves decreased until the zero-g mark was reached, which occurred sometime after 0.100 s. The brown CDR initially showed a small offset from the blue CDR and the DAS as indicated by the first peak value, but settled out to an approximate negative 6-g offset after 0.100 s. The 6-g offset was 0.1% of the brown CDR's full-scale range and was in the same range as the sensitivity in the sensor itself. The range on the brown CDR was simply too high to accurately capture the data at these comparatively low levels, which is an important point to note. The blue CDR, however, performed well as indicated by its pulse peak values, duration, and general shape that matched the DAS data very well.

Finally, with confidence gained from the results of the blue CDR data, the data from the luggage CDR were examined. As noted previously with regard to the failure initiation and propagation, the luggage played a large role in the overall structural response of the test article. The compression and rebound of the luggage at impact interacted with the lower floor structure and created a distinct failure pattern in the seat track and floor supports. After the luggage was removed from the fuselage lower cavity post-test, the CDR located in one of the bags was removed and the recorded data were downloaded. The vertical acceleration data are plotted in Figure 3.15.

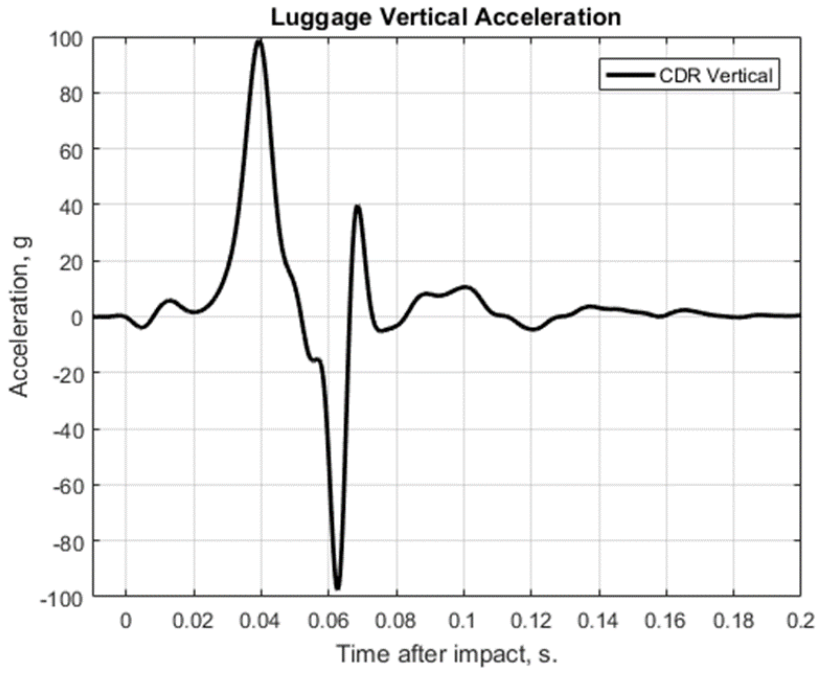

Figure 3.15. Forward section luggage vertical acceleration

The CDR measured two distinct peaks in the luggage response: the first at 0.040 s after impact and the second (in the negative direction) at 0.063 s after impact. These two events were the result of the luggage interaction with the soil (event #1) and the luggage rebound into the floor support lateral stiffeners (event #2). Three images were taken from the camera focused on the rear portion of the forward section. This camera viewed the bag containing the CDR, so correlation of the event data and video was possible. Figure 3.16 shows the image series of the luggage response using the two peak times identified from Figure 3.15. The bag containing the CDR is circled.

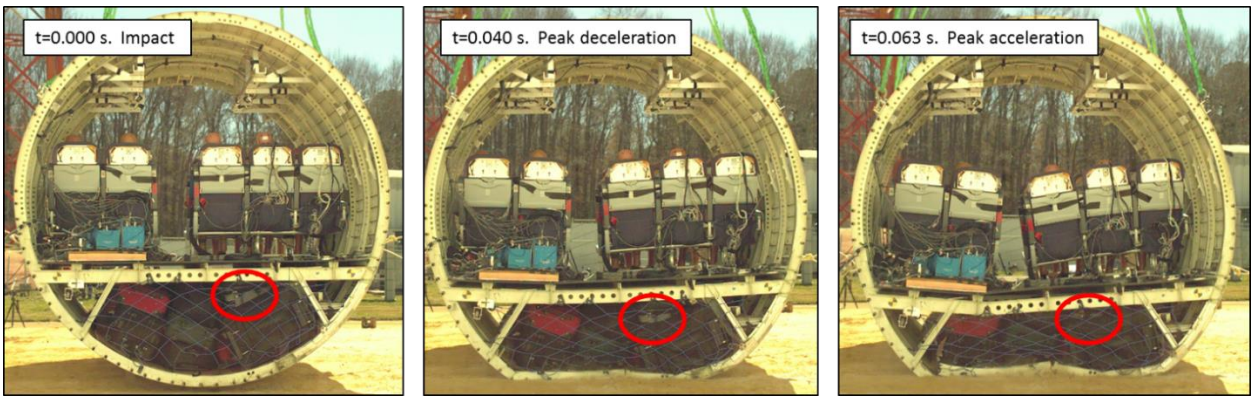

Figure 3.16. Luggage response image series

The first positive acceleration peak of 98 g shown in the data was the maximum deceleration due to the compression of the luggage, including the bag containing the CDR at impact. The high spike at 0.040 s resembles a compaction portion of a response curve from typical materials that exhibit compaction such as foams or honeycombs. This timing also agreed within a few milliseconds to

the image series obtained from of the forward view of the section, as shown the top right image in Figure 3.2. The second acceleration, shown as a negative 96.6 g value in Figure 3.15, was caused by the luggage rebound after maximum compression. This acted as a bearing surface for the floor support lateral stiffeners to react against as they continued downward through the impact event. This was also likely around when the failures occurred in the floor support lateral stiffeners.

The luggage response was considered such an important part of the test that additional component level tests on the luggage were done for the acquisition of luggage material properties. These tests are described in Section 4.

Soil measurements were taken around the impact site. The soil used for testing is known as Gantry Unwashed Sand, which is a silty sand (SM) using the Unified Soil Classification System (Thomas, et al., 2008). The sand was made into a 2-ft tall horizontal surface at the impact site. The strength and stiffness properties of the soil were measured approximately 1 hour before the test occurred. The soil moisture content was sampled at three locations. An average of 11.4% was measured at the time of the test. The California Bearing Ratio (CBR) (ASTM Standard D1883, 2016) was also measured and is shown in Figure 3.17.

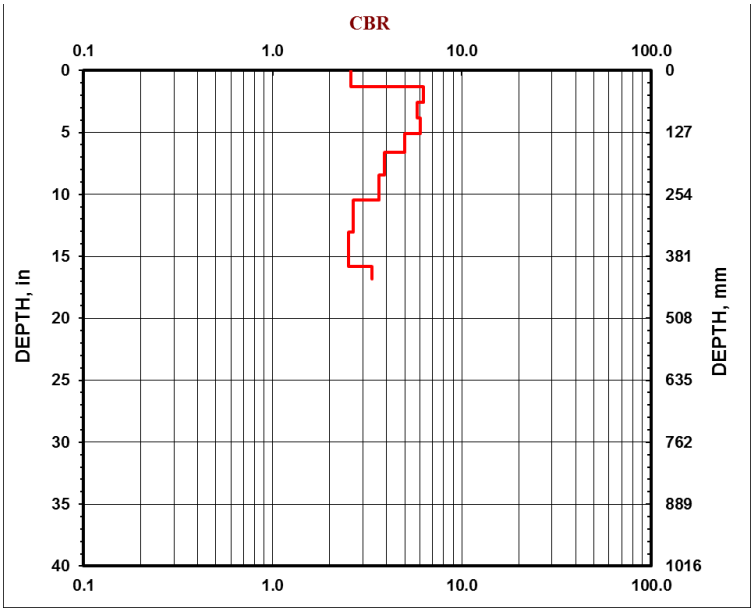

Figure 3.17. CBR for soil in forward section test

The CBR can be considered a measure of the stiffness as a function of the depth of the soil. There was initially a large jump from the top surface going to approximately 2 in down into the soil, which was the difference between the top layer of loose soil and the initial compacted layer underneath. From there, the stiffness steadily decreased until a depth of 15 in. was reached. Afterward, the soil began to stiffen, as evidenced by the curve moving to the right in Figure 3.17. However, the readings were stopped at this depth and no further analysis completed because this depth was well below the indentation made by the test article.

The soil indentation was measured once the test article was removed from the test area. Because most of the deformation was in the fuselage itself, a large indentation was not made in the soil.

Only ripples in the soil were created from the stringers located on the bottom skin. Indentations ranging from 0.25 in. to approximately 1.5 in. were measured at locations around the impact site. As shown in the CBR measurements, at this depth the soil showed a jump in stiffness. Consequently, the deformations were primarily contained to the outermost layer of loose soil. Figure 3.18 shows the impact area with the outline of the fuselage footprint highlighted.

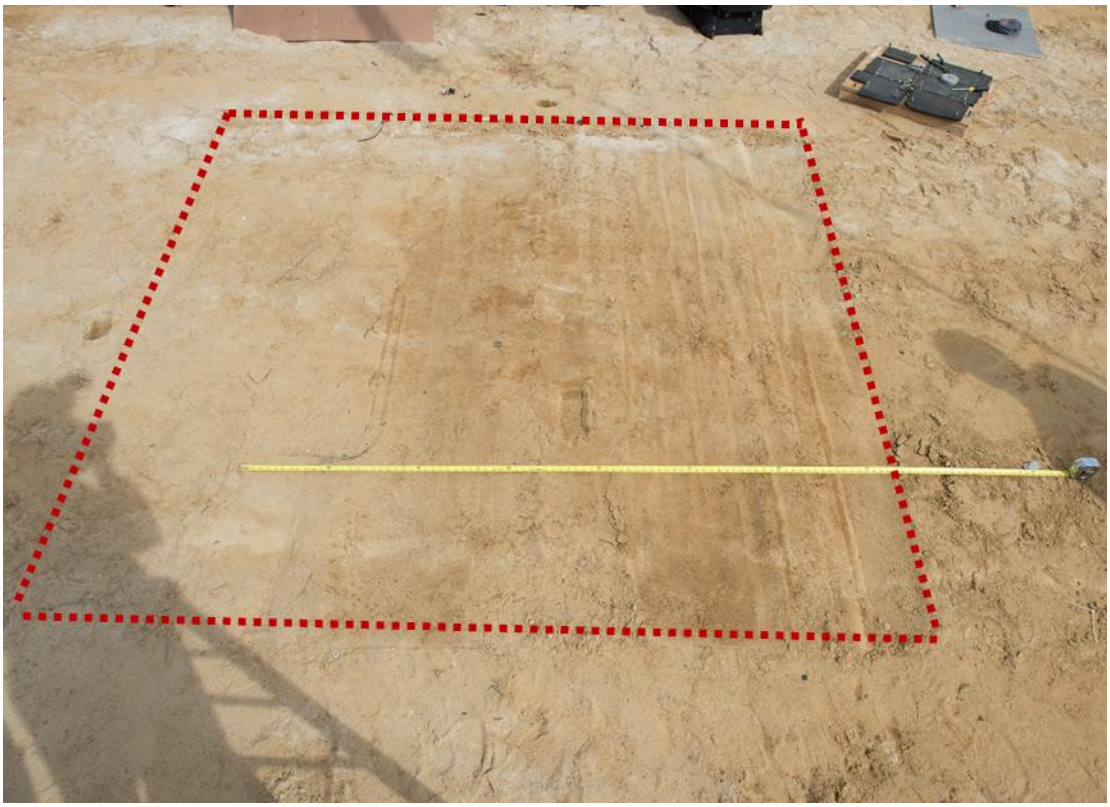

Figure 3.18. Forward section soil indentation results with test article outline

After examining the airframe deformation and responses, responses of the occupants were evaluated to determine the magnitude of loads and likelihood of injury. Figure 3.19 shows the front row of occupants post-test. The ATD seated in seat 8 was leaning into the aisle, restricting any potential egress. The ATDs seated in seats 7 and 9 were also leaning toward the aisle. The outboard ATDs seated in seats 6 and 10 were upright. The inward lean in most ATDs was due to the fuselage floor supports failing, primarily inboard of the lower stanchions. This caused the weight of the ATDs and seats to sag onto the underfloor luggage.

Figure 3.19. Forward section front row ATDs (Seats 6 through 10)

A view of the rear row ATDs appears in a pieced together composite view in Figure 3.20. A composite view was only available for the rear row ATDs because the section needed to be partially disassembled to examine the rear row in detail. In the rear row, the post-test ATD positions were similar to the front row. ATD 3 was leaning into the aisle, almost contacting ATD 4. The large amount of deformation in seat 3 was also noticeable, which included the headrest separating from the seat frame. The 95th percentile ATD 2 also showed a lean toward the center. However, ATDs 1 and 4 remained upright and ATD 5 showed an outward lean toward the outside of the test article.

Figure 3.20. Forward section rear row ATDs (Seats 1 through 5)

The ATD data were examined and determined the probability of injury. The occupant lumbar data Figure 3.21 shows the time histories on the left and the peak value measured on the right.

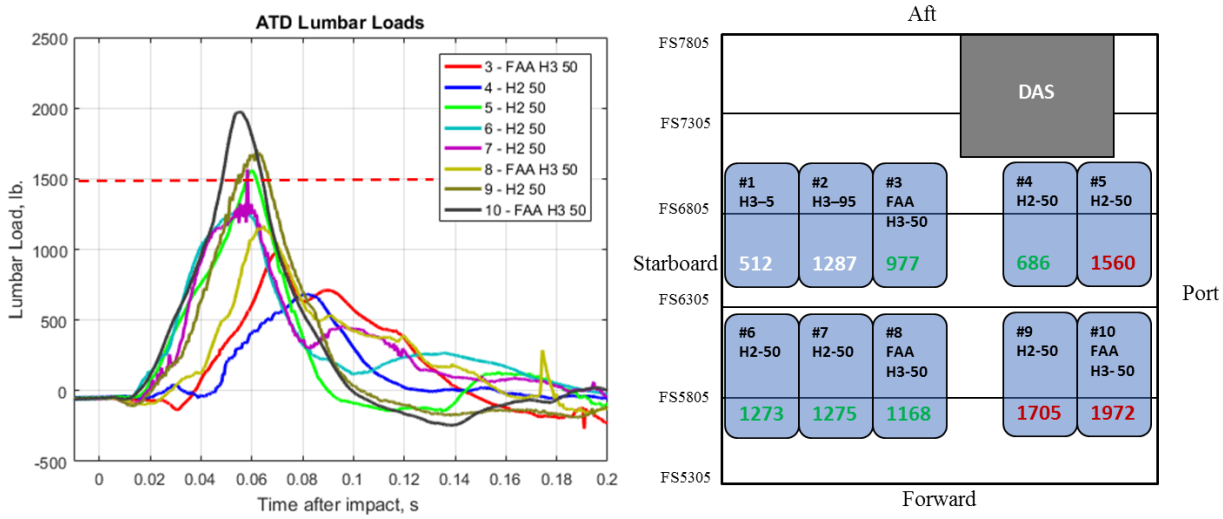

(a) (b)

Figure 3.21. Forward section ATD lumbar load time history (a) and highlighted peak values (b)

The time histories of the ATD lumbar loads fell into two distinct shapes for the eight ATDs plotted in Figure 3.21. ATDs 1 and 2 are not plotted on the chart, and the peak value is included in the illustration for comparative purposes only. These two ATDs were included in the test to obtain data points for non-typical sized ATDs. They were not evaluated for injury because there are no current lumbar load injury criteria for these ATD sizes. The 50th percentile ATDs experienced environments that produced lumbar loads both above and below the 1,500 lb. limit as specified by (FAA, 14 CFR § 25.562, 1998). This is indicated by the red dashed line in Figure 3.21 on the left.

There were three ATDs that exhibited lower peak values and a longer pulse duration. ATDs 3, 4, and 8 measured the lowest peak values. The load time history from ATD 4 differed from the others possibly because of the failures in the floor supports located underneath ATD 4. This resulted in an inadequate surface in which to react the occupant loads. This ATD (and its seat) sank further into the floor than any other of the ATDs in the test, which was confirmed by examining the onboard video.

ATDs 3 and 8 exhibited marginally lower lumbar load results due to their position in the cantilevered portion of the triple seat configuration. Because there was no reaction device, such as a seat leg or other surface, these loads were lower on average, and the deformations in the horizontal seat pan support tubes were greater than for the other seats.

Head accelerations were examined for the determination of head injury. The ATDs seated in the rear row are plotted on the left, and the ATDs seated in the front row are plotted on the right in Figure 3.22.

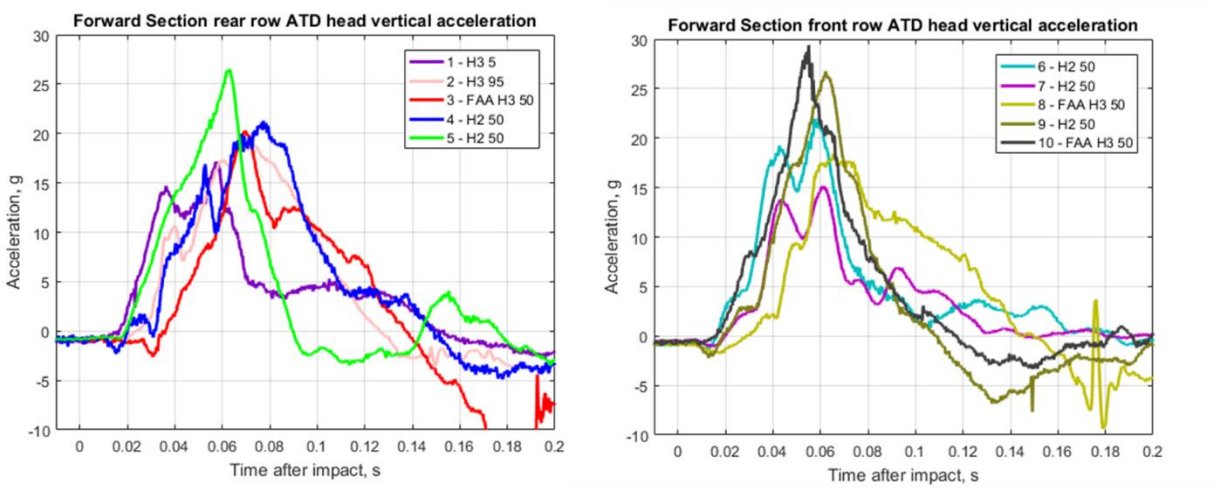

(a) (b)

Figure 3.22. Forward section ATD head vertical acceleration—rear row (a) and front row (b)

The head vertical acceleration peak values measured by the ATDs were less than 30 g for all ATDs and for some less than 20 g. The maximum head acceleration was recorded in ATD 10 at 28.5 g, and the second highest acceleration in ATD 5 at 26.4 g. Both of these seats were the window seat in the double seat configuration. The acceleration in ATD 5 had the shortest duration at 0.090 s and exhibited a triangular pulse shape. All other pulse durations ranged from 0.109 s to 0.183 s. The head accelerations from both the vertical and horizontal directions were used in computations of Head Injury Criteria (HIC). HIC, as defined in the Federal Motor Vehicle Safety Standards (FMVSS) No. 208 (U.S Dept. of Transportation, 2020), is a way of evaluating acceleration data from an ATD during a crash test and equating it to the probability of skull fracture. The equation is:

$$HIC = \max\left(\frac{1}{t_2 - t_1}\int_{t_1}^{t_2} a(t) * dt\right)^{2.5} * (t_2 - t_1)$$

The variable a(t) is the root-sum-square of the head acceleration time history obtained from the test, which has moving end points of t_1 and t_2. This report uses a 36 millisecond-moving window and a limit of 1000 for a 50th percentile ATD. The HIC value of 1000 gives the probability of a skull fracture (Abbreviated Injury Scale ≥ 2) at 48% (Schmitt, et al., 2004) and is used as a limit in (FAA, 14 CFR § 25.562, 1998). Table 3.1 shows the results for all of the ATDs in the test.

Table 3.1. Forward section test ATD HIC values

ATD Type - Size	Seat #	HIC Value
H3 – 5	1	28.3*
H3 – 95	2	58.5*
FAA H3 – 50	3	39.4
H2 – 50	4	59.1
H2 – 50	5	55.9
H2 – 50	6	45.6
H2 – 50	7	15.9
FAA H3 – 50	8	34.6
H2 – 50	9	68.4
FAA H3 - 50	10	60.5
**For reference only*		

The lack of a high spike in the acceleration time histories indicated that the ATD heads did not strike the seat back or other surfaces. Consequently, all HIC values were well below the established limits with a low probability of injury. Finally, pelvic acceleration was examined on each of the ATDs. Figure 3.23 shows the results from the rear row ATDs on the left and front row ATDs on the right.

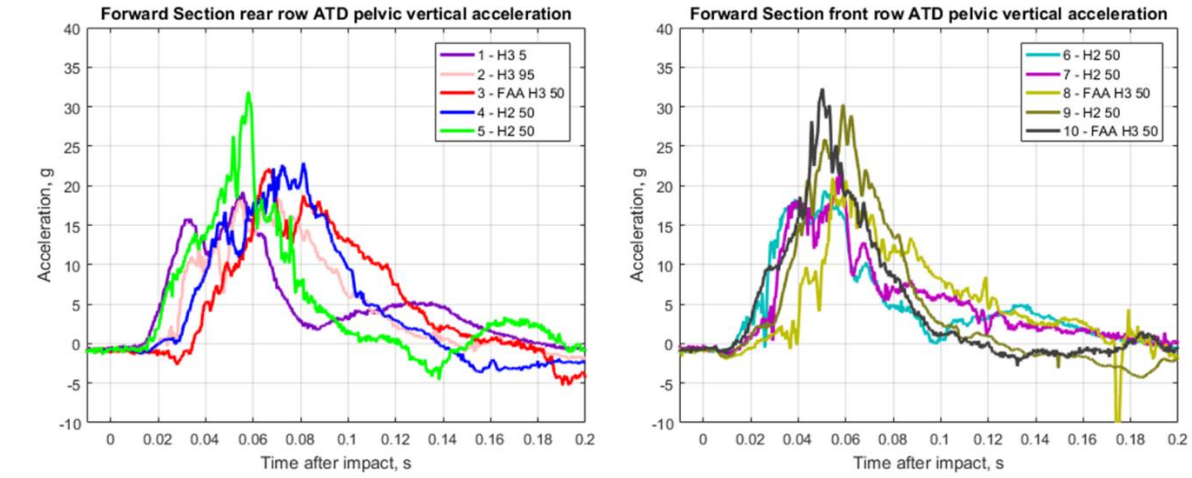

(a) (b)

Figure 3.23. Forward section ATD pelvic vertical acceleration—rear row (a) and front row (b)

The pelvic responses, although not required for specific injury criteria in 14 CFR § 25.562, were examined as a check to the lumbar loading. This was because the physical locations in which the pelvic measurements were taken were close to the load cell used for the lumbar load measurement. Ideally, the two shapes of the curves should be similar, and trends resulting from higher and lower

magnitudes of peak values should be in general agreement. The highest pelvic accelerations for the rear row were recorded in ATD 5. The peak acceleration of 31.6 g occurred 0.58 s after impact and before the peak values from the rest of the seats in the rear row. Similarly, ATD 1 had the fastest onset rate of acceleration with an initial localized peak of 15.7 g occurring 0.032 s after impact. ATD 3 had the slowest onset rate with its acceleration reaching a peak of 21.9 g at 0.068 s after impact. Similarly, the front row ATD pelvic data were compared to the lumbar load data. ATDs 9 and 10 showed the largest magnitude of accelerations of 29.8 g and 32.3 g. These were the two highest values of pelvic acceleration for all the ATDs and corresponded to the two highest values of lumbar load.

After removing the ATDs, the seats were examined for permanent deformation. Both the front and rear triple seats are shown in Figure 3.24. Both seats exhibited similar post-test deformation shapes.

(a) (b)

Figure 3.24. Post-test triple seats—rear (a) and front (b)

The maximum seat deformation occurred on seats 3 and 8, which are both overhung. - Both seat frame rear tubes deformed to a maximum of approximately 4.5 in. vertically when measured at the aisle armrest location. The luggage guard buckled at the aisle seat rear attachment location, which lead to a crack in the material. The middle and window seats and seat leg structure were undamaged for both of the triple seats. The double seats appeared undamaged when conducting post-test inspections. Figure 3.25 shows the underside of the triple seat in the rear row, noting the bent rear seat frame tube and cracked luggage guard.

Figure 3.25. Post-test rear triple aisle seat deformation (seat 3)

4. COMPONENT LEVEL LUGGAGE TEST RESULTS

The luggage interaction with the floor was previously identified as an item of interest for determining fuselage response. To acquire material property data on the luggage, two component-level dynamic impact tests were performed only on the luggage components. Two tests were conducted using a 50-ft drop tower located at LandIR. Each test consisted of filled bags, picked at random out of a set of old luggage, that were randomly stacked at a configuration of two bags wide and three bags tall at the base of a drop tower. For each test, both cloth and rigid style bags were included and stacked at random to achieve a "global" average luggage response. The bags were compressed via an instrumented 620 lb. falling mass guided down the tower by a series of rails. Figure 4.1 shows the test setup for the luggage compression test.

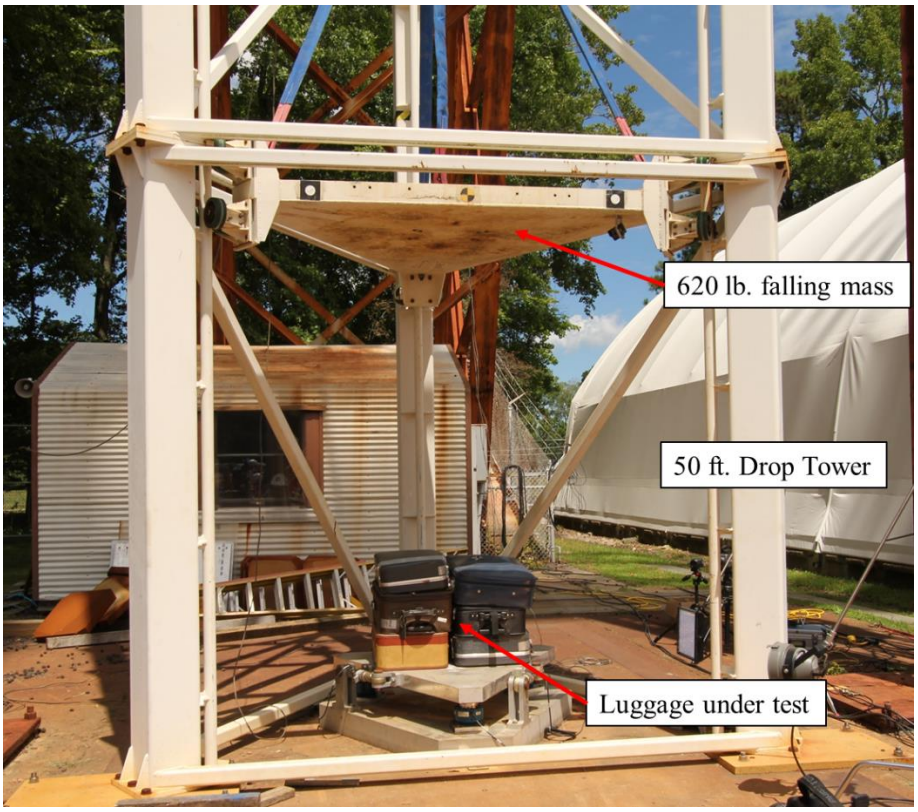

Figure 4.1. Luggage component test setup

The first test was conducted with the impact velocity of the falling mass at 18 ft/s. The total luggage weight was 128.6 lb. A pre- and post-test picture is shown in Figure 4.2. Post-test inspections revealed that the impact shattered the rigid bags but left the soft bags mostly intact. The items inside were not examined for damage.

(a) (b)

Figure 4.2. Luggage test 1 pre-test (a) and post-test (b)

The acceleration versus time response as measured on the instrumented falling mass is shown in Figure 4.3. All luggage acceleration data from both tests were filtered at a Butterworth 4-pole low-

pass filter with cutoff frequency of 300 Hz. The acceleration response can be interpreted as either a triangle or trapezoid with a duration of 0.127 s. The acceleration reached a peak of 13.3 g, which occurred 0.060 s after impact. If assuming a trapezoid shape, the average acceleration on the plateau was 11.9 g when using the initial and final peaks at 0.060 s and 0.078 s as endpoints.

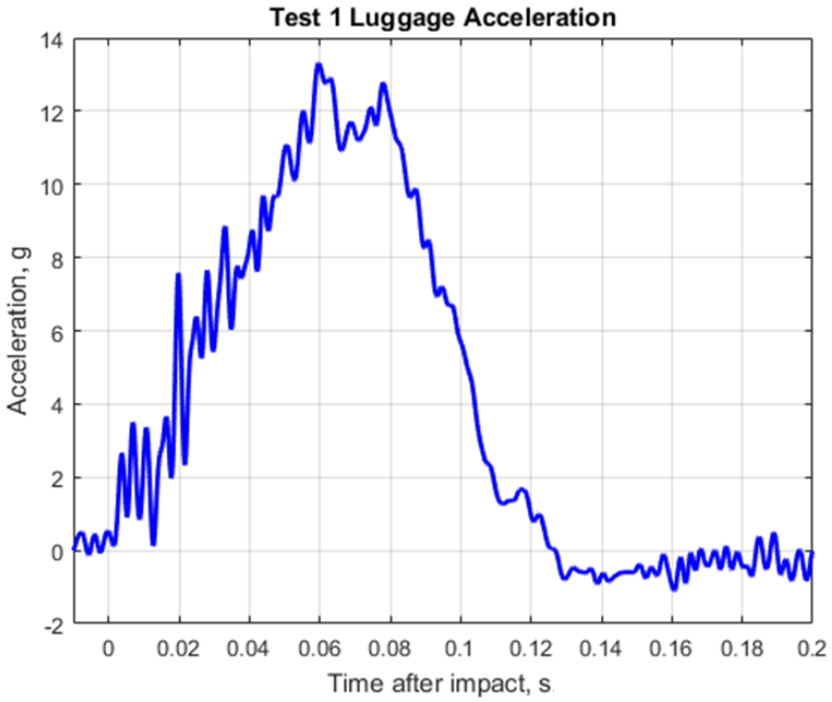

Figure 4.3. Test 1 luggage acceleration

The acceleration data were then converted into crush stress versus relative deflection data to achieve a result like a material property stiffness curve. Individual bag dimensions were measured and then averaged to obtain an average bag size. This average was used in the bag footprint area calculations, with the footprint being twice the average measured width multiplied by the average length. The total height was found by multiplying the average bag height times three. The acceleration was double integrated and then divided by the total height to achieve relative deflection. The acceleration was multiplied by the drop mass weight and then divided by the footprint area to achieve crush stress. The data for test 1 is plotted in Figure 4.4.

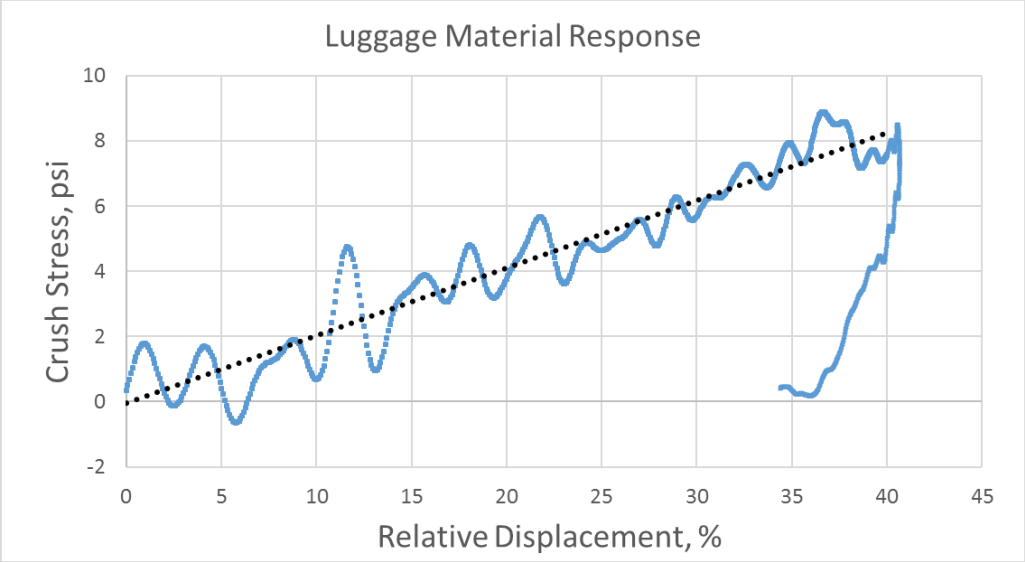

Figure 4.4. Test 1 luggage response

A linear trend line was fit to the loading portion of the curve to smooth out the large amounts of oscillations and noise leading up to approximately 40%. The slope of this trend line was 20.7 psi. There was no plateau in the curve, presumably because of the lack of residual available kinetic energy needed to further crush the bags after the initial loading region of the curve was reached. Test 2 added additional kinetic energy into the luggage to reach the sustained crush region portion of the crush curve.

Test 2 was conducted like test 1. Six different bags were used, but the methodology in developing the crush curve was identical. In test 2, the impact velocity was 24.5 ft/s, which was 85% more of the initial kinetic energy at impact. The total luggage weight for test 2 was 147.4 lb. Figure 4.5 shows a pre- and post-test picture of test 2.

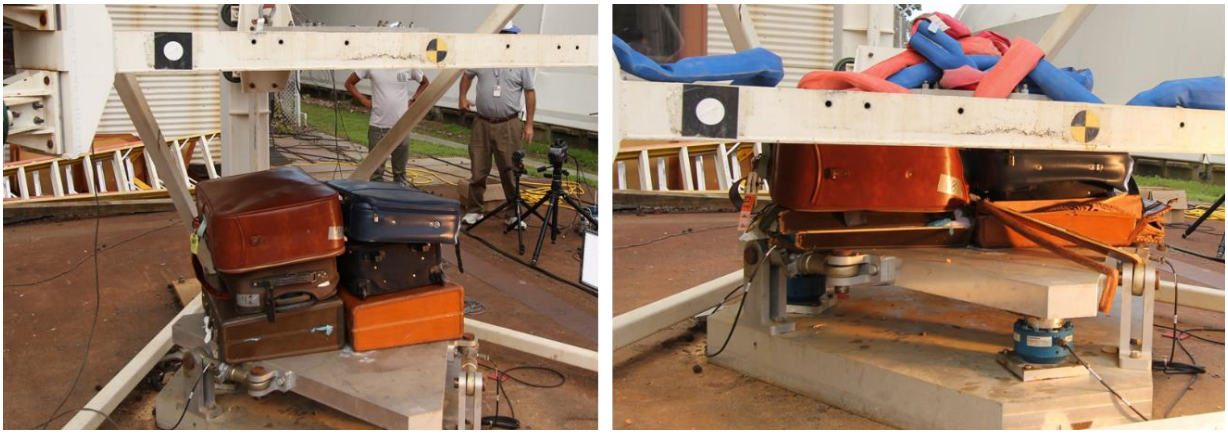

(a) (b)

Figure 4.5. Luggage test 2 pre-test (a) and post-test (b)

The acceleration data are shown in Figure 4.6. There were large amounts of oscillations in the data through the first 0.020 s of contact, which was the amount of time taken for the impact mass to fully engage the tops of different sized bags. Once fully engaged, the acceleration averaged 10.6 g between 0.020 s and 0.070 s. The final acceleration reached a peak value of 19.4 g at 0.079 s after initial contact, which was when maximum crush displacement of the impact mass occurred. After the maximum acceleration, the impact mass rebounded and the luggage unloaded.

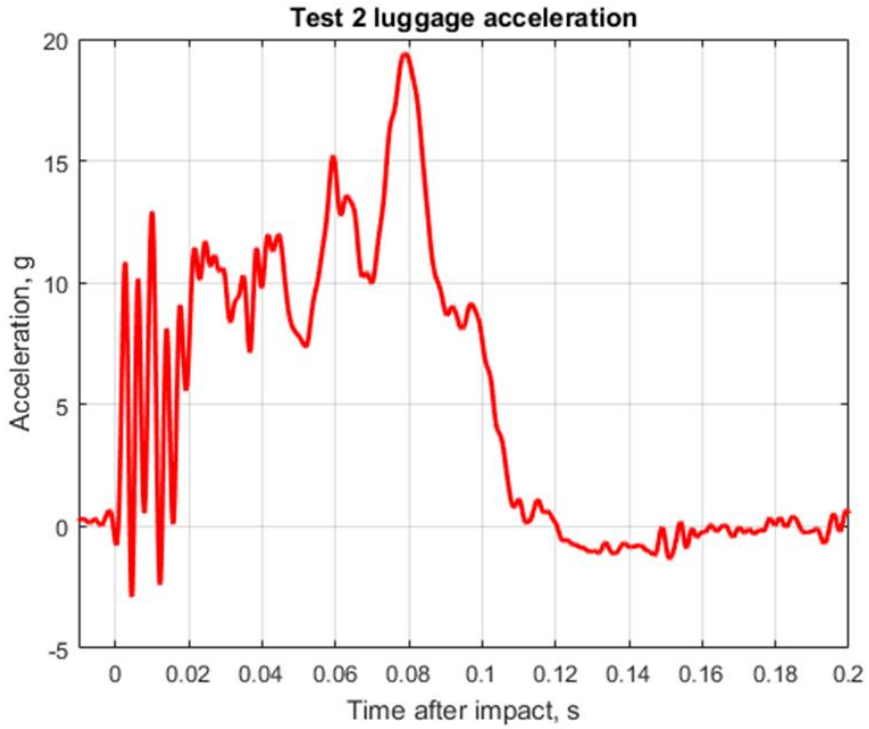

Figure 4.6. Test 2 luggage acceleration

The crush stress versus relative displacement is plotted in Figure 4.7. An exact curve fit was difficult to determine when examining the data. This was due to large oscillations at the beginning of the data along with the potential for a beginning of material compaction toward the end. One interpretation resolved a linear slope of 8.0 psi up until 22.7% of relative displacement, a plateau of 5.55 psi until 48.8% of relative displacement, and compaction until 57.1% of relative displacement. A second interpretation characterized the response as an elastic-plastic material behavior, starting with a linear slope of 8.0 psi until 22.7% relative displacement and then a linear slope of 9.1 psi in the plastic regime. There are additional valid interpretations.

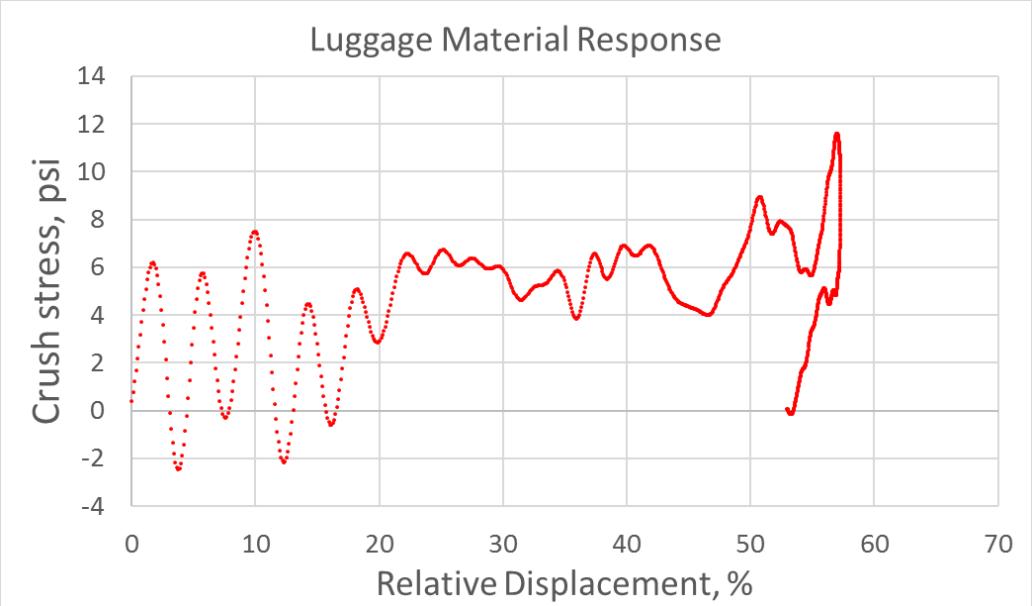

Figure 4.7. Test 2 luggage response

5. WINGBOX SECTION STRUCTURAL RESPONSE RESULTS

The wingbox section test occurred on June 29, 2017. An image series as captured from the front high-speed camera is shown in Figure 5.1 with notable events highlighted.

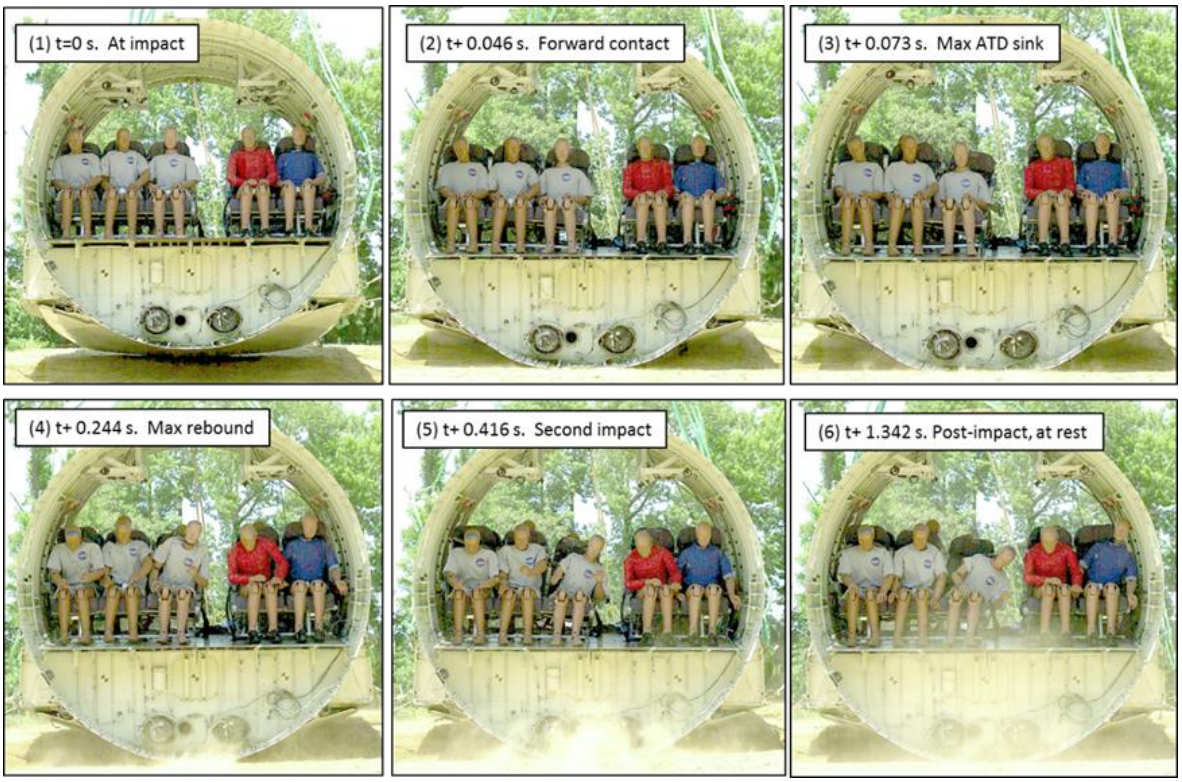

Figure 5.1. Sequence of test events for the wingbox section test, forward view

The initial contact of the aft portion of the test article onto the sloped soil surface was considered the initial impact, depicted in the top left image of Figure 5.1. Between impact and t+0.046 s, the test article rotated about the rear impact point, terminating with the forward portion of the test article initiating ground contact at t+0.046 s, which is depicted in the top-middle image. No sliding between impact at t+0.046 s was evident from the videos, so the horizontal acceleration between these two times was presumed to be from the test article rotation. The next notable time occurred when the onboard ATDs experienced their maximum downward vertical motion, also known as maximum sink position, occurring at t+0.073 s. The test article and ATDs appeared to exhibit uniform motion between t+0.073 s and t+0.244 s, until both test article and ATDs rebounded to their maximum unloaded positions. There was a second impact of the test article at t+0.416 s. During the second impact, the test article uniformly contacted the soil surface without rotational motion. The test article came to rest shortly thereafter. A final position of the test article is depicted in the lower right portion of Figure 5.1. This shows the test article at rest at a time well beyond the final motion during the test. An additional side view image sequence illustrates the fuselage motion, especially the fuselage rotation during the impact event. See Figure 5.2.

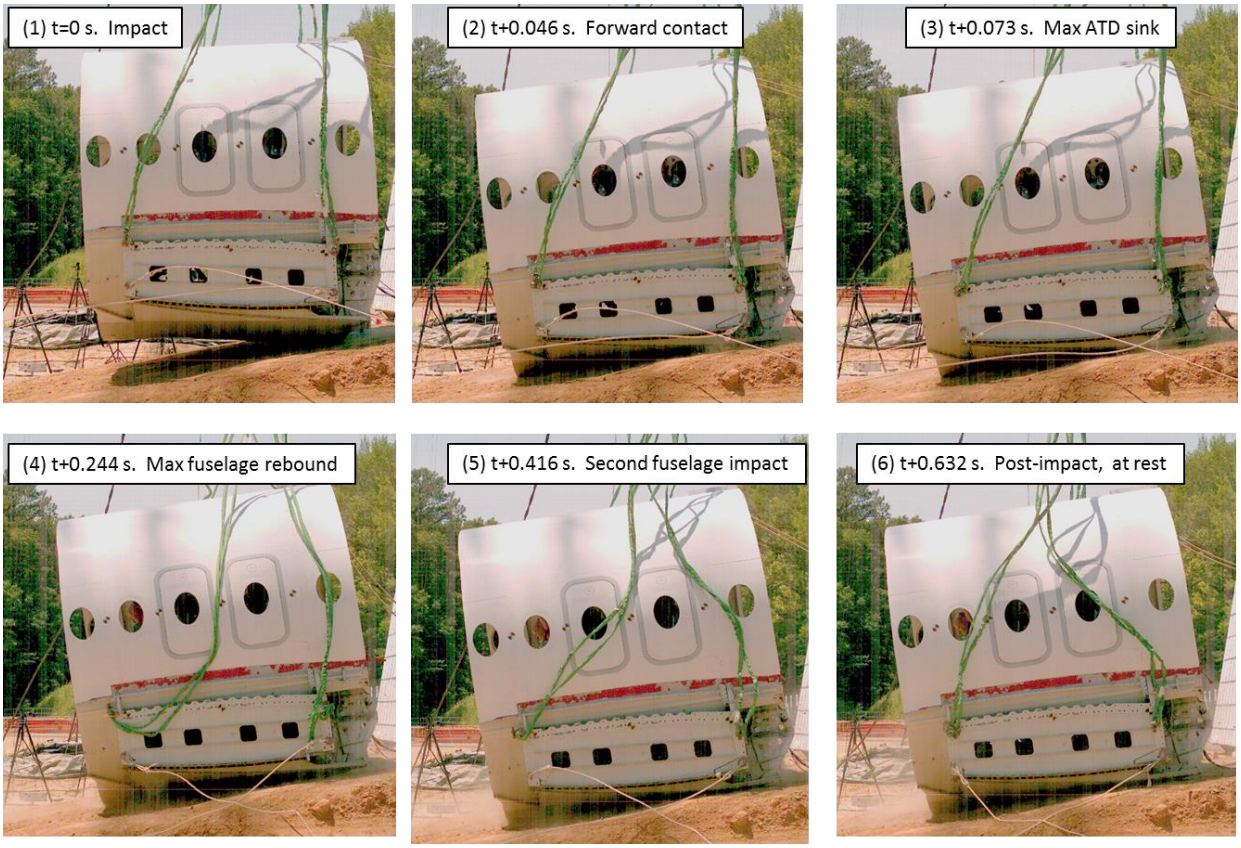

Figure 5.2. Sequence of test events for the wingbox section test, port side view

The image sequence in Figure 5.2 depicts the motion of the wingbox section from the port side and corresponds to discrete times highlighted in Figure 5.1. The initial contact with the rear portion of the fuselage is shown in the upper left image. A gap underneath the forward portion of the section is also shown. In the top middle image, the gap closed due to the rotation about the rear portion of the fuselage. The top right image shows the section at ATD maximum sink. This image

is included for reference because the ATDs were not visible in the port side camera. At t+0.244 s, maximum upward rebound occurred in the test article. The bottom middle image shows the second contact, which occurred at t+0.416 s. The bottom right image shows the final frame of captured video from the camera after all the major impact events.

The velocity results were resolved from a series of four black and yellow bowtie targets placed between the window openings at mid-cabin height. The target data showed the aft portion of the test article impacted the soil surface first at a pitch as determined from the floor of 2.9 degrees nose down with a vertical velocity of 29.5 ft/s. The pitch down in combination with the sloped soil created induced local vertical and horizontal velocities. The four velocity traces were translated into the test article local coordinate system using calculations based on the pitch angle time history. This is shown in Figure 5.3, noting that positive horizontal velocity indicated forward motion of the test article. Positive vertical velocity indicated downward motion of the test article. We smoothed the velocities using a 5-point moving average without filtering. The individual velocity curves from each target followed the same general trends, so the data were taken as a whole with individual traces averaged together for reporting overall values. The numbered vertical red bars correspond to image times shown in Figure 5.1 and Figure 5.2.

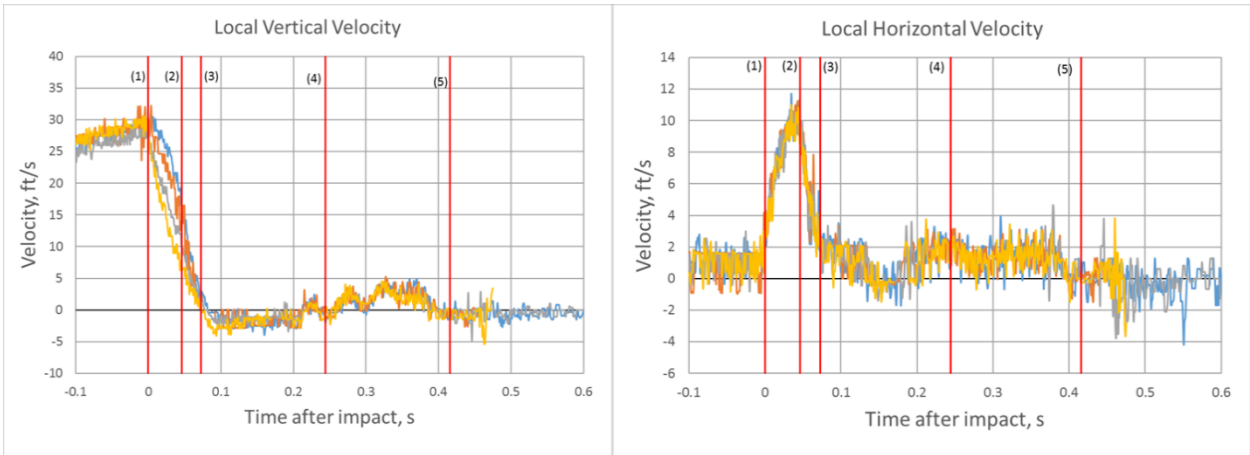

(a) (b)

Figure 5.3. Velocity time histories for Wingbox section test—vertical (a) and horizontal (b)

The local vertical velocity was 29.1 ft/s downward and the local horizontal velocity 1.1 ft/s forward at initial impact, which is designated by line 1. The rotation of the test article after impact caused the local horizontal velocity to reach 9.6 ft/s in the horizontal direction, which occurred immediately before forward test article contact at 0.046 s, indicated by line 2. Both the horizontal and vertical velocities approached zero at the maximum ATD sink at 0.073 s. During the rebound (between lines 3 and 4), the vertical velocity averaged 1.6 ft/s in the upward direction ending at 0.244 s after impact. The second impact occurred with a forward velocity of 1.3 ft/s and a vertical velocity of 1.5 ft/s, which is noted in the data between lines 4 and 5. After the second impact, the motion stopped, noted by a zero velocity after line five and the test article came to rest. The rotation rate of the section is next plotted in Figure 5.4.

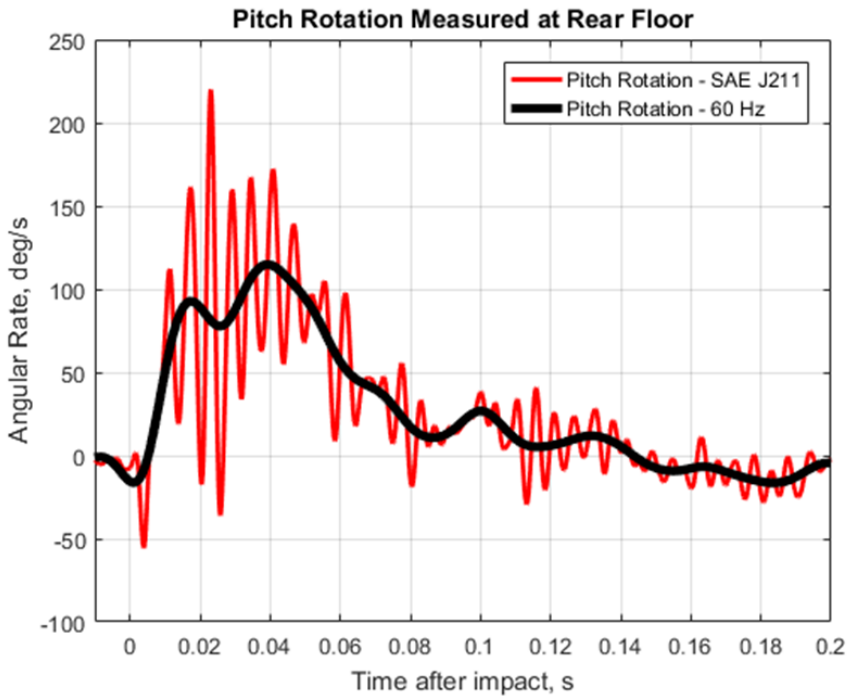

Figure 5.4. Rotational rate for wingbox section test

Although the rotational rate was filtered in accordance to SAE J211, it still had a large amount of oscillation. Thus, the data was filtered using a lower Butterworth 4-pole 60 Hz lowpass filter. This curve shows a rise after impact until 92.6 deg/s was reached at 0.017 s and then a gradual dip at 0.026 s until the pitch rotation reached a maximum value of 114.7 deg/s at 0.039 s. As noted by the images in Figure 5.2, the main portion of the rotation during the test was between impact and 0.046 s after impact, where forward contact was made. There was additional rotational motion due to the ATD sink until 0.073 s after impact. The data obtained from the rotational rate sensor confirmed these results.

Due to the initial pitch angle and sloped soil surface, crush displacement at both the forward and aft ends of the test article was examined because the slope could potentially cause non-uniform crush behavior. At the forward position, two photogrammetric targets placed on the forward wingbox stiffener structure at FS 9805 were tracked to determine forward subfloor crush. This data is shown in Figure 5.5. Note that the time scale shown in Figure 5.5 is shifted to reference the initial impact of the aft portion of the test article impacting the soil surface. Due to the rotation of the test article at impact, the forward portion of the test article impacted approximately 0.046 s after rear impact, which is reflected in the displacement data crossing the x-axis mark at this time.

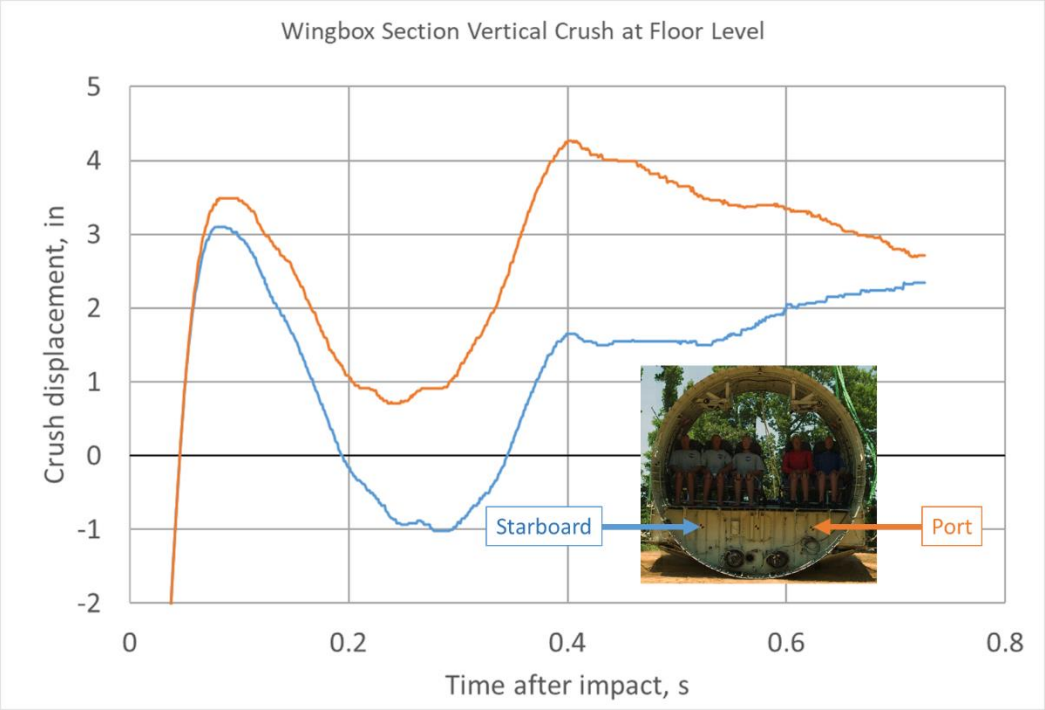

Figure 5.5. Wingbox section subfloor crush deformation—forward view

The data obtained from the forward view follows a pattern exhibited in the forward section response. There is an initial peak deformation immediately after impact, followed by a rebound between 0.25 and 0.3 s after impact. Next, there was a settling into a post-test crush position starting at 0.4 s. after impact. The initial peaks for both the port and starboard side targets produced similar responses of 3.49 inches and 3.10 inches respectively. However, the targets settled into a post-test deformation of 2.71 inches and 2.35 inches for the port and starboard sides respectively.

The aft response was dominated by the lower cavity portion of the wingbox section, located below the wingbox truss structure and the outer skin of the aircraft. There were vertical stanchions running through the lower cavity. These stanchions buckled during the impact, which caused the lower cavity to experience most of the subfloor deformation. Figure 5.6 shows pre- and post-test views of the lower cavity structure.

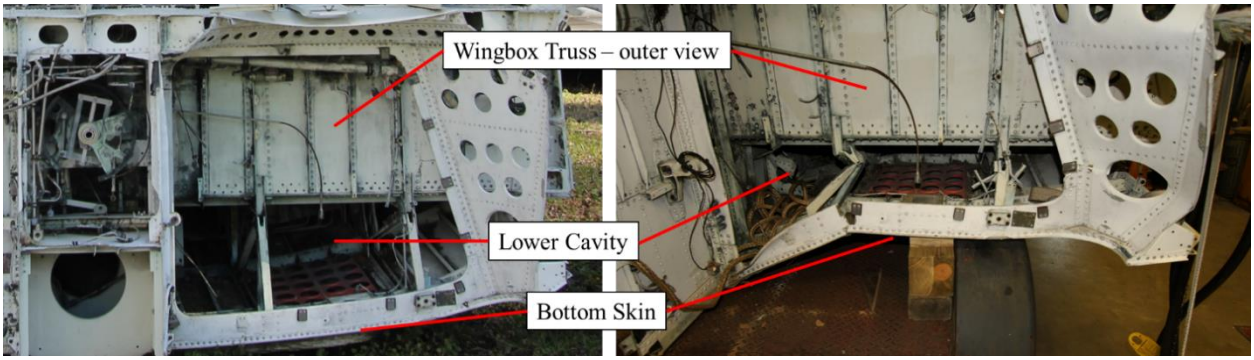

(a) (b)

Figure 5.6. Wingbox lower cavity pre-test (a) and post-test (b)

Deformation was determined by measuring the distance between the bottom skin and the bottom of the wingbox truss structure before and after impact. The measurements showed the total deformation of the lower structure at the aft location of the wingbox section to be approximately 6.48 inches. This deformation occurred at the locations outboard of the large vertical stiffeners running down the center of the structure. The vertical stiffeners did not deform during the impact but penetrated into the soil approximately 7 to 3inches from the aft to the forward location.

Additional images were taken from an onboard camera mounted inside the wingbox truss structure. Figure 5.7 shows a still image from a video taken from the camera post-test, which verified that the truss structure did not exhibit deformation or failure during the test.

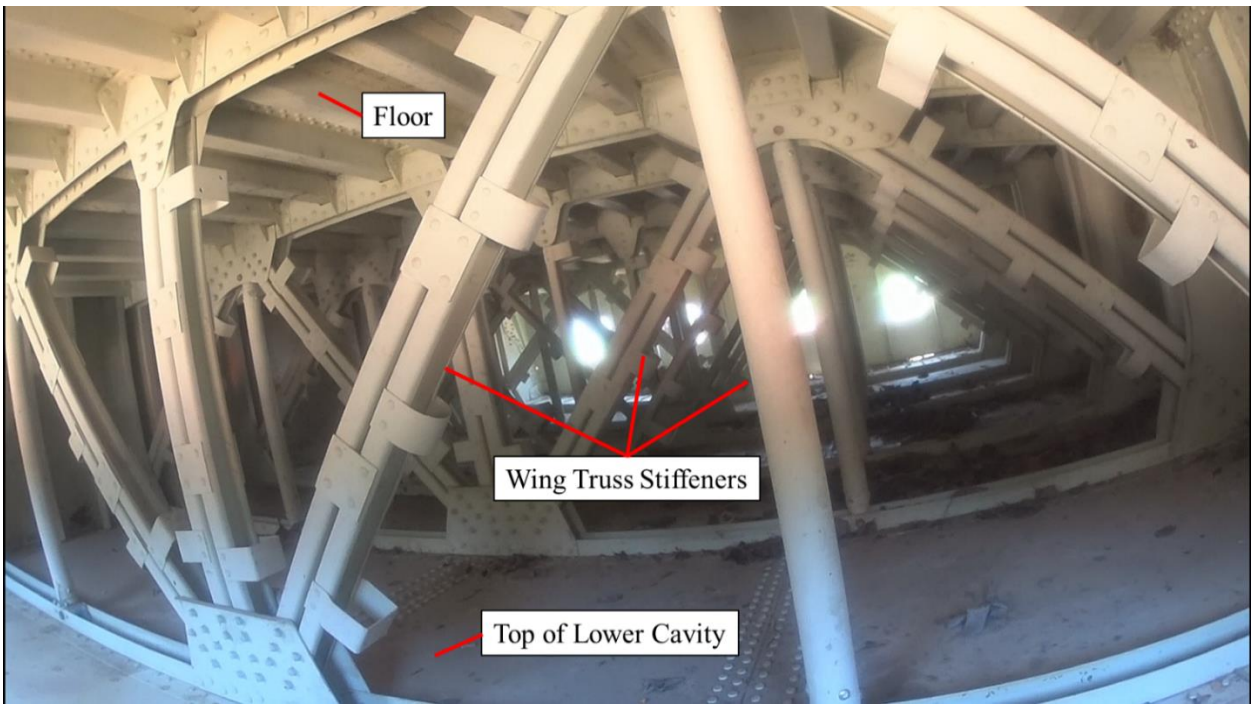

Figure 5.7. Wingbox section truss structure post-test

Other than the aft lower cavity region, the test article did not show noticeable signs of structural damage. The wingbox truss structure appeared to be undamaged, and the seat tracks did not show signs of fracture or tearing. Similar to the forward section, the structure above the floor did not appear damaged. Additionally, all four emergency exit doors opened nominally post-test, which indicated no permanent deformation or warpage around the door frames. Figure 5.8 shows the doors pre-test and the openings post-test on the port side of the test article.

(a) (b)

Figure 5.8. Wingbox section port emergency exit doors pre-test (a) and removed post-test (b)

The soil moisture content at three locations and had an average of 8.4% at the time of the test. CBR measurements were also taken at three locations around the impact point. The CBR data showed a high bearing capacity at and near the surface of the soil with a gradual decrease as the depth increased. The capacity reached a minimum at approximately 12 in. depth and then began to increase again. This trend was similar to those from the forward section soil, which was expected because the same soil was used. However, the CBR surface results were higher, and the moisture content lower than the measurements taken in the forward section test. The differences were due to the wingbox test taking place in the summer when the temperature was much higher. The higher temperature led to the evaporation of the surface moisture, which caused the soil to dry out and exhibit a stiffer response at the surface. The results of the location near the forward impact point are shown in Figure 5.9.

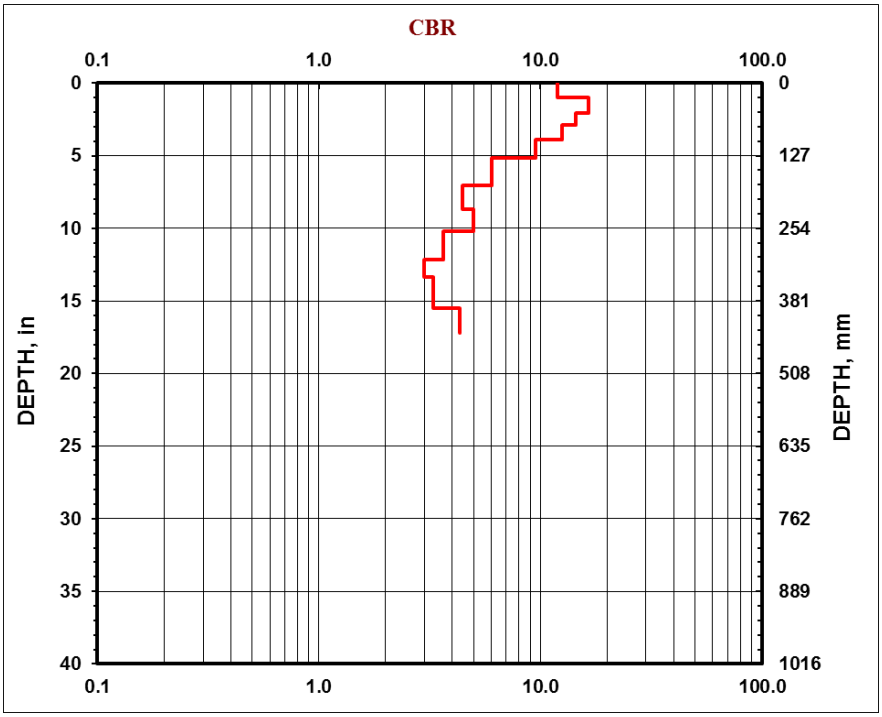

Figure 5.9. CBR for soil in wingbox section test

The impact caused a distinct impression in the soil. Specifically, the impression exhibited two distinct parallel vertical lines with the deepest penetration near the aft of the test article and gradually becoming shallower when moving toward the front. The parallel lines were created by vertical stiffeners located at the bottom of the test article, approximately 9 in. outboard from the test article's geometric centerline. Because the aft portion of the test article impacted first, the rear features, including the vertical stiffeners, made the deepest impression in the soil surface. Generally, the rest of the soil mound was undeformed due to the impact. Figure 5.10 shows the indentation of the soil surface from the test. The two vertical indentations are noted, and the top of the image is toward the aft end of the section.

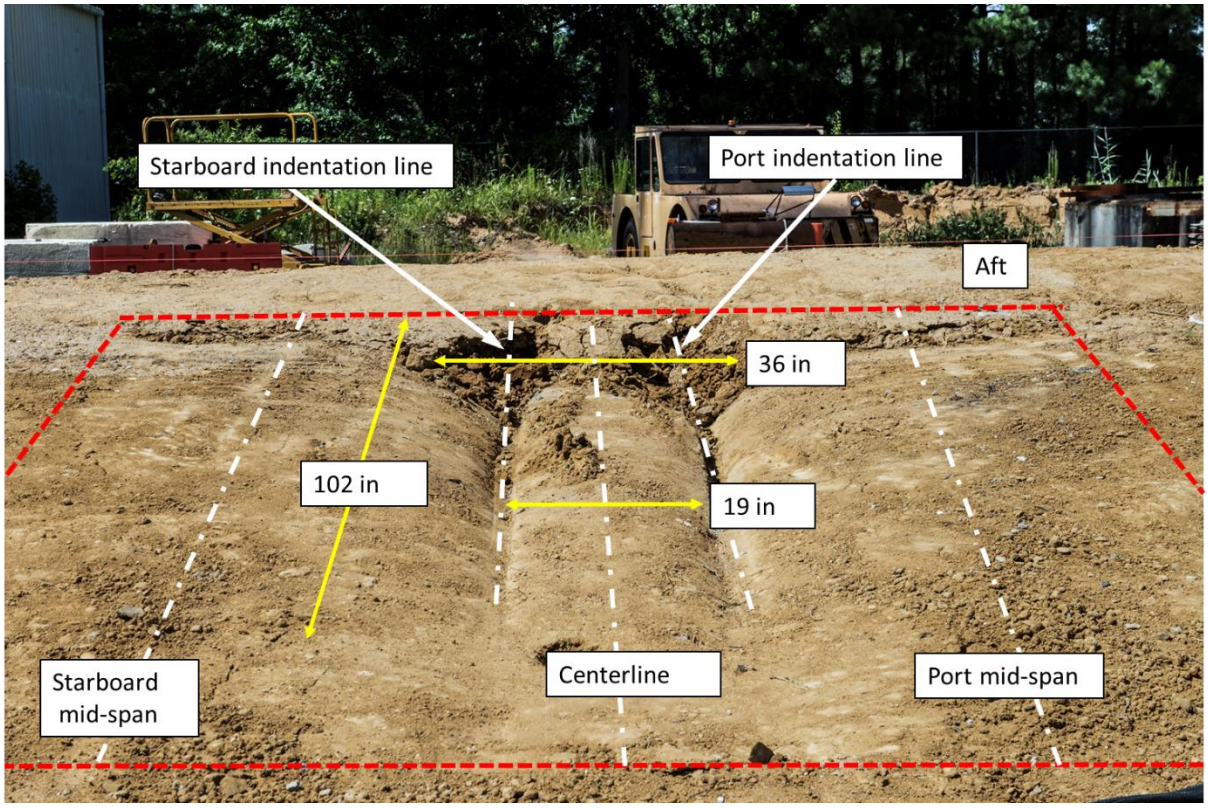

Figure 5.10. Wingbox section soil indentation results with test article outline

Penetration measurements were taken at three locations in the crater, depicted in Figure 5.10. Measurements for the starboard indentation line, which is the vertical line on the left in Figure 5.10, the middle between the indentation lines, and the port indentation line, which is shown to the right in Figure 5.10, were taken. The results are shown in Table 5.1.

Table 5.1. Wingbox section crater depth measurements

Position from aft (in)	Starboard indentation depth (in)	Centerline depth (in)	Port indentation depth (in)
15	7.0	4.25	7.25
22	8.0	4.0	7.0
37	8.0	4.0	8.0
47	6.0	3.25	7.5
62	6.0	2.5	6.0
76	4.75	2.75	5.25
102	3.0	3.0	3.0

The soil crater measurement data marked differences between the vertical stiffener and bottom span locations. In the aft impact location, vertical stiffener penetration was 7 in. deep on the starboard side and 7.25 in. deep on the port side. The location of the mid-spans corresponding to

the lower cavity locations of the test article lightly penetrated the soil. The differences were notable because accelerations obtained at the different measured locations provided a local loading profile. The acceleration data was compared between the aft subfloor accelerometer for the vertical stiffener accelerations and the CDR for the lower cavity accelerations. Figure 5.9, left, shows the locations of both accelerometers in the post-test damaged view to contrast the difference in their locations. The data are shown in Figure 5.11, right. The data were not time synchronized, so manual shifting was implemented on the CDR data to give a more direct comparison. The data in Figure 5.11 are filtered using a Channel Frequency Class 60 low-pass filter for visualization.

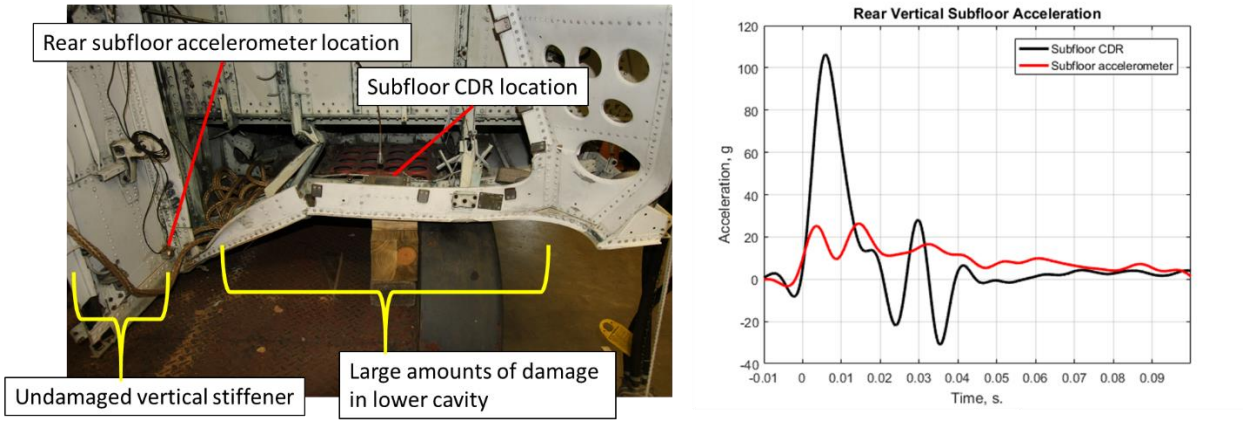

(a) (b)

Figure 5.11. Wingbox section aft lower sensor locations (a) and acceleration results (b)

The filtered CDR data showed a triangular shaped pulse with a peak acceleration of approximately 106 g and duration of approximately 0.021 s. This is using the first data point for which the acceleration trace crossed the zero-g mark after maximum. In contrast, the subfloor accelerometer located on the vertical stiffener produced accelerations that more closely matched the results from the airframe floor accelerometers. The vertical stiffener remained undamaged during the impact but produced the deepest soil crater where penetration occurred (shown in Figure 5.10) in a controlled manner throughout the initial rotation, front impact, and ATD max sink. The soil penetration, along with the rotation, limited the peak magnitude of 26.0 g with a duration of 0.100 s.

Figure 5.12 shows an image series of the aft lower cavity crushing that illustrates the differences in deformation where the two sensors were mounted. Note that the horizontal lines in the images are artifacts of the camera sensor unrelated to the test, test setup, or results, and ignored when interpreting the images.

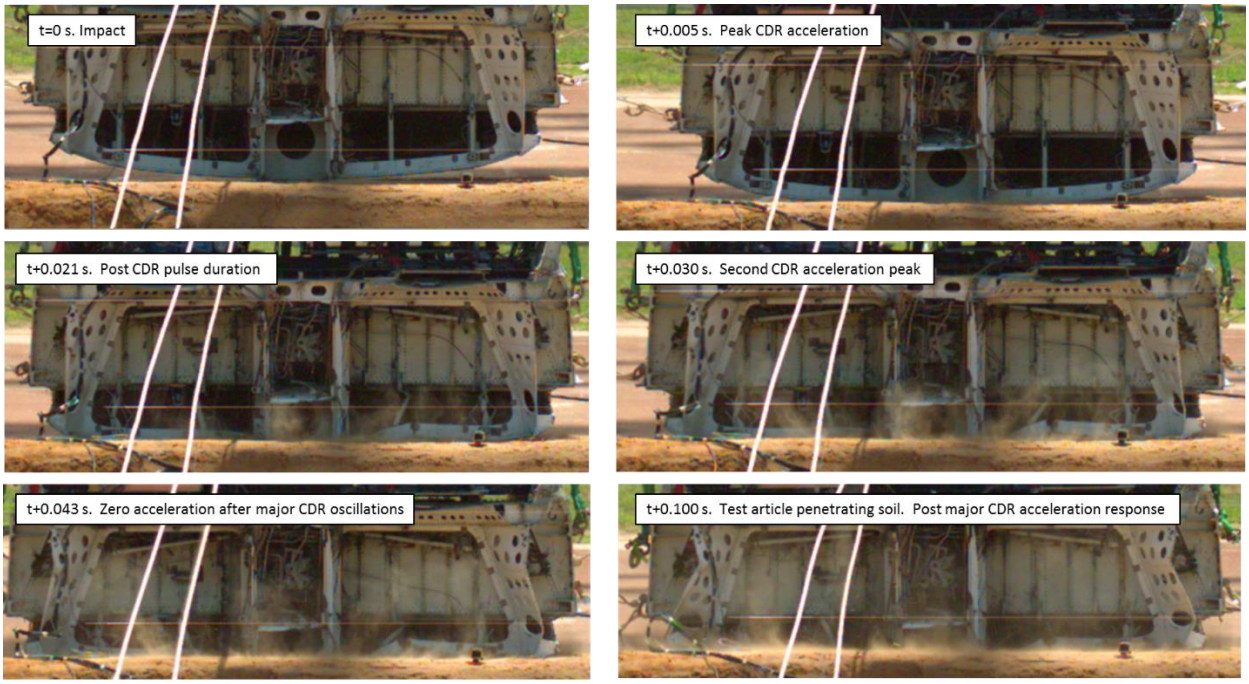

Figure 5.12. Aft lower cavity deformation image series

The initial contact between the aft portion of the test article and the soil surface is shown in the upper left image in Figure 5.12. The peak CDR acceleration, shown in the upper right, was 106 g and occurred 0.005 s after initial contact. Between impact and this time, there was not any noticeable deformation in the lower cavity occurring. The impact shape and magnitude of the acceleration response were a result of contact between the bottom skin's large surface area and soil. It was only after the 106-g peak that the lower cavity deformation initiated. The CDR pulse shape crossed the first zero-g mark at 0.021 s, shown in the middle left image. After 0.021 s, the lower cavity deformation continued to occur. The oscillation in the CDR data was from the flexing of the panel where the CDR was mounted during the failure of the lower cavity, shown in the middle right and lower left images. After 0.100 s, the major acceleration pulses for both the data logger and the accelerometer on the vertical stiffener concluded.

Local horizontal accelerations for the sensors mounted at the floor level of the wingbox section are plotted in Figure 5.13 for the starboard side and Figure 5.14 for the port side.

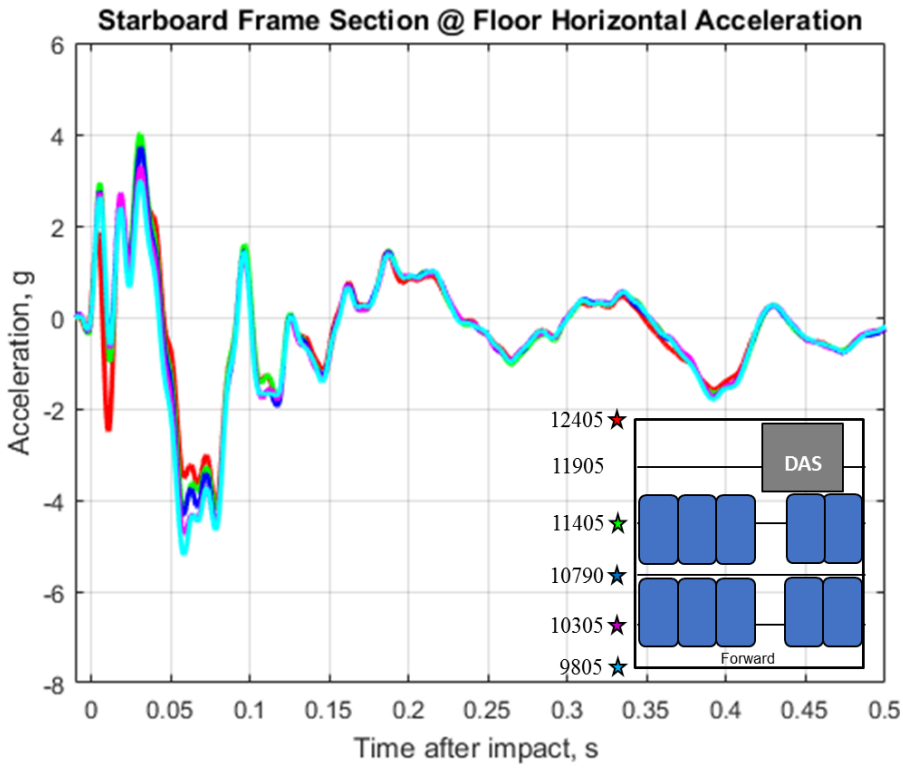

Figure 5.13. Starboard floor/frame horizontal accelerations from wingbox section

Horizontal acceleration results from all accelerometers closely matched each other throughout most of the impact event. There were minor differences in some of the initial peak (both positive and negative) values that occurred before 0.100 s. Positive acceleration peaks of 4.0 g occurred at FS 11405 during the test article rotation up until initial forward impact, which occurred at 0.046 s. After forward impact, the acceleration reached negative values, which ranged from 4.1 g at FS 12405 to 5.2 g on at FS 9805 approximately 0.058 s after impact. The large negative accelerations resulted from the restriction of further fuselage tip over because of the interaction with the soil impact surface immediately after the initial rotation. The rebound of the fuselage occurred between 0.073 s and 0.244 s after impact, corresponding to the positive acceleration recorded by the accelerometers at all locations toward a maximum of approximately 1.4 g at 0.192 s after impact, which was the middle of the rebound event. The horizontal accelerations reached a value of 1.7 g at 0.393 s around when the second impact occurred. After the second impact, there were no additional notable acceleration events. The horizontal accelerations on the port side of the fuselage were examined and are shown in Figure 5.14.

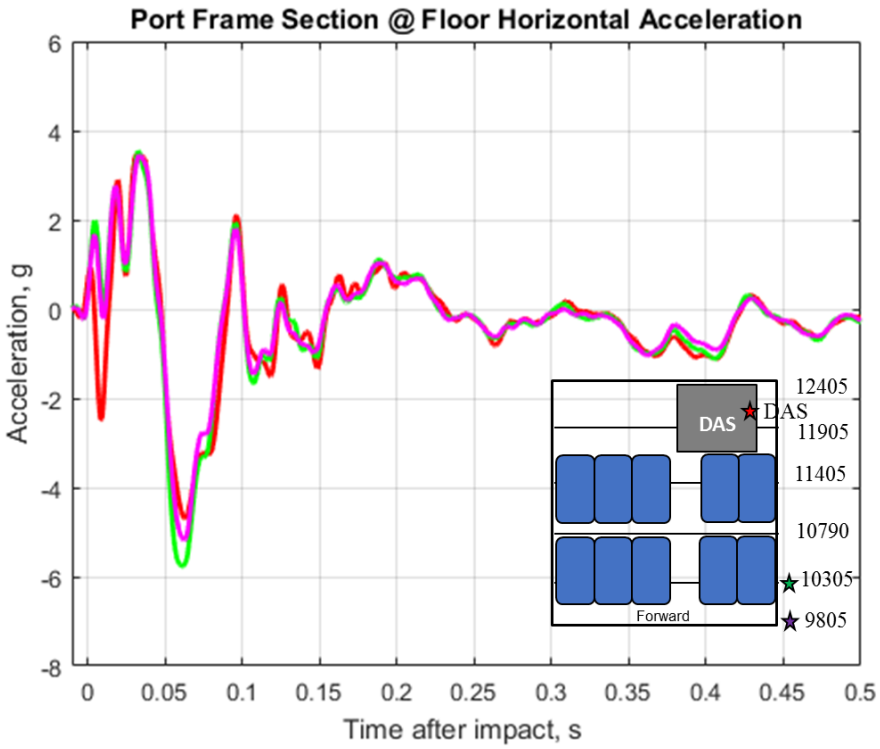

Figure 5.14. Port floor/frame horizontal accelerations from wingbox section

The accelerometer at FS 11405 did not function during the test, so an accelerometer on the DAS plate, near FS 12405, was used in its place. Acceleration traces for all accelerometers closely matched throughout the impact event, with minor differences in the negative peaks occurring at 0.064 s. Positive acceleration peaks of 3.5 g occurred during the test article rotation until initial forward impact at 0.046 s. The acceleration traces went negative, reaching between -4.7 g on the DAS plate to -5.7 g on FS 10305 until they crossed the zero-g mark again at 0.084 s after initial impact. The general shapes of the acceleration curves were like the accelerations measured on the starboard side of the fuselage. These shapes were caused by the same factors acting on the starboard side. The rebound of the fuselage occurred between 0.073 s and 0.244 s after impact. The rebound caused positive accelerations measured by all accelerometers with almost identical response traces. After a localized maximum at 0.118 s, there were no other significant events recorded by the port side accelerometers.

The starboard vertical accelerations at the floor/frame junctions are shown in Figure 5.15. In general, the pulses were trapezoidal shaped with a total duration of approximately 0.100 to 0.120 s. The average plateau value was between 9.8 g and 12.2 g for times between 0.02 s and 0.05 s after impact. An initial peak occurred at approximately 0.008 s after initial test article/soil contact. The peak values were greatest at the aft of the test article and decayed as the location moved toward the front. The highest peak of approximately 39.0 g occurred at FS 12405, which was followed by a peak of 26.3 g at FS 11405. The accelerations decayed with no discernable peaks exhibited after 0.08 s after impact.

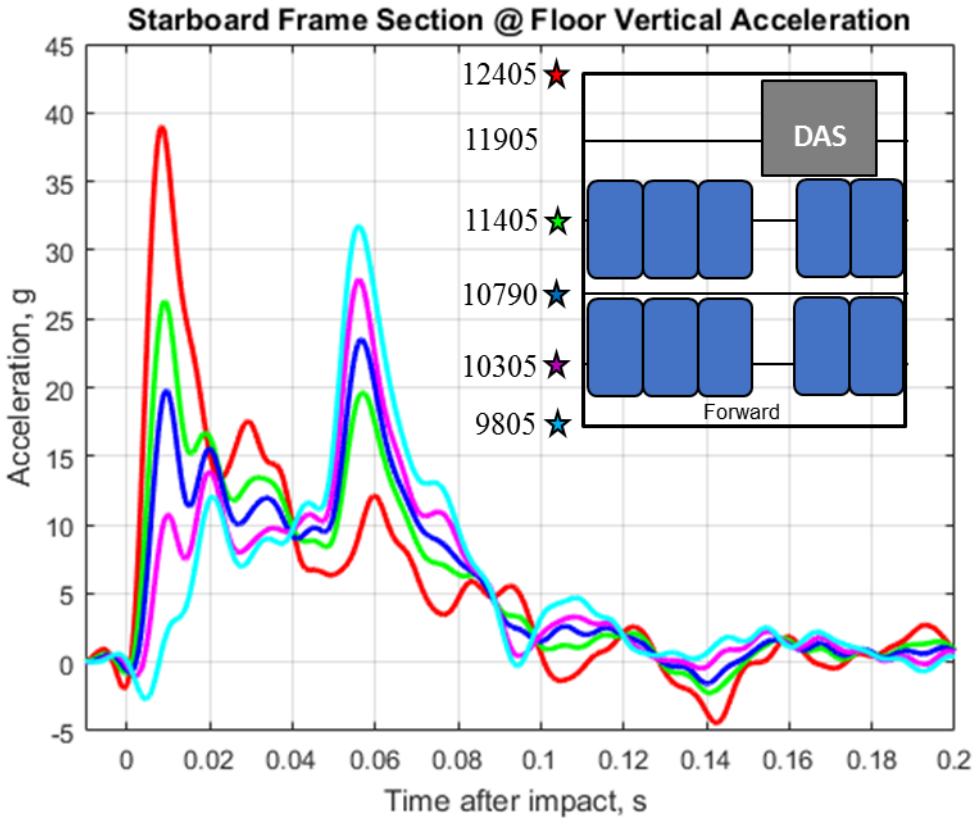

Figure 5.15. Starboard floor/frame vertical accelerations from wingbox section

The second peak occurred approximately 0.055 s after impact, which was shortly after the forward portion of the test article made contact with the soil surface due to the rotation of the test article at impact. In contrast to the trend observed in the initial peak values for the response, the greatest magnitude in the second peak occurred in locations at the front of the test article. Specifically, the highest magnitude peak occurred at FS 9805, which exhibited an acceleration magnitude of approximately 31.7 g. The peak then decreased rearward until 12.1 g was observed at FS 12405. The acceleration data on the port side of the airframe, are plotted in Figure 5.16.

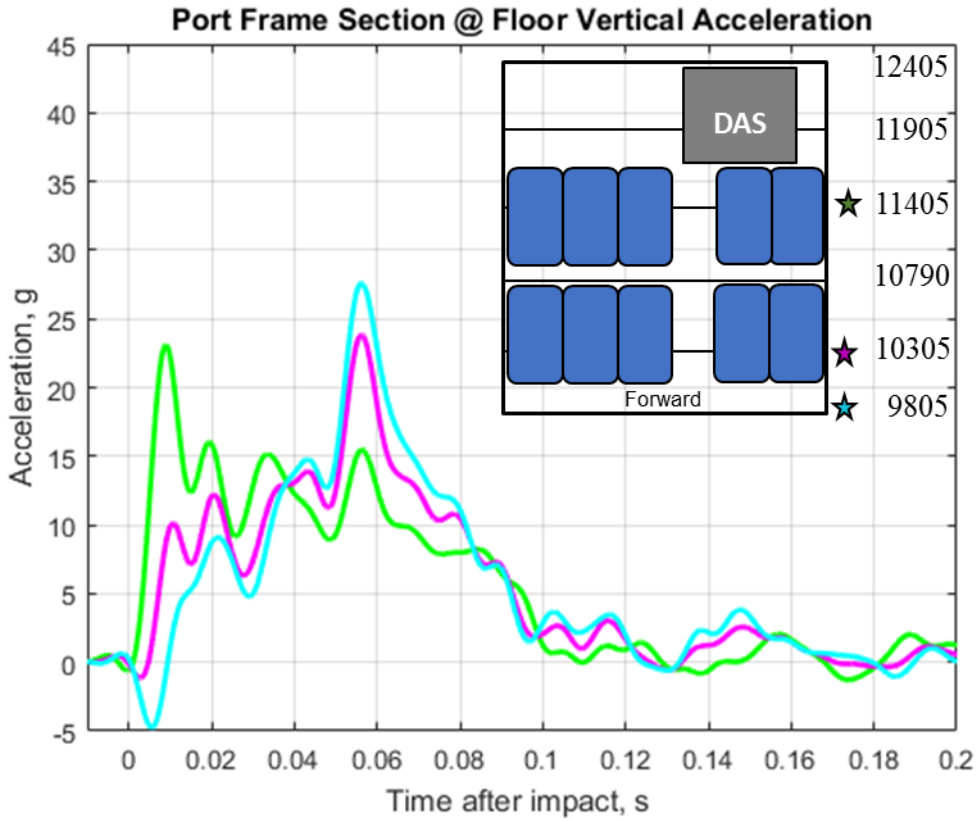

Figure 5.16. Port floor/frame accelerations from wingbox section

Although the port side of the wingbox section was not as heavily instrumented as the starboard side, the data collected from the instrumented locations closely mimicked the response from the starboard side. The acceleration data obtained from FS 11405 showed an initial peak at the beginning of the response with a peak value of 23.1 g occurring at 0.009 s after initial contact. This value was close to the 26.3 g peak recorded on the starboard side at this location. Similar to the starboard data, both FS 10305 and FS 9805 did not show an initial peak at the beginning of the response. The peak acceleration at these locations occurred at the end of the response, similar to the starboard side behavior. At 0.060 s after impact peak values of 27.6 g, 23.8 g, and 15.5 g were measured for FS 9805, FS 10305, and FS 11405, respectively. These values correspond to values of 31.7 g, 27.8 g, and 19.7 g at the same locations on the starboard side. The average values computed between 0.020 s and 0.05 s after impact were 12.0 g, 11.0 g, and 10.4 g at FS 11405, FS 10305, and FS 9805. These values were similar to the values obtained on the starboard side. The overall response at the floor locations for both the starboard and port sides were in general agreement. Only slightly higher peak acceleration values occurred at the end of the response on the port side. The acceleration results at the seat bases were examined. The rear row vertical seat acceleration is plotted in Figure 5.17.

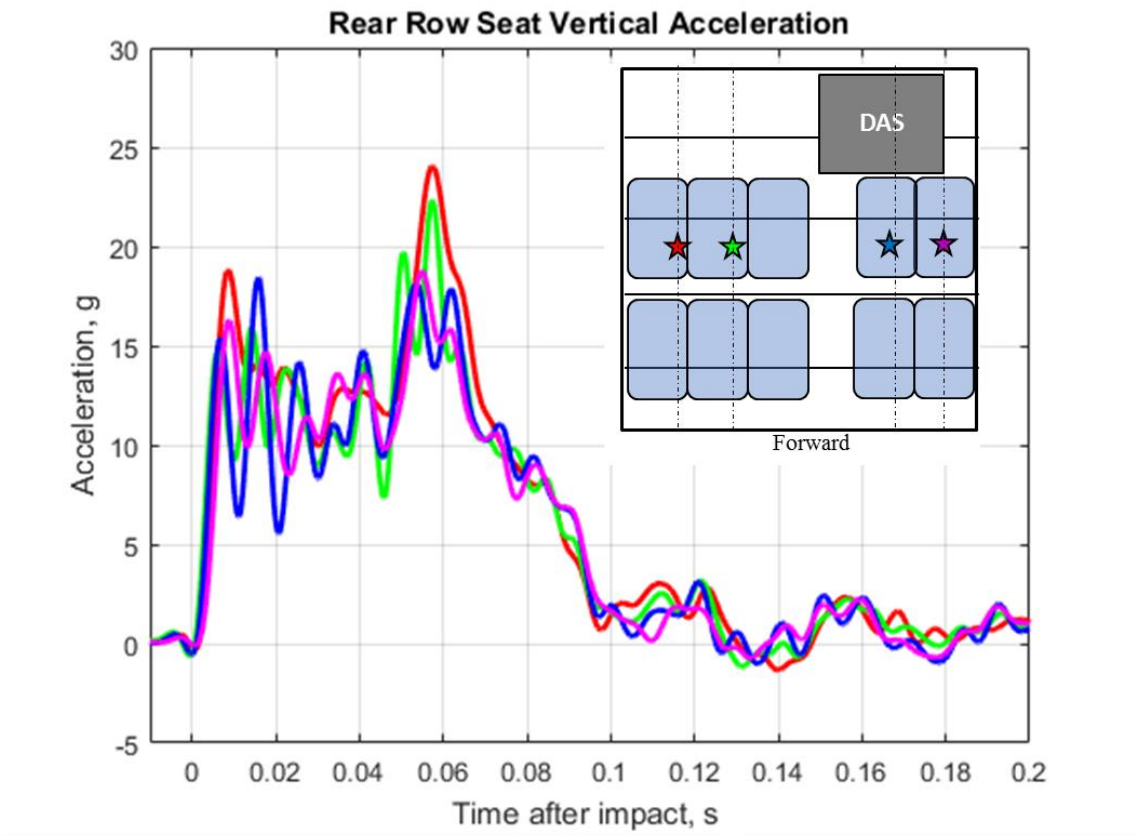

Figure 5.17. Rear row seat vertical accelerations from wingbox section

All the rear row seat leg accelerations exhibited a trapezoidal shaped pulse response. A small initial peak appeared at the beginning of the response. There was a well-defined peak at the end. For the triple outer measurement location, the peak at the end of the response reached a value of 24.1 g, which was the highest for all locations measured. If assuming a trapezoidal shaped response, accelerations averaged between 0.010 and 0.046 s were 11.5 g, 12.8 g, 11.2 g, and 11.8 g for the triple outer, triple inner, double inner and double outer seat leg base locations. The response duration was approximately 0.097 s for all locations measured. The front row vertical seat acceleration data are plotted in Figure 5.18.

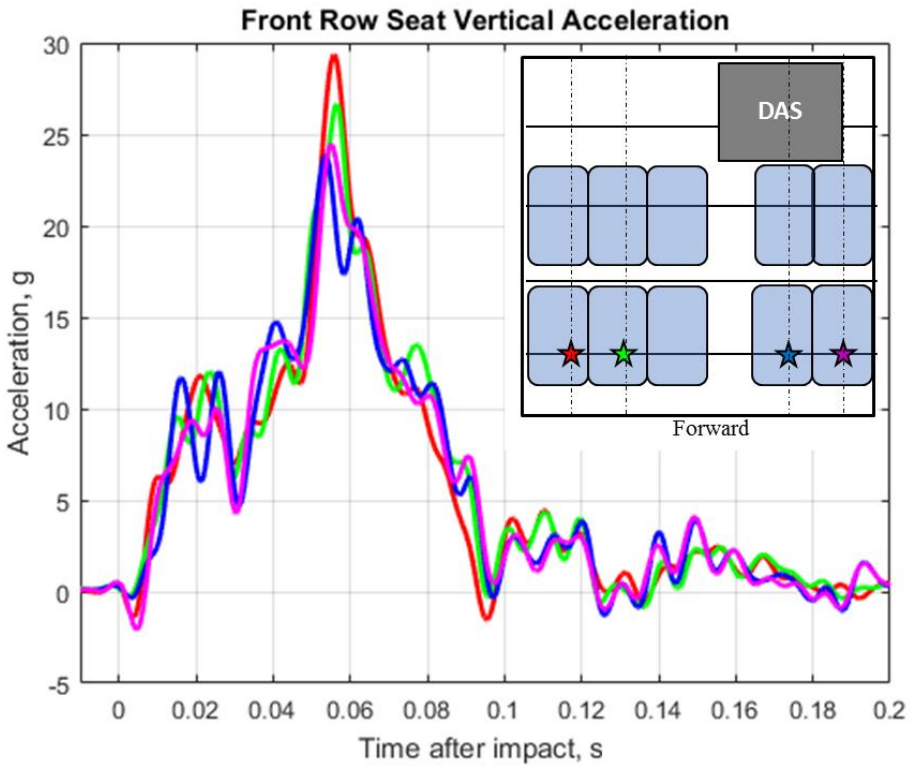

Figure 5.18. Front row seat vertical accelerations from wingbox section

The seat leg vertical acceleration responses for the front row of seats did not exhibit the same response as the rear row. The four seat leg locations exhibited nearly uniform responses. The only major difference was their peak accelerations at 0.055 s after impact. The acceleration data ranged between 23.8 g on the double inboard seat leg to 29.3 g on the triple outboard seat leg. Because these seats were located approximately over FS 10305, the timing the peak occurred was in general agreement with the timing of the floor/frame acceleration data at FS 10305. The duration of all responses was approximately 0.095 s, which was in general agreement with the rear row results.

The horizontal accelerations from the rear seat location are shown in Figure 5.19. The general trend matched the trend in the floor/frame horizontal acceleration data, as shown in Figure 5.13 and Figure 5.14. An initial oscillation occurred for the first 0.02 s after impact, which lead to an initial peak of 4.6 g from the port side outboard seat base accelerometer in blue. A minimum acceleration of 6.5 g was recorded on the port side outboard accelerometer. Note that the port side inboard seat base accelerometer measured the maximum positive acceleration, which occurred at 0.032 s after impact. The port side outboard seat base accelerometer measured the maximum negative acceleration that occurred at 0.064 s after impact. All four responses followed the same shape. Differences in the maximum negative accelerations were in the range of 2–3 g. This did not significantly affect the overall response because the total magnitude of the response was less than 8 g, which is depicted in the limits of the chart. The results suggested minor differences between the side and middle of the section. Other than slight differences in maximum values, the acceleration curves generally matched in magnitude and in shape.

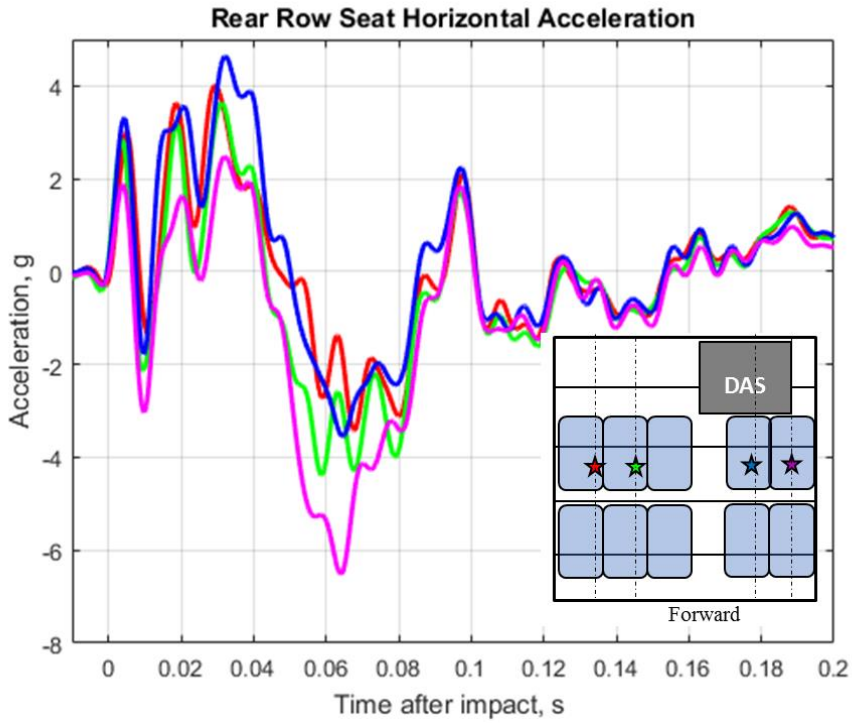

Figure 5.19. Rear row seat horizontal accelerations from wingbox section

As shown in Figure 5.20, the horizontal accelerations recorded in the forward seats matched the trends seen in the rear seats and floor/frame accelerations. An initial oscillation occurred for the first 0.030 s after impact. A maximum of 3.6 g occurred at 0.031 s after impact in the triple outboard accelerometer location. However, the responses were similar for all locations at this time. All accelerations then trended negative, leading to maximum negative accelerations of 5.8 g and 5.9 g at the double outer and inner seat leg locations. The triple side accelerations measured maximums of 4.7 g. These accelerations were less than those on the double side and a slightly different shape that resembled a trapezoid between 0.04 s and 0.10 s. Other than noted differences, the acceleration curves generally matched in magnitude and shape.

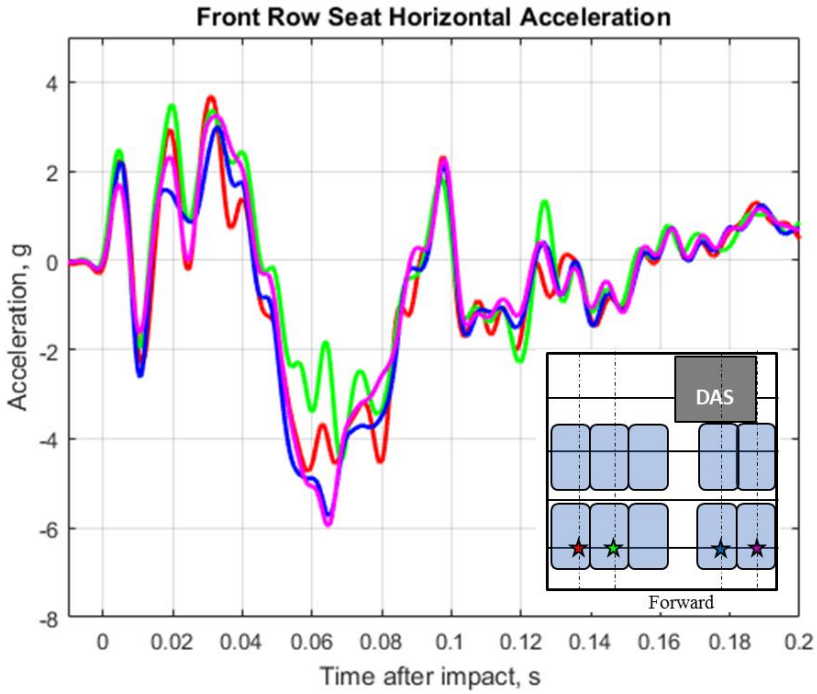

Figure 5.20. Front row seat horizontal accelerations from wingbox section

The results from the CDRs on the floor were examined. The acquired CDR data were compared with measurements from an adjacent accelerometer like what was examined in the forward section. However, unlike the forward section test, the brown CDR did not trigger and collect impact data. The sensor's threshold trigger limit was accidentally set too high, which caused faulty triggering and was noted for future testing. Data was obtained from the blue CDR and appears in Figure 5.21 with horizontal and vertical direction results.

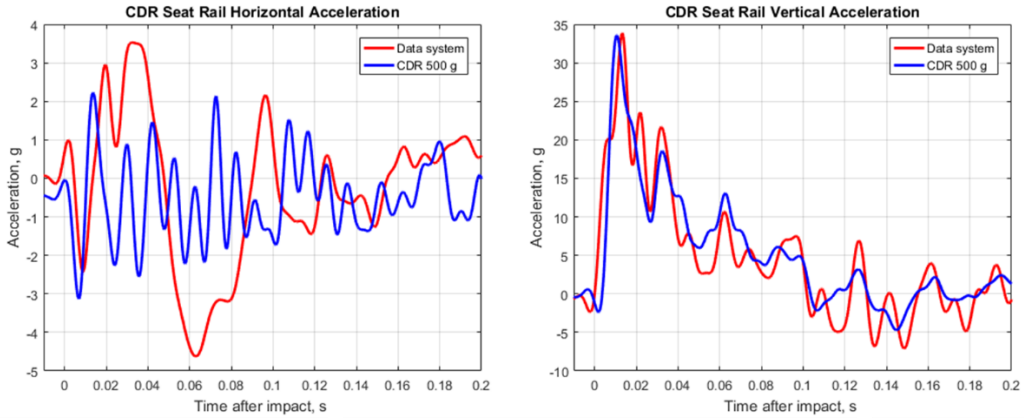

(a) (b)

Figure 5.21. CDR seat rail acceleration for wingbox section test—forward direction (a) and vertical direction (b)

The results from the CDRs showed good agreement in the vertical direction and less than ideal agreement in the forward direction. In the forward direction, both curves exhibited initial negative peak values immediately after impact that were similar in magnitude and time. The DAS acceleration measured 2.4 g and the CDR measured 3.1 g. After the initial spike, the curves deviated. The data system measured positive acceleration between 0.014 s and 0.048 s, reaching a second negative peak of 4.6 g. In contrast, the CDR showed oscillations with no defined curve shape. However, in the vertical direction, the two measurements matched well. In the vertical direction, both the CDR and data system show peaks at 0.013 s after impact, which ranged between 33.6 g on the CDR and 33.8 g for the data system. As with the forward section test, the CDRs were not synchronized to the data system or cameras. Therefore, a manual time shift was implemented, using the peak value timing information as reference. After the initial peak, both vertical measurements decayed toward the zero-g mark and crossed it at 0.101 s for the data system and 0.104 s for CDR. The difference of only 0.003 s is remarkable.

The hat rack bin ballast results displayed the same trends as the floor level accelerations, as shown in Figure 5.22. The aft-most attachment location at FS 11405 measured an initial peak of 28.5 g and then settled into an average acceleration of 12.1 g when the data were averaged between 0.020 s and 0.060 s after impact. In contrast, the forward-most attachment location at FS 10305 exhibited a peak of 30.3 g near the end of the plateau region of the response. However, averaged data over the same 0.020 s and 0.060 s plateau region gave a response of 12.6 g.

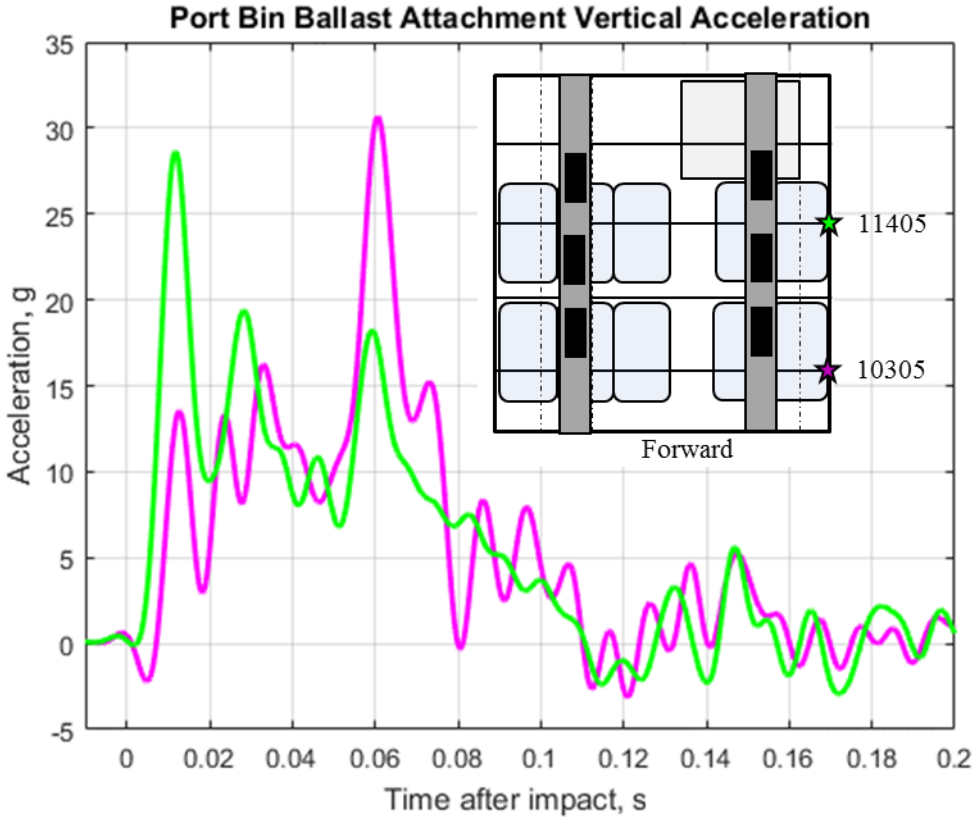

Figure 5.22. Overhead bin attachment location vertical accelerations

As Figure 5.23 shows, accelerations recorded on the hat rack bin ballast mass were a higher magnitude than either the bin attachment or floor accelerations. These accelerations did not exhibit a trapezoidal pulse. Instead, there was an oscillatory response of between 26.6 and 27.2 Hz for all instrumented ballast locations on the port and starboard sides centered about zero g. The oscillations were caused by ballast masses and c-channels swaying at the end of the cantilever attachment arms post-impact. The accelerations also followed the general trend seen in other portions of the data, in which aft locations show an initial peak due to aft ground contact, and the forward locations show the peak after forward ground contact. The magnitudes for the peaks were 45.9 g for the FS 11405 location and 47.3 g for the FS 10305 location. Finally, the oscillation frequency in the ballast mass was approximately 2.5 times higher than the forward section oscillation frequency. From a structural standpoint, the higher frequency indicates a stiffer response at impact.

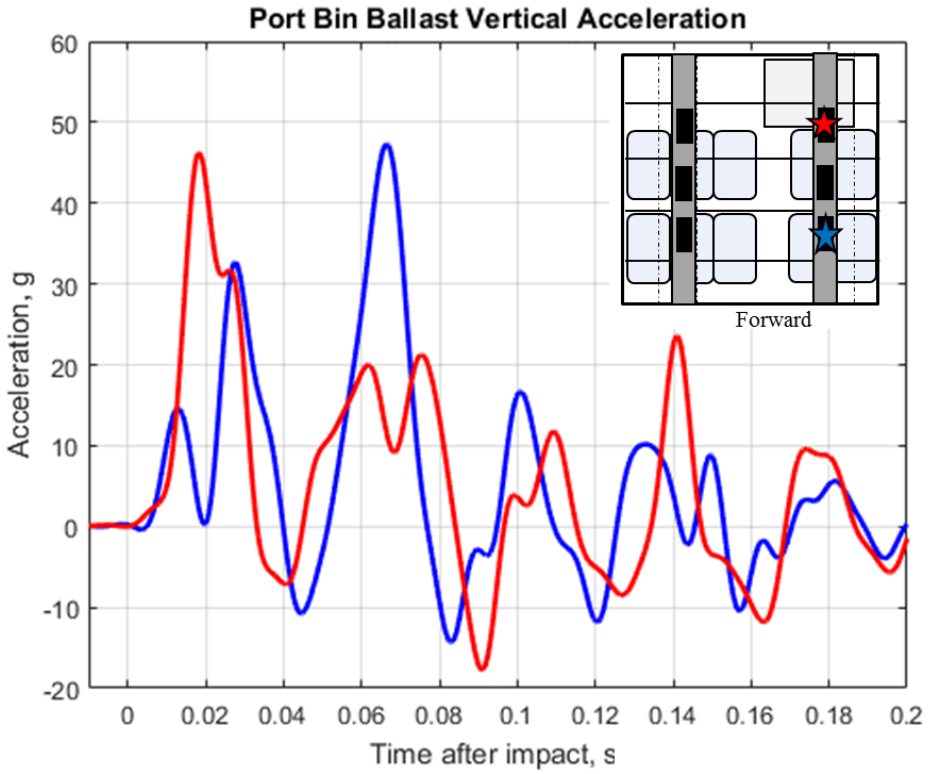

Figure 5.23. Port side bin ballast accelerations from wingbox section

ATD data were examined. Nine of the ATDs were seated upright with their hands on their knees, in an identical position to that of the forward section test. ATD 3 was unique in that it was positioned in the "brace" position, configured by leaning its chest forward and positioning its head such that it was nearly touching the seat #8 seat back. Its arms were down at its side and rested below its knees with the hands located near its shins. Figure 5.24 shows a view of ATD 3, positioned in the brace position, just before impact.

Figure 5.24. ATD 3 in the brace position

On overhead view of the post-test configuration for the ATDs is shown in Figure 5.25. ATDs 1, 4, 6, 7, and 9 all appeared to lean directly forward. ATD 3 appeared to be in the same position as before the test. ATDs 5 and 10 leaned both backward and sideways, toward the window. They were in a similar position as in the forward section test. Finally, ATD 8 appeared to be leaning purely sideways, into the aisle.

Figure 5.25. Wingbox section post-test ATD positions

After capturing the post-test ATD positioning, the ATD data were examined and determined the probability of injury. The first occupant data examined were the ATD lumbar loads. Figure 5.26 shows the time histories on the left and the peak values on the right.

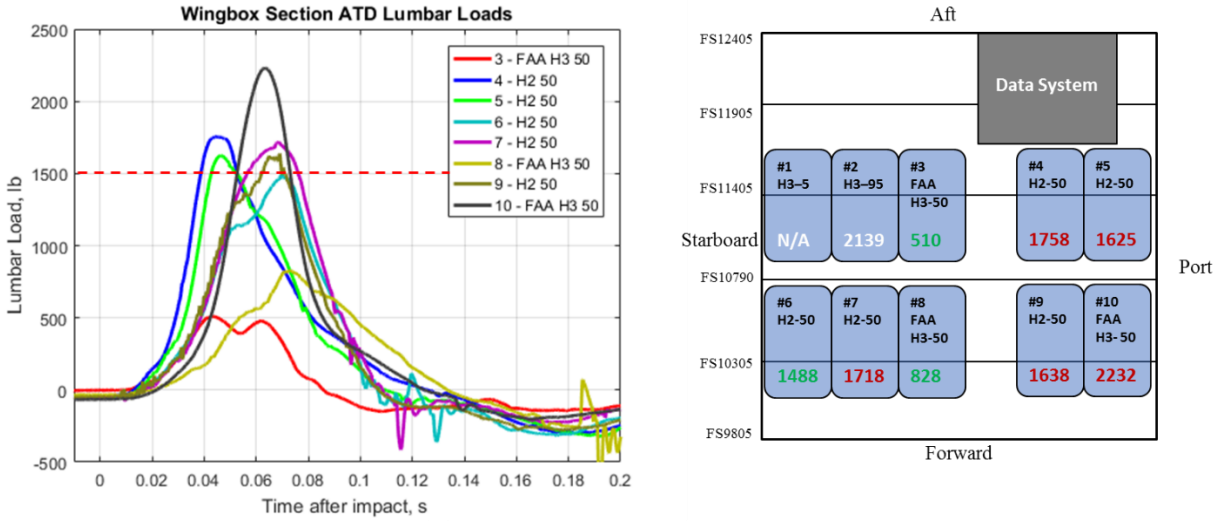

(a) (b)

Figure 5.26. Wingbox section ATD lumbar load time history (a) and highlighted peak values (b)

The wingbox section test resulted in higher lumbar loads for six of the ATDs as compared to the forward section test. The exceptions were ATDs 3 and 8, which were seated in the cantilever seats on the triple side. However, in addition to being seated in the cantilever seat, ATD 3 was positioned in the brace position and not directly upright. The resultant peak load and the overall pulse shape of ATD 3 were much less than the other ATDs because of this positioning change. ATD 8 saw a lumbar load approximately 300 lb. less than in the forward section test due its location in the cantilever seat only. The lower lumbar value result for ATD 8 was caused by additional deformation of the seat itself because the specific accelerations were higher in the seat leg in this test. Finally, the results from non-standard sized ATDs are shown in Figure 5.24 on the right. The 95th percentile ATD seated in seat 2 had a significant increase in load in the wingbox section test. However, data were not collected for the 5th percentile ATD seated in seat 1.

Head vertical accelerations were examined for to determine head injury. In Figure 5.27, the ATDs seated in the rear row are plotted on the left and ATDs in the front row are plotted on the right.

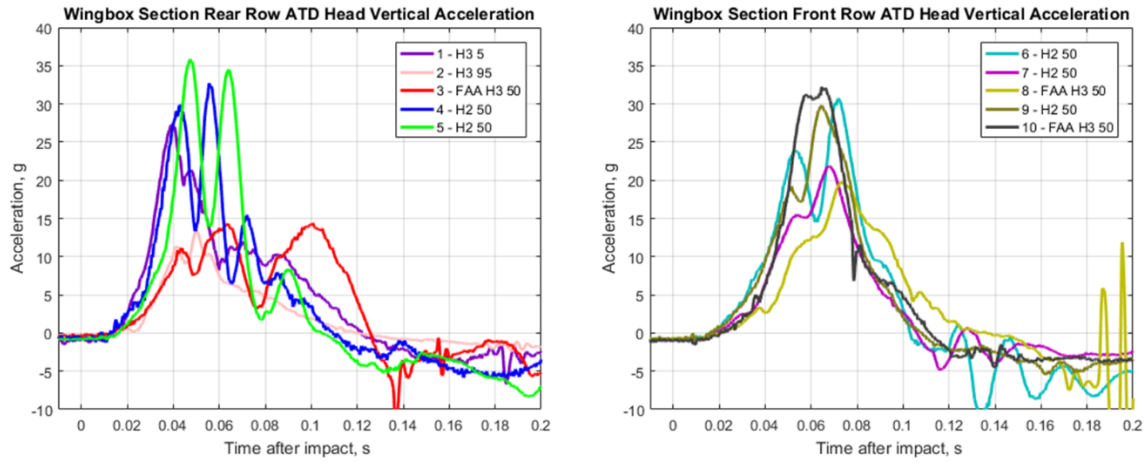

(a) (b)

Figure 5.27. Wingbox section ATD head vertical acceleration—rear row (a) and front row (b)

The head accelerations in the rear row exhibited two distinct types of responses. The first, which occurred in ATDs 1, 4 and 5, had a higher acceleration onset rate. There was a higher initial peak earlier than for ATDs 2 and 3. ATDs 1, 4, and 5 had peak acceleration values of 27.3 g, 32.7 g, and 35.9 g. ATDs 2 and 3 had a much slower acceleration onset rate with a much lower peak value of acceleration. ATD 2 had a peak value of 13.3 g and ATD 3 had 14.2 g. The response for ATD 3 was explained by the difference in the brace positioning of that ATD, but the response from ATD 2 is currently unexplained.

For the rear row, the results are similar between all the seats. The onset rate of all accelerations was similar, except for ATD 8. ATD 8 had the slowest onset rate and lowest peak acceleration value of 19.7 g. The other ATDs measured peak acceleration values of 30.7 g, 21.9 g, 29.8 g, and 32.2 g for 6, 7, 9 and 10. Results for the horizontal acceleration data are plotted in Figure 5.28.

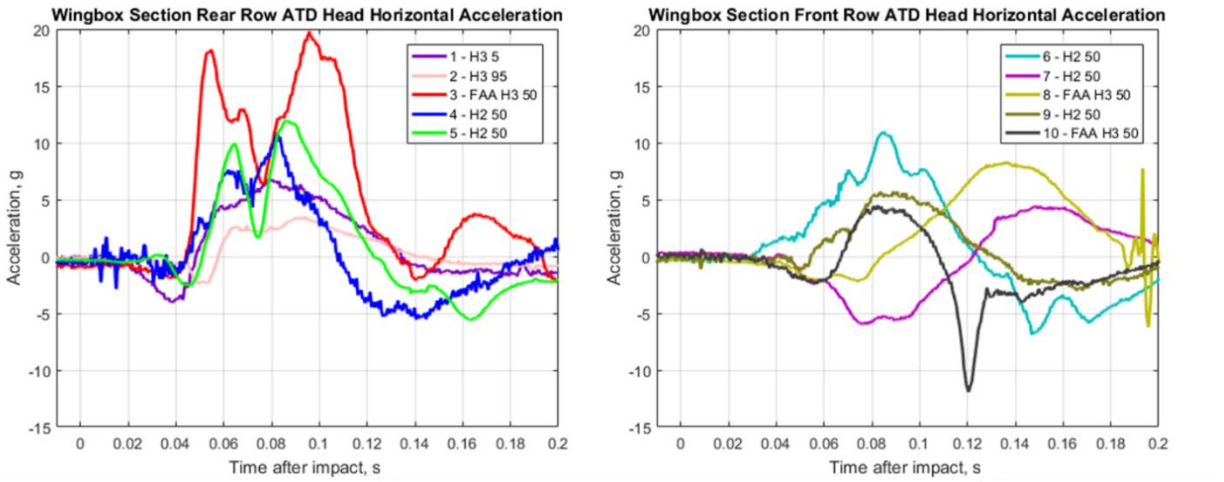

(a) (b)

Figure 5.28. Wingbox section ATD head horizontal acceleration. Rear row (a) and front row (b)

The horizontal head accelerations measured by the ATDs varied widely between location, size, and type. The most noticeable response was in ATD 3, which was well above the magnitudes of the accelerations seen in the other ATDs due to the difference in its positioning. In the brace position, ATD 3's head was oriented mainly in the horizontal direction as opposed to the other ATD heads, which were aligned mainly in the vertical direction. This difference led ATD 3 to measure 19.8 g peak acceleration that occurred 0.096 s after impact. The next highest response was obtained in ATD 5, which had a peak acceleration of 11.8 g.

The rear row accelerations for ATDs 3, 4, and 5, which were all 50th percentile ATDs, showed a similar double peak response shape at different magnitudes. In contrast, the 5th and 95th percentile ATDs showed the lowest acceleration peaks and the longest magnitudes. There was no discernable trend in the responses for the ATDs seated in the front row. Additionally, the response curves for all of the ATDs did not begin until after 0.020 s after impact and did not end until well after 0.200 s for some of the ATDs located in the front row. The timing offset indicated that the ATD response lagged that of the airframe.

The head acceleration values were used in the HIC computation, similar to what was done for the forward section data. The results of the HIC computation are shown in Table 5.2.

Table 5.2. Wingbox section test ATD HIC values

ATD Type - Size	Seat #	HIC Value
H3 – 5	1	48.6*
H3 – 95	2	9.1*
FAA H3 – 50	3	54.4
H2 – 50	4	75.6
H2 – 50	5	107.2
H2 – 50	6	86.9
H2 – 50	7	47.2
FAA H3 – 50	8	32.9
H2 – 50	9	77.9
FAA H3 – 50	10	99.4
**For reference only*		

The absence of a high spike in the acceleration time histories indicated that the ATD head did not strike the seat back or other surfaces. The low HIC results from ATD 3 were unexpected because the head was resting against the seat 8 seat back, and the expected forward motion would cause a strike into the seat 8 seat back. However, the actual forward motion due to the rotation of the fuselage was not high enough to cause the ATD's head to strike the seat back with any noticeable acceleration. For all seats, all HIC values were well below the established limits, which indicated a low probability of skull fracture.

Finally, pelvic acceleration was examined on each of the ATDs. Figure 5.29 shows the results from the vertical accelerations both from the rear row ATDs on the left and the front row ATDs on the right.

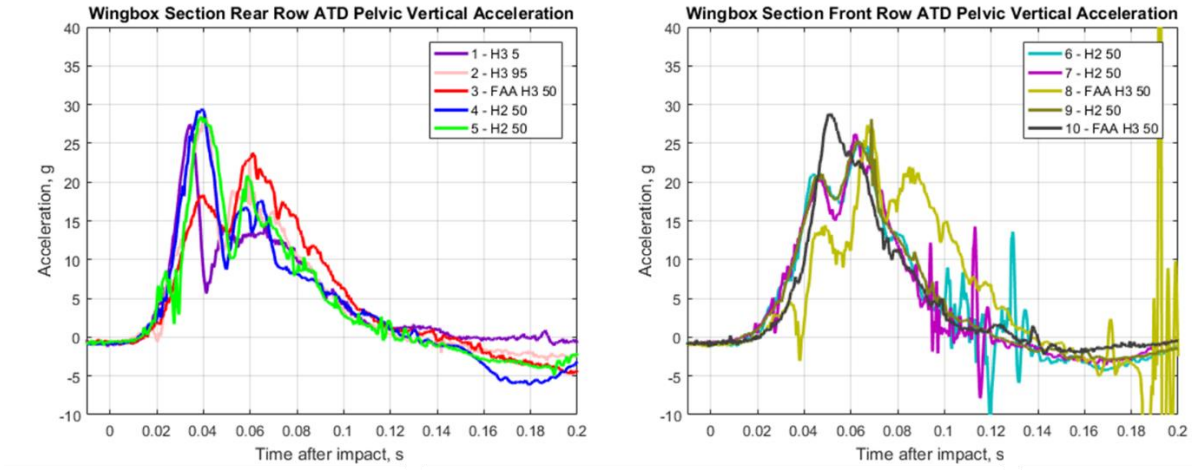

(a) (b)

Figure 5.29. Wingbox section ATD pelvic vertical acceleration—rear row (a) and front row (b)

The pelvic responses were again checked as a backup to the lumbar loading because the accelerometer locations in the pelvis were close to the load cell used for the lumbar load measurement. In the rear row, the responses were all very similar, both in magnitude and shape for ATDs 1, 2, 4, and 5. ATD 3 had a different response than the rest, which was expected due to the difference in ATD 3 positioning. The peak pelvic accelerations for ATDs 1, 2, 4, and 5 were 27.4 g, 28.4 g, 29.4 g, and 28.3 g, which occurred at 0.034 s, 0.041 s, 0.039 s, and 0.039 s after impact. ATD 3 measured a peak acceleration of 23.7 g, which occurred at 0.061 s after impact. The general shapes of all of the response curves were similar.

ATDs 6, 7, and 9 followed similar trends when examining the pelvic vertical acceleration response and ATDs 8 and 10 had differences. ATD 10 measured a peak acceleration of 28.8 g, which occurred at 0.051 s after impact. ATD 8 measured a peak acceleration of 26.9 g, which occurred 0.067 s after impact. In contrast, the ATDs seated in seats 6, 7, and 9 measured peak accelerations of 25.3 g, 26.1 g, and 25.2 g. These occurred between 0.062 s and 0.064 s after impact. The horizontal pelvic accelerations measured in the ATDs is shown in Figure 5.30.

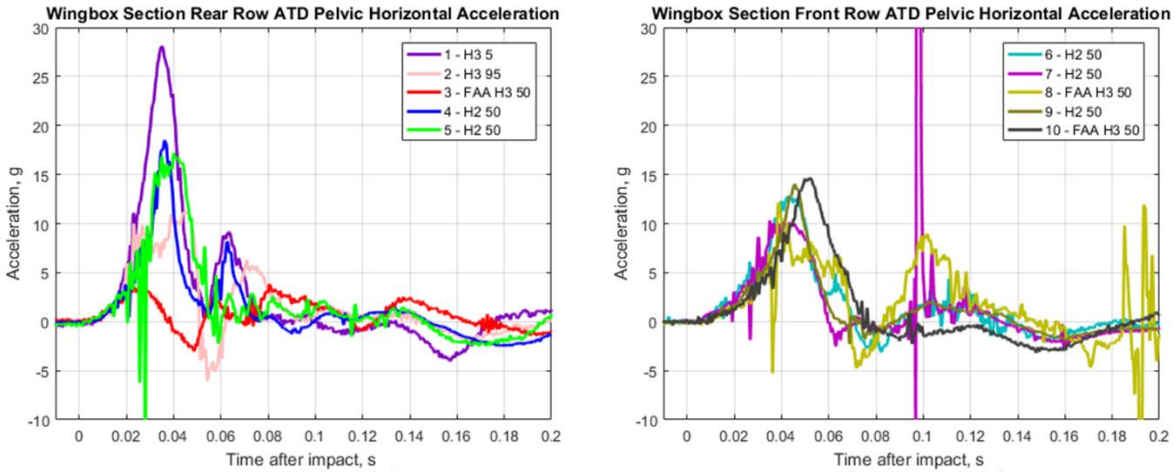

(a) (b)

Figure 5.30. Wingbox section ATD pelvic horizontal acceleration—rear row (a) and front row (b)

The horizontal pelvic responses showed the rear row did not exhibit clear acceleration trends. The 5th sized ATD seated in seat 1 measured the largest acceleration peak of 28.1 g at approximately 0.035 s after impact. The peak could partially be due to the ATD's small size, allowing it to move around in the seat even when fastened into the seat with the seatbelt. The next highest peak accelerations from the rear row ATDs were from seats 4 and 5. ATDs 4 and 5 measured peak acceleration values of 18.5 g and 17.2 g. They generally followed the same post-peak acceleration trend. These results are followed up by the peak acceleration of 11.3 g measured from the 95th sized ATD seated in seat 2. Finally, ATD 3 showed a different response magnitude and shape due to its positioning. This ATD measured a small 3.5 g peak approximately 0.025 s after impact, after which the accelerations reached a maximum negative peak of 3.0 g. The acceleration generally hovered around the zero-g mark post-negative peak, with no notable events happening after 0.06 s. The small horizontal accelerations could be due to the lack of horizontal motion the ATD could undergo because its head was essentially positioned against the seat back of seat 8 and its pelvis buckled tightly into the seat. There was a possibility that it was wedged into its braced position, unable to move forward or backward during the impact.

In the forward row of seats, the data followed similar trends. The onset rate for all ATDs was similar, and all ATDs reached initial peak values between 0.040 s and 0.055 s after impact. All curves are triangular with a duration between 0.060 s and 0.080 s. ATD 7 measured a spike at approximately 0.100 s. The magnitude is 284 g, which is out of the range of Figure 5.30. This spike was likely caused by an anomalous electrical signal from the experimental data system used in the ATD. There was no evidence in the video or other test data that the pelvic section in this ATD registered a structural acceleration in this range.

6. APPLICABILITY OF RESULTS TO AIRCRAFT CRASHWORTHINESS DISCUSSION

These two tests were conducted, in part, to collect data to evaluate the characteristics of transport category aircraft crashworthiness on two actual aircraft sections. There are numerous possible

criteria to evaluate crashworthiness of an aircraft, but this example borrowed from past criteria for aircraft development. The four general criteria to evaluate crashworthiness follow:

1. Retention of items of mass
2. Maintenance of occupant emergency egress paths
3. Maintenance of acceptable acceleration and loads experienced by the occupants
4. Maintenance of a survivable volume

These metrics guided aircraft design features for crashworthiness in literature (FAA, 2007, U.S. Army Aviation Systems Command, 1987) and useful when considering a new transport category aircraft crashworthiness rule. One specific criteria for an aircraft certified by the FAA using a Special Condition (SC) (FAA, 2014) stipulates that crashworthiness must be met on aircraft sections, either through "analysis using validated analytical tools or by direct-test evidence" in conditions of up to 30 ft/s in the vertical direction. Other SCs issued for other new composite aircraft (FAA, 2007) are similar.

Criteria #1 stipulates items such as overhead bins, seats, items in the galley, and other items of mass onboard the aircraft must not come loose during an impact. For overhead bins specifically, an attachment failure could lead to a bin detachment, causing a direct strike to an occupant or possible blockage of an aisle, leading to difficulty in occupant egress. Criterion #2 stipulates the egress paths must be maintained. This criterion relates to mass retention addressed in criteria #1 but also suggests that the floor or floor supporting structures must remain intact. Criteria #3 addresses the occupant loading levels, specifically limits defined in 14 Code of Federal Regulations (CFR) § 25.562, which are imposed using a 50^{th} percentile Hybrid II (or equivalent) ATD. Criteria #4 addresses the airframe deformation around the occupant with acceptable limits defined for occupant egress.

The four criteria can be addressed using "direct-test evidence" from the data acquired on the two tests. For criteria #1 - In both tests, the overhead items of mass were simulated with aluminum c-channels and ballast, and the attachment fasteners were intentionally oversized to ensure they would not fail. This arrangement means criteria #1 cannot be addressed directly. However, accelerations on the ballast and attachment locations were measured, and a dynamic load factor at the attachment locations is reported. It is hoped that the dynamic load factor provides insight into the actual loading at the attachment locations during a dynamic event, as opposed to an inertial loading conditions as stipulated in 14 CFR § 25.561 (FAA, 1997). If this airframe was actually under consideration for certification, the corresponding fasteners and other structure could be sized appropriately. For criteria #2, the occupant egress paths can be addressed. The forward section showed failures in many of the floor supports, but floor failures caused the floor panels to bear against the underfloor luggage. Different interpretations can be made whether the egress path was maintained. If this test article was actually undergoing certification, the ultimate decision would be left to the certification expert. In the wingbox section, the floor did not fail, and the egress path was maintained. In criteria #3, the occupant lumbar loads were exceeded for the majority, but not all, of the ATDs in both tests. The wingbox section results had overall higher values. Using the most conservative case and reporting only the highest loaded ATD as the basis for evaluation, both tests would fail this criterion. However, if a less conservative criteria is used, such as the average or the median of the ATD loads, different results can be expected. This could lead to a pass condition depending on interpretation of the data. For criteria #4, the forward section showed 5

inches of maximum dynamic deformation and 1 inch of permanent deformation through the fuselage ovalization. However, the wingbox section had negligible deformation. The wingbox section passed this criterion, and further evaluations are necessary to determine whether a maximum of 5 inches of dynamic deformation would intrude into the occupant's survivable volume.

Results obtained using the four criteria are mixed as to whether the sections would exhibit a pass or fail if this aircraft were undergoing actual certification. One consideration is that the size of the F28 sections (and corresponding aircraft) are much smaller than an A350-900 or other wide-body aircraft. The size of these sections made them potentially unable to demonstrate adequate crashworthiness at 30 ft/s as stipulated in the referenced SCs. Had the sections been tested at 20 ft/s vertical velocity, representing a reduction of the kinetic impact energy by 44%, all four criteria might have been met. Thus, it is important to consider different limits in the criteria based on aircraft size, weight, or other defining factors.

Relative performance of the seats used in these tests needs to be addressed. The seats were certified to the most recent FAA guidelines (FAA, 14 CFR § 25.562, 1998) and removed from an in-service aircraft. However, the seats were designed for a different aircraft and modified–mainly in the seat leg spacing. The modification allowed for the triple aisle seat to be at a large overhang but potentially out of specification limits for how the seats were originally certified. The low lumbar loads measured in the ATDs seated in the cantilevered triple aisle seats were a result of the large amount of seat support tube deformation that might or might not represent the actual certified seat used in the F28.

Additionally, it should be considered whether to use double seats for the port side of the airframes from the modification of a triple seat. There is a difference in weight supported by the double seats used in the test (approximately 170 lb. per 50^{th} percentile ATD for a total of approximately 350 lb.) versus what is typically supported by the seats in their unmodified triple configuration, which can be assumed as an additional 170 lb., leading to a 520 lb. total weight. If a seat designed for 520 lb. of weight is only loaded with 350 lb. of weight, the seat design might be too stiff when evaluating the ATD response. However, triple and double seat designs share common materials and parts, resulting in reduced development and certification costs. Taken a step further, the performance of a triple-made-into-a-double seat is identical to the performance of a designed double seat due to the commonality of parts and design. There are no further conclusions but care was taken to ensure that the results for the ATDs seated in the cantilever seats are well documented.

The wingbox section test was an opportunity to configure a test with induced forward motion rather than just repeat a second purely vertical impact condition. The wingbox section test article was tipped a small angle forward, which then impacted a sloped surface. The angles were kept relatively small – approximately 2.9 degrees for the test article and 10 degrees for the surface– because it was unknown whether the test article would tip over. The small potential for a tip over is uncertain, so precautions were taken and hardware added to the test article. During the test, the test article experienced a small amount of rotation that briefly induced approximately 9.4 ft/s velocity in the forward direction. This was not enough rotation to cause tip over. The forward motion did not significantly affect either the airframe or occupant response. The airframe survived the test with minimal damage, and the ATDs did not show signs of head strike due to the added forward motion. To noticeably influence the forward direction, the test article should be tilted to

an angle of 20 or more degrees. A 20-degree angle gives a local horizontal velocity of 10.3 ft/s at impact when using a 30 ft/s vertical condition. For a rotation to occur at impact, the surface should have an angle greater than 20 degrees. The rotation of the test article through the impact would allow for the horizontal velocity to be even higher.

7. CONCLUSION

During 2017, two vertical drop tests were conducted on two partial sections removed from a Fokker F28 MK4000 aircraft as a part of a joint NASA/Federal Aviation Administration (FAA) effort to investigate the crashworthiness characteristics of Transport Category Aircraft. The first test was a pure vertical drop test of a relatively uniform forward section, which included an underfloor area for luggage. The second test was a canted drop test onto a sloped surface of a portion of the fuselage representing the wingbox stiffened structure. In both tests, accelerometers were installed on the floor, seat track, luggage, and overhead bin to measure responses in the two airframe sections. The seats were (FAA, 1998 CFR § 25.562) certified and removed from an in-service Boeing 737 aircraft. They were modified to attach the floor tracks of the F28 aircraft A triple seat configuration was located on the right side and a dual configuration on the left. In addition, ten Anthropomorphic Test Devices (ATDs, a.k.a. crash test dummies) were used in each test to measure the potential of onboard occupant injury. Self-contained data recorders, which logged accelerations and rotational rates, were also used on the seat tracks and lower structure for evaluation as potential crash recording devices in future tests. Finally, the starboard side of each section was painted with a stochastic black and white speckle pattern for use in full field photogrammetric imaging techniques.

The first test, named the forward section test, was of a forward portion of the F28 fuselage between FS 5305 and FS 7805. There was underfloor space for the addition of 922 lb. of luggage, which was loosely stacked four bags wide by four bags deep by three bags high. The test impacted at a nearly zero-degree pitch angle with an impact velocity of 28.9 ft/s. Both tests impacted a bed of soil. All the data were successfully collected on the airframe, ATD, and crash data recorder (CDR) sensors. Post-test inspections showed a number of failures in the floor support structure and bottom skin. However, the portion of the fuselage above the floor exhibited little to no deformation. A permanent deformation of approximately 1 inch was observed post-test. The luggage interaction played a large role in the response of the section. Many of the failures of the floor supports were caused by a specific bag interaction with the floor structure. The ATDs show mixed results when examining the lumbar loads. Some were above the 1,500 lb. limit and others were below. The two ATDs seated in the overhung seats measured the lowest loads out of all of the ATDs, with the exception of ATD 4, which was affected by the floor failure at its seat base.

A wingbox section was used for the second test, which was located between FS 9805 and 12405. This test pitched the test article forward approximately 2.9 degrees onto a 10-degree sloped soil surface. The test article did experience forward motion, which was not significant enough to affect the response of the fuselage or ATDs. Most of the fuselage deformation occurred in the lower cavity below the wing truss support structure. The rest of the test article appeared undamaged. The ATDs measured higher loads than in the forward section, which was expected because there was less fuselage deformation. All the ATDs were over the 1,500 lb. limit, except for the ATDs seated in the overhung seats and ATD 6, which was just slightly under the 1,500 lb. limit. The

braced positioned ATD 3 showed different response shapes when comparing both its acceleration and lumbar load data with other ATDs. ATD 10 was consistently on the high end of the responses.

To induce a larger horizontal velocity into the test impact conditions, a larger test article pitch angle onto a larger slope on the impact surface is needed. However, testing these larger angles is challenging because of the extra steps to properly zero the measurement sensors, restrain the test article to prevent tip over, and position the ATDs accurately for impact. These challenges need to be addressed before testing.

A series of luggage component tests were conducted to evaluate the luggage response by itself. The luggage showed similar acceleration time histories for both tests conducted using different sets of individual bags at differing impact conditions. This suggests that luggage response is generally consistent and mostly unaffected by bag type, size, or contents. Additionally, the data suggest the luggage response can be simulated both physically and computationally using materials having properties that represent either elastic-plastic response or a response that is linear elastic-constant crush-compaction. Typically, foams exhibit the second type of response. An evaluation of various density foams would identify a suitable luggage substitute for future tests.

Three CDRs were used in the tests to evaluate their use as an alternative portable data acquisition system and as usable data collection tools. The CDRs used in the luggage from the forward section test and in the lower cavity in the wingbox section test provided valuable data to quantify the responses at these locations. A second set of CDRs were used as comparisons to the conventional data systems. The results showed very good agreement in the lower ranged CDRs when compared to the ruggedized data systems and give confidence in using the CDRs in tight or otherwise inaccessible spaces normally unavailable for instrumentation. Because these CDRs are lightweight and portable, they can be used to collect these types of data. It is important to note that the CDR ranges need to be set within the sensor's measurement range and not within the sensitivity of the sensor.

The results collected show notable differences in the forward and wingbox section responses. The forward section floor accelerations showed an initial peak of approximately 21 g and a relatively uniform response of approximately 7 g throughout the impact event. This section exhibited large amounts of subfloor crushing, floor stiffener failures, and seat deformation upon impact. . These results are contrasted by the wingbox section accelerations, which showed large differences when comparing accelerations from the rear and the front of the FS. The rear had an initial peak of 39 g and the front section only 32 g, and uniform responses of 12.2 and 9.8 g, respectively. Additionally, the wingbox section test induced a forward motion caused from the rotation at impact. Except for the lower cavity, there was minimal deformation in the wingbox section, and ATD responses were consistently higher than those for the forward section.

Finally, a discussion that compares the test data to four crashworthiness criteria was presented. The crashworthiness criteria are: retention of items of mass, maintenance of occupant emergency egress paths, maintenance of acceptable acceleration and loads experienced by the occupants and maintenance of a survivable volume. It was not the purpose of the tests or this report to categorize the F28 aircraft as crashworthy. However, the data can be used as test cases for an aircraft crashworthiness certification process that uses the four criteria presented. Results pertaining to each of the four criteria and supporting rationale behind each pass or fail judgement are presented.

As stated in the report, one consideration is that the size of the F28 sections (and corresponding aircraft) are much smaller than an A350-900 or other wide-body aircraft. The size of these sections made them potentially unable to demonstrate adequate crashworthiness at an impact velocity of 30 ft/s as stipulated in the referenced SCs. Had the sections been tested at 20 ft/s vertical velocity, representing a reduction of the kinetic impact energy by 44%, all four criteria might have been met. Thus, it is important to consider different limits in the criteria based on aircraft size, weight, or other defining factors.

It is hoped that the data obtained from the tests, along with the lessons learned from the criteria, can be used as guides for future work in transport category aircraft crashworthiness.

8. REFERENCES

Annett, M.S., Littell, J.D., Jackson, K.E., Bark, L.W., DeWeese, R. L., McEntire, B.J. (2014). Evaluation of the First Transport Rotorcraft Airframe Crash Testbed (TRACT 1) Full-Scale Crash Test. (NASA-TM-2014-218543).

ASTM Standard D1883, 2016. "Standard Test Method for California Bearing Ratio (CBR) of Laboratory-Compacted Soils." ASTM International, West Conshohocken, PA..

FAA Report. (1993). Vertical Drop Test of a Metro III Aircraft. (DOT/FAA/CT-93/1).

FAA Report. (1995). Vertical Drop Test of a Narrow-Body Fuselage Section with Overhead Stowage Bins and Auxiliary Fuel Tank System On Board. (DOT/FAA/CT-94/116).

FAA Report. (1998). Vertical Drop Test of a Beechcraft 1900C Airliner. (DOT/FAA/AR-96/119).

FAA Report. (1999). Vertical Drop Test of a Shorts 3-30 Airplane. (DOT/FAA/AR-99/87).

FAA Report. (2000). Vertical Drop Test of a Narrow-Body Transport Fuselage Section with a Conformable Auxiliary Fuel Tank Onboard. (DOT/FAA/AR-00/56).

FAA Report. (2006). Vertical Drop Test of an ATR 42-300 Airplane. (DOT/FAA/AR-05/56).

Fasanella, E.L. and Alfaro-Bou, E. (1986). Vertical Drop Test of a Transport Fuselage Section Located Aft of the Wing. (NASA-TM-89025).

Fasanella, E.L., Alfaro-Bou, E. and Hayduk, R.J. (1986). Impact Data from a Transport Aircraft During a Controlled Impact Demonstration. (NASA-TP-2589).

Federal Aviation Administration. "Emergency Landing Conditions: General." 14 CFR § 25.561. Amended July 29, 1997.

Federal Aviation Administration. "Emergency Landing Dynamic Conditions." 14 CFR § 25.562. Amended May 17, 1998.

Federal Aviation Administration. (2007). Special Conditions: Boeing 787-8 Airplane; Crashworthiness. *Federal Register, 72*(186), 32021–322023.

Federal Aviation Administration. (2014). Special Conditions: Airbus A350-900 Airplane; Crashworthiness, Emergency Landing Conditions. *Federal Register, 79*(143). 43237–43239.

Federal Aviation Administration. (2015). Aviation Rulemaking Advisory Committee, Transport Airplane and Engine Issues, *Federal Register, 80*(107), 31946–31948.

Fokker. (1999). "Fokker Fellowship F28 Weight and Balance Manual." Revised January 1, 1999.

Gowdy, V., DeWeese, R., Beebe, M., Wade, B., Duncan, J., Kelly, R., and Blaker, J. (1999). A Lumbar Spine Modification to the Hybrid III ATD For Aircraft Seat Tests. (SAE TP 1999-01-1609). General, Corporate, and Regional Aviation Meeting and Exposition. Wichita, KS.

Kellas, S., and Jackson, K.E. (2008). *Multi-Terrain Vertical Drop Tests of a Composite Fuselage Section.* Proceedings from the American Helicopter Society 64th Annual Forum. Montreal, Canada.

Littell, J.D. (2015). Crash Tests of Three Cessna 172 Aircraft at NASA Langley Research Center's Landing and Impact Research Facility. (NASA-TM-2015-218987).

Littell, J.D. (2016). Experimental Photogrammetric Techniques used on Five Full-Scale Aircraft Crash Tests. (NASA-TM-2016-219168).

Schmitt, K.-U., Niederer, P. and Walz, F. (2004). "Trauma Biomechanics: Introduction to Accidental Injury." Verlag Berlin Heildelberg New York: Springer.

Society of Automotive Engineering. (1995). "J322-1 Instrumentation for Impact Test – Part 1 – Electronic Instrumentation." SAE international, 400 Commonwealth Drive, Warrendale, PA.

Thomas, M.A., Chitty, D.E., Gildea, M.L., T'Kint, C.M. (2008). Constitute Soil Properties for Unwashed Sand and Kennedy Space Center. (NASA CR-2008-215334).

U.S. Army Aviation Systems Command. (1987). Aeronautical Design Standard. Rotary Wing Aircraft Crash Resistance. (ADS-36).

U.S Dept. of Transportation. "Occupant Crash Protection." Federal Motor Vehicle Safety Standard No. 208 (2020).

Williams, M.S. and Hayduk, R.J. (1983). Vertical Drop Test of a Transport Fuselage Section Located Forward of the Wing. (NASA-TM-85679).

Williams, M.S., and Hayduk, R.J. (1983). Vertical Drop Test of a Transport Fuselage Center Section Including the Wheel Wells. (NASA-TM-85706).